7-30-2020 2:30 PM

Experimental and Numerical Study of Precast Concrete Pipe with Single Elliptical Steel Cage Reinforcement

Abdullah Samir Ramadan, *The University of Western Ontario*

Supervisor: Nehdi, Moncef, *The University of Western Ontario*

A thesis submitted in partial fulfillment of the requirements for the Master of Engineering Science degree in Civil and Environmental Engineering

Abstract

Reinforced concrete pipe (RCP) with single elliptical (SE) reinforcement offers cost savings and is permitted by Canadian and American standards. Yet, its use has not yet gained momentum primarily due to limited knowledge of its structural performance. This study explores the structural behaviour of full-scale 1050 mm and 1200 mm diameter RCP reinforced with SE cold drawn steel wire cage under the Three-Edge Bearing Test. Results indicate that RCP with SE reinforcement designed per current standards did not meet the specified 0.3-mm crack and ultimate load capacity. Hence, pertinent provisions in CSA A257.2 and ASTM C76 for RCP need to be updated with specific and more suitable guidance for SE cage RCP. The study also investigates the effect of the SE cage rotation on the structural capacity of the pipe through finite element modelling. The model indicates a significant reduction in ultimate load capacity from the cage rotation.

Keywords

Precast Pipe; Reinforced Concrete; Three-Edge Bearing Test; Design; Standard; Elliptical Reinforcement; Structure; Finite Element Modelling; Design Code.

Summary for Lay Audience

Concrete is the second most consumed material in the world today, second only to water. Concrete used in construction applications is typically reinforced with a steel mesh or cage in order to increase its strength and resistance to cracking. The wet concrete is poured on the steel mesh/cage in a mould, permanently encasing the steel once dried up. Reinforced concrete pipes (RCPs) has been reliably used in North America for over a century to transport sanitary and storm sewage. As such, they are an important and durable component of modern civil infrastructure. RCP market share has seen a steady decline over the years due to competition from the plastic pipe industry and lack of technological advancements.

The most common reinforcement configuration used in the industry is the double circular (DC) steel cage configuration for mid-size diameter pipes. RCP with single elliptical (SE) steel cage reinforcement offers cost savings up to 30% and is permitted by Canadian and American RCP design standards as an alternative to the DC steel cage. Yet, its use has not gained momentum, primarily due to limited knowledge of its practical application in the industry. This study explores the practical application of full-scale 1050 mm and 1200 mm diameter RCP with SE steel cage under a standard load test. Results indicate that RCP with SE steel cage designed according to current Canadian and American standards did not meet the specified load limits. Hence, relevant requirements in design standards for RCP need to be updated with specific and more suitable guidelines for SE cage RCP design. The study also investigates the effect of rotation of the SE cage on the load capacity of the pipe through computer modelling programs. The computer models indicate significant reduction in the pipe load capacity due to the rotation of the cage from its original position.

Co-Authorship Statement

This thesis has been structured according to the integrated-article format following the guidelines and regulations of the School of Graduate and Postdoctoral Studies (SGPS) at Western University. Chapters 3 and 4 of the Thesis have been submitted for publication to peer-reviewed technical journals. All experimental work, numerical work, data analysis, and writing draft manuscripts for publications was carried out by the candidate under the direct supervision of Professor M.L. Nehdi. Any other co-authors assisted in the experimental testing, numerical modelling, and development for the final version of the publications.

Ramadan, A., Younis, A.-A., Wong, L. S., and Nehdi, M. L. "Investigation of structural behavior of precast concrete pipe with single elliptical steel cage reinforcement," *Engineering Structures, Elsevier*, Vol. 219, pp. 1-17, 2020.

Ramadan, A., Shehata, A., Younis, A.-A., Wong, L. S., and Nehdi, M. L. "Modeling structural behavior of precast concrete pipe with single elliptical cage reinforcement," *Structures*, Elsevier, Vol. 27, October 2020 Issue, pp. 1-14, 2020

Ramadan, A., Younis, A.-A., Wong, L. S., and Nehdi, M. L. (2019) "Reinforced Concrete Pipe Design with Single Elliptical Steel Cage Reinforcement" 7th International Specialty Conference on Engineering Mechanics and Materials, Proceeding of the Annual Conference of the Canadian Society for Civil Engineering, Laval, Canada

Dedication

To:

My Mother: Noha Abou Radi

My Father: Samir Ramadan

My Brother: Bilal Ramadan

My Late Grandmother: Lotfie Sleiman

My Late Grandfather: Abdulkader Abou Radi

Acknowledgments

First and foremost, I would like to thank God for providing me with the strength and ability to complete this thesis.

I would like to extend my sincere thanks to my supervisor Prof. Moncef L. Nehdi for providing me with this opportunity and for his continuous support and assistance, I will always be grateful for that.

I would also like to extend my deepest gratitude to Liu Sammy Wong for his technical guidance, efforts, support, and facilitating communication with Con Cast Pipe.

I would like to acknowledge the support of Con Cast Pipe for manufacturing the tested full-scale reinforced concrete pipes and for providing their apparatus for testing. Special thanks to all the staff and workers at Con Cast Pipe who were extremely welcoming and supportive throughout the research project.

I would like to extend my deepest appreciation to my dear friend and research partner Aziz Younis for his encouragement, suggestions, and assistance throughout this research project. I will always cherish our friendship.

I would also like to sincerely thank all the amazing faculty and staff here at Western University, their dedication and work behind the scenes make achievements like this possible.

I am extremely grateful to all my friends and colleagues that have always supported and encouraged me through this experience. The life-long relationships that I have developed throughout have been one of the highlights of my time at Western University. I wish them all success in the future.

Finally, I would like to acknowledge with a deep sense of love and respect my family, especially my parents. The sacrifices they have made and the prayers and support they have provided have been immense. I dedicate all my achievements to them and will forever be in their debt. This would not have been possible without them.

Table of Contents

List of Tables

List of Figures

List of Symbols

D_{HL}	Load the first visible hairline cracks appears (N/m/mm)
D_{MHL}	Load when second visible hairline crack appears (N/m/mm)
$D_{\delta=0.36\%}$	Load when the pipe deflects 0.36% of the internal diameter (N/m/mm)
$D_{0.3}$	Load when the crack width reaches 0.3 mm width with minimum length of 300 mm (N/m/mm)
D_{peak}	First maximum linear value followed by a declined in load (N/m/mm)
D_{10mm}	Load when the pipe deflects 10 mm (N/m/mm)
D_{ult}	Maximum load the pipe can withstand (N/m/mm)
y1	Vertical displacement at pipe and should be positive indicating downward movement (mm)
y2	Vertical displacement at the pipe invert and should be negative indicating downward movement (mm)
δ	Deflection of pipe (mm/m/mm)
δ_{HL}	Deflection of pipe at D_{HL} (mm/m/mm)
$\delta_{0.3}$	Deflection of pipe at $D_{0.3}$ (mm/m/mm)
δ_{peak}	Deflection of pipe at D_{peak} (mm/m/mm)
δ_{ult}	Deflection of pipe at D_{ult} (mm/m/mm)
$R_{0.3}$	Post-crack load ratio ($D_{ult}/D_{0.3}$)
R_{peak}	Post-peak load ratio (D_{ult}/D_{peak})

S_{HL}	Pipe stiffness at first visible crack (N/mm)
$S_{0.3}$	Pipe stiffness at crack load (N/mm)
S_{peak}	Pipe stiffness at first peak load (N/mm)
$S_{\delta=0.36\%}$	Pipe stiffness when pipe deflects 0.36% of the internal pipe diameter (N/mm)
Di	Internal pipe diameter (mm)
h	Pipe wall thickness (mm)
Asi	Inner area of steel (mm^2/m)
Aso	Outer area of steel (mm^2/m)
l_o	Longitudinal wire spacing (mm)
fc'	Concrete compressive strength (MPa)
fy	Steel yield strength (MPa)
E_c	Concrete modulus of elasticity (MPa)
E_s	Steel modulus of elasticity (MPa)
G_f	Fracture energy (MPa)

List of Abbreviations

ACPA	**American Concrete Pipe Association**
DC	**Double Circular**
EC	**Equivalent Class**
FS	**Factor of Safety**
FEM	**Finite Element Modelling**
PL	**Prism Load**
RCP	**Reinforced Concrete Pipe**
SE	**Single Elliptical**
SFRC	**Steel Fibre-Reinforced Concrete**
SCM	**Supplementary Cementitious Material**
TEBT	**Three-Edge Bearing Test**
VAF	**Vertical Arching Factor**

Chapter 1

1 Introduction

1.1 Background

Reinforced concrete pipes (RCP) are a crucial component of modern civil infrastructure and have been transporting sanitary and storm sewerage for over a century with reliable performance. A need to standardize and produce high quality RCP products resulted in the formation of the American Concrete Pipe Association in 1907. Urbanization and the shift of population density from rural areas to cities has led to the tremendous growth and use of RCP present-day (American Concrete Pipe Association, 2020).

Despite that RCP is still a primary choice for drainage, the industry has been experiencing declining market share due to the emergence of the lightweight flexible pipe industry, coupled with tepid technological advancements (Masterson, 2017). Flexible steel-reinforced HDPE pipe of up to 2100 mm in diameter has been promoted as an alternative to RCP for storm and sanitary drainage (armtec, a Division of WGI, n.d.). Flexible pipes are characterized by their ability to deform more than 2% of their diameter without cracking, relying heavily on the surrounding bedding material to transfer the vertical loads imposed on them. Conversely, rigid pipes such as RCP are structurally resilient and can resist external load, allowing them to better handle lower quality bedding material. Flexible pipes have the advantage of being resistant to chemical attacks and abrasions. However, they have an inferior fire resistance relative to RCP. The lightweight flexible pipes are more adaptable for installation as they can be cut on site for length adjustments compared to RCP which have a standard length, reducing the flexibility of on-site installation (KWH PIPE, n.d.).

Standards such as ASTM C76 (ASTM C76-16, 2016) and CSA A257.2 (CSA A257-14, 2014) provide provisions for RCP reinforcing steel design. Up to three reinforcing steel cages are commonly used by the manufacturer to fulfill design requirements. Single layer circular cage is common in smaller diameter RCP (typically less than 900 mm). Double layer circular cages are common in mid-size diameter pipes ranging between 600 mm to 1800 mm or larger diameter up to 2400 mm pipes with lower class. Triple layer cages with an elliptical layer supplementing the double circular cages are common for large diameter and higher-class RCP.

1.2 Research Need and Objectives

Recent research on RCP has focussed on using steel fibre or hybrid fibre as reinforcement, potentially reducing or completely eliminating the need for conventional reinforcing steel in the fabrication process, and thus making RCP manufacturing less labor intensive (Haktanir et al., 2007) (Figueiredo et al., 2012) (Mohamed et al., 2015) (Abolmaali et al., 2012) (Park et al., 2015). However, using steel fibre-reinforced concrete (SFRC) for RCP manufacturing has not been widely adopted due to complications with attaining desired structural behaviour and finished product. Hydrostatic performance of SFRC pipes was also reported as a challenge (Wong, 2016). Furthermore, substantial changes in the manufacturing process and the cost incurred in additional quality control to produce SFRC pipes created a roadblock for the technology. Therefore, using a single elliptical conventional reinforcing cage for RCP without altering the normal manufacturing process is considered an attractive option.

While current Canadian and American standards allow for using single elliptical (SE) reinforcement as an alternative to conventional double circular (DC) reinforcement, this option is not commonly used by the industry due to difficulties in manufacturing the cage into a true elliptical shape. Although single circular cage is not uncommon for small diameter RCP (less than 900 mm), the lack of research to validate its structural performance discouraged its use in larger pipe sizes. SE steel reinforcement design can be more effective since the steel reinforcement can be positioned more favourably at the tensile faces of the pipe under loading. Elimination of the outer layer of steel reduces the needed reinforcement

and the associated labour, thus enhancing the RCP competitiveness. There is potential material cost saving of over 30% of steel based on CSA A257 (CSA A257-14, 2014) and ASTM C76 (ASTM C76-16, 2016) design standards. Since there is no previous research on the behaviour of RCP with SE cage reinforcement, the main scope of the present thesis is to investigate the structural behaviour of RCP with single elliptical cage reinforcement in order to introduce its application into the industry.

1.3 Original Contributions

This research investigates the applicability of RCP with SE cage reinforcement as an alternative to the conventional DC cage reinforcement used in mid-sized diameter pipes. Accordingly, a knowledge gap is filled concerning the structural performance of RCP with SE cage reinforcement. Specific original contributions include:

1. Investigating the manufacturing process of elliptical steel cage reinforcement. Findings outlined the challenges and modifications undergone in order to manufacture elliptical reinforcing steel cages.
2. Studying the structural performance of RCP with SE cage reinforcement under the three-edge bearing test. The study compared the performance of SE RCP with that of RCP reinforced with conventional steel double cage in order to assess applicability of SE pipe to the RCP industry.
3. Developing a finite element model for RCP with SE cage reinforcement to assess the load capacity of the pipe. The model evaluated the effect of SE cage rotation manufacturing or installation process and assessed the effect of the cage rotation on the structural capacity of the pipe.

1.4 Thesis Structure

The following thesis has been structured according to the integrated-article format following the guidelines and regulations of the School of Graduate and Postdoctoral Studies (SGPS) at Western University. The thesis consists of five chapters covering the

scope and objectives of the study; to assess the structural performance of RCP with SE cage reinforcement.

Chapter 1 is an introductory chapter which provides the background of the topic and an insight into the research needs, research objectives, and the original contributions of the research.

Chapter 2 provides an overview of the precast concrete pipe industry including: standards and specifications that regulate the RCP industry, testing methods, manufacturing process of RCP, and design process of RCP. Furthermore, an overview of previous research on RCP with conventional double cage reinforcement is presented.

Chapter 3 presents an experimental study on full-scale precast concrete pipe with SE cage reinforcement under the three-edge bearing test. The elastic and plastic performance of the pipe in addition to the failure mechanisms are investigated in order to evaluate the effect of the elimination the outer layer of reinforcement in the DC cage configuration. Furthermore, the manufacturing process of the elliptical cage is also investigated in the chapter.

Chapter 4 presents the development of a finite element model of RCP with single elliptical cage reinforcement. The model explores the effect of the mis-orientation of the SE cage on the structural capacity of the pipe. Furthermore, the model investigates the effect of the non-symmetrical shape of the SE cage and associated serviceability performance.

Finally, chapter 5 summarizes the research outcomes and conclusions, along with providing recommendations for future research.

1.5 References

Abolmaali, A., Mikhaylova, A., Wilson, A., & Lundy, J. (2012). Performance of steel fiber–reinforced concrete pipes. *Transportation Research Record: Journal of the Transportation Research Board*, *2313*(1), 168–177. https://doi.org/10.3141/2313-18

American Concrete Pipe Association. (2020). *Brief History of the ACPA*. http://www.concretepipe.org/about-us/

armtec, a Division of WGI. (n.d.). *BOSS 3000®SRPE Pipe, Large diameter steel reinforced polyethylene pipe.* (p. 8).

ASTM C76-16. (2016). *Specification for Reinforced Concrete Culvert, Storm Drain, and Sewer Pipe*. ASTM International. https://doi.org/10.1520/C0076-16

CSA A257-14. (2014). *Standards for Concrete Pipe and Manhole Sections*. CSA Group.

Figueiredo, A., de la Fuente, A., Molins, C., & Aguado, A. (2012). *A New Approach on Crushing Strength Test for Fibre Reinforced Concrete Pipes*. 1082–1095.

Haktanir, T., Ari, K., Altun, F., & Karahan, O. (2007). A comparative experimental investigation of concrete, reinforced-concrete and steel-fibre concrete pipes under three-edge-bearing test. *Construction and Building Materials*, *21*(8), 1702–1708. https://doi.org/10.1016/j.conbuildmat.2006.05.031

KWH PIPE. (n.d.). *Flexible Pipe vs. Rigid Pipe* (p. 6).

Masterson, R. (2017). *Concrete Pipe & Block Manufacturing in Canada*. IBISWorld, Industry Report 32733CA.

Mohamed, N., Soliman, A. M., & Nehdi, M. L. (2015). Mechanical performance of full-scale precast steel fibre-reinforced concrete pipes. *Engineering Structures*, *84*, 287–299. https://doi.org/10.1016/j.engstruct.2014.11.033

Park, Y., Abolmaali, A., Beakley, J., & Attiogbe, E. (2015). Thin-walled flexible concrete pipes with synthetic fibers and reduced traditional steel cage. *Engineering Structures*, *100*, 731–741. https://doi.org/10.1016/j.engstruct.2015.06.049

Wong, L. S. (2016). *Full Scale Manufacturing of Steel Fibre Reinforced Concrete Pipe*. 2016 Annual Conference of the Canadian Society for Civil Engineering, London, Ontario.

Chapter 2

2 Literature Review

2.1 Introduction

RCP design and acceptance criteria are dictated by international standards that specify requirements such as the reinforcement area, structural load test, and hydrostatic performance. Wong and Nehdi provide an in-depth critical analysis of the requirements of international standards representing a quarter of the world's population (L. Wong & M.L. Nehdi, 2018). For the purpose of this thesis, the study will focus on the North American standards CSA A257 (CSA A257-14, 2014) and ASTM C76 (ASTM C76-16, 2016). The three-edge bearing test (TEBT) is the main structural load test acceptance criteria for RCP, and forms one of four acceptance criteria for RCP in Canada. Other acceptance criteria include absorption test, hydrostatic test, and visual inspection.

As mentioned earlier, CSA A257 and ASTM C76 provide requirements for steel reinforcement area for RCP. Up to three reinforcing steel cages are used by manufacturers to satisfy design requirements. **Figure 2.1** shows the cross-sections of three conventional reinforcing configurations in RCP design. Single layer cage is common in smaller diameter RCP (typically less than 900 mm). Double layer cages are common in mid-size diameter pipes ranging between 600 mm to 1800 mm or larger diameter up to 2400 mm pipes with lower class. Triple layer cages with an elliptical layer supplementing the double circular cages are common for large diameter and higher-class RCP. The shaded areas in **Figure 2.1** outline the tension zone under three-edge bearing load where reinforcement is needed for structural considerations.

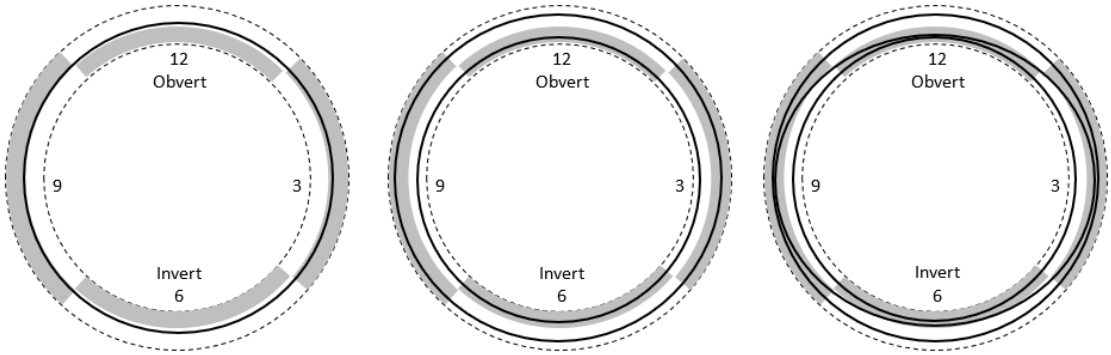

Figure 2.1-Typical Reinforcing Steel Cage for RCP (Left) Single Cage, (Mid) Double Cage, and (Right) Triple Cage.

The following chapter provides an insight into the structural load test for RCP, manufacturing process of RCP, design methods for RCP, and previous studies on RCP with different reinforcements.

2.2 Reinforced Concrete Pipe Testing Standard

The structural load capacity of RCP is assessed according to its design crack load and the ultimate load. The design crack load is determined by a threshold crack measurement where a 0.3 mm (0.01 inch) wide and 300 mm (12 inches) long crack is produced during the TEBT. The ultimate load is defined as the maximum applied load the pipe can withstand. According to the testing procedure outlined in CSA A257.0 Section 4, the crack is measured manually during the test by visual observation using a 0.3-mm thick leaf gauge (**Figure 2.2**).

Figure 2.2-Leaf Gauge Measuring 0.3 mm Crack.

The test is destructive applying a concentrated load via a hydraulic loading beam along the crown of the pipe and two rubber bearing strips support at the invert along the full length of the pipe barrel (**Figure 2.3**). The distance between the two lower bearing strips is a function of the internal diameter of the pipe. The minimum allowable distance between the lower two rubber bearing strips is 25 mm. It is essential for the testing machine to be rigid such that the load can be applied without a deflection greater than 1/720 of the pipe length. The load is applied at a load rate of 7 to 37 kN/min/m until formation of crack that meets the limit stated in the standard (CSA A257-14, 2014). TEBT according to ASTM C497 is similar to CSA A257 but with higher load rate up to 109.4 kN/min/m before reaching 75% of the design crack load. The pipe sample is then loaded at a slower rate of 43.8 kN/min/m until the 0.01-inch crack limit is reached (ASTM C469 / C469M-14, 2014). The actual 0.3-mm or 0.01-inch crack load collected from the test is then normalized to Newton per meter length per millimeter internal diameter, referred as $D_{0.3}$, or pound per foot length per foot internal diameter $D_{0.01}$ in the US, respectively. The ultimate load that the pipe can withstand is also normalized and referred to as D_{ult}. The pipe is required to exceed the ultimate load of its design class in order to pass the TEBT. The required crack load and ultimate load for each class of pipe are listed in **Table 2.1**.

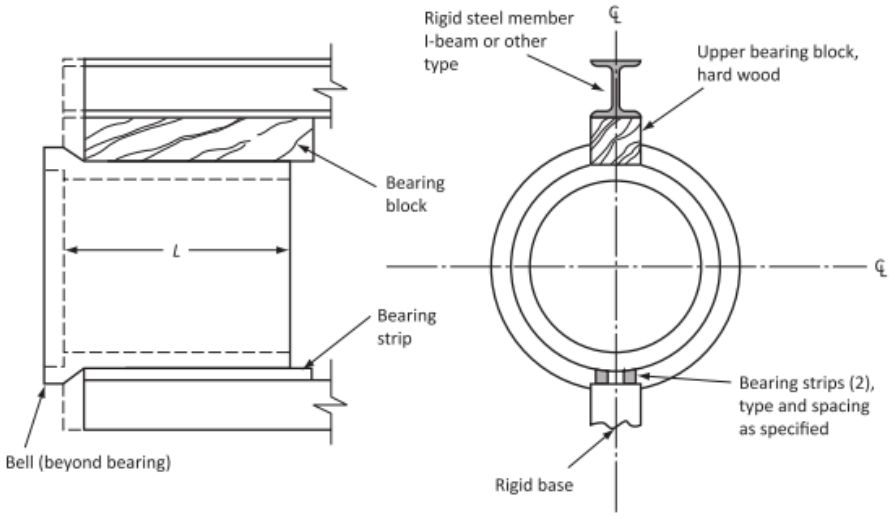

Figure 2.3-Standard TEBT Setup (CSA A257.2-14).

Table 2.1-Required Crack Load and Ultimate Load for each Class of Pipe in Canada and US

Canada (CSA A257.2) – N/m/mm				US (ASTM C76) – lb/ft/ft			
Class	**Design crack load D0.3**	**Design Ultimate Load Dult**	**Safety Factor Dult/D0.3**	**Class**	**Design crack load D0.01**	**Design Ultimate Load Dult**	**Safety Factor Dult/ D0.01**
				I	800	1200	1.5
50D	50	75	1.5	**II**	1000	1500	1.5
65D	65	97.5	1.5	**III**	1350	2000	1.5
100D	100	150	1.5	**IV**	2000	3000	1.5
140D	140	175	1.25	**V**	3000	3750	1.25

2.3 Reinforced Concrete Pipe Fabrication

Typical manufacturing of RCP commences with the fabrication of the reinforcing steel cage. The commonly used steel reinforcement is deformed cold-drawn wires conforming to ASTM A1064 (ASTM A1064/A1064M-18a, 2018). The wire is continuously and helically rapped and fusion-welded around several longitudinal wires along the axis of the pipe. The fabrication process is computer controlled and fully automated using welding machines, as shown in **Figure 2.4**.

Figure 2.4-Cage Welding Machine.

Figure 2.5 shows a typical steel cage ready to be used for RCP production. The cage is staged on the metal pallet that forms the bell (female) end of the pipe. The fully automated pipe making system feeds the pallet with the cage into the core and jacket of the mould. The cage is then anchored into position by several retractable knifes from the jacket of the mould, before a dry cast mix concrete is placed. Concrete is introduced from a hopper and fed into the mould at a computer-controlled rate, followed by consolidation through intense vibration. After pressing the metal header that forms the spigot (male-end) of the pipe, the pipe is then removed from the mould. After the heavy vibration process, the zero-slump concrete can maintain the shape of the pipe without additional support. The pipe is then carefully moved by a crane into an accelerated steam curing chamber, which has an integrated system that inputs a specific curing profile of heat and moisture usually for 8 to 10 hours. CSA A257 permits a maximum curing temperature of 70°C. After curing, the metal pallet and header are removed from the hardened pipe. The pipe is then rotated in its final horizontal position for marking, final inspection and storage. The entire manufacturing cycle is fully automated and controlled (L. S. Wong, 2016).

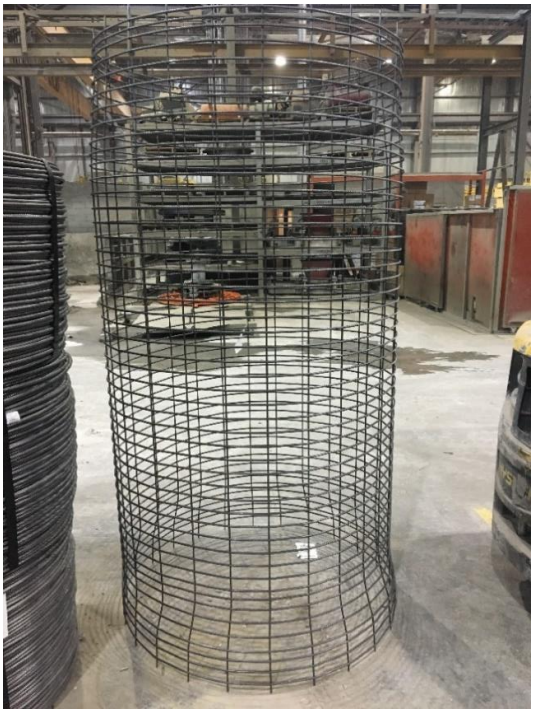

Figure 2.5-Welded Reinforcing Steel Cage for RCP.

2.4 Reinforced Concrete Pipe Concrete Mixture

As mentioned earlier, zero-slump concrete is commonly used in the production of RCP to achieve high early strength and allow the pipe to support its own weight once the mould is removed. Zero-slump concrete, also known as negative slump concrete, is concrete that has a slump of between zero to 25 mm (Arnold et al., n.d.). ACI 211.3R-02 specifies the water to cement ratio used for zero-slump concrete, which is influenced by various factors including particle shape and grading of the aggregates, air content and temperature of the concrete, effectiveness of mixing, addition of chemical admixtures, and the method of consolidation. Supplementary cementitious materials (SCM), such as natural pozzolans, fly ash, ground granulated-blast-furnace-slag, and silica fumes can be added to the concrete mixture. The addition of SCM can decrease cracking and permeability, which protects the pipe from chemical attacks. Both fine and coarse aggregates may be used in zero-slump concrete, however, having a higher ratio of fine to coarse aggregates increases the workability of the mixture. The maximum recommended nominal aggregate size is 19 mm for no-slump concrete (Arnold et al., n.d.).

2.5 Reinforced Concrete Pipe Design

2.5.1 General

TEBT establishes the structural load capacity of the pipe by applying a concentrated load along the crown of the pipe. In practical applications, however, the load distribution is far more distributed over the circumference of the pipe under buried conditions. Once buried, the concrete pipe is part of a composite system comprising the pipe and surrounding soil envelope that interact together and contribute the structural behaviour of the system (American Society of Civil Engineers, 15-98). There are two approaches that are widely used and accepted for the design of RCP; direct design and indirect design. The direct design considers the effect of the interaction between the pipe and soil envelope to determine the loads, pressure distributions, moments, and shear after which the required reinforcement to resist the load is calculated, while the indirect design adopts a more empirical approach.

2.5.2 Construction of Reinforced Concrete Pipe

The earth pressure distribution along the walls of the pipe is dependant on the construction method adopted. Four common construction methods exist: trench construction, positive embankment construction, negative embankment construction, and jacking construction. In the trench construction methods, the pipe is installed in a narrow trench, which is excavated in the undisturbed soil, and then covered with backfill soil extending to the natural ground surface. In the positive embankment construction method, the pipe is installed on the original ground surface, or compacted fill, after which the pipe is covered by backfill or embankment. In the negative embankment construction method, the pipe is installed in a shallow trench of such depth that the top of the pipe is below the natural ground surface, or compacted fill, after which the pipe is covered by backfill or embankment, which extends beyond the natural ground surface. Finally, jacking construction is used when it is difficult to apply excavation and backfill methods, thus the pipe is advanced horizontally underground (American Concrete Pipe Association, 2011).

The pipe experiences the most critical load case in the positive embankment construction method. In the trench construction method, the weight of the backfill is resisted by both the pipe and the frictional forces along the walls of the trench, as established by Anson Marston in 1910. As the trench becomes wider, the frictional forces are offset by an increase in the weight of the backfill. The embankment condition is reached if the trench walls become too far away from the pipe. The further the walls are from the pipe, the less support the pipe has in resisting the weight of the backfill, thus increasing the vertical loads resisted by the pipe. The transition width is the width of trench at a certain depth where the trench load is equal to the embankment load. A pipe should be designed as an embankment construction type for a width greater than the transition width (American Concrete Pipe Association, 2007).

2.5.3 Background

A research project at Iowa State University in the late 1920’s was conducted based Anson Marston’s theories on earth loads with the objective of determining the supporting strength of a buried rigid pipe. The findings were later published by Spangler in 1933, introducing

the term bedding factor to relate the supporting strength of a buried pipe to the strength obtained from more severe TEBT. Spangler concluded that the bedding factor is dependant on the width and quality of contact between the pipe and bedding, in addition to the magnitude and vertical height of the lateral pressure acting on the buried pipe. Furthermore, Spangler determined four standard bedding types used in field installations (A, B, C, and D). The bedding is the soil which is positioned underneath the pipe with the role of distributing the vertical forces around the lower exterior surface of the pipe, thus reducing the stresses in the pipe wall. Marston and Spangler's research forms the basis of the indirect design method for RCP (American Concrete Pipe Association, 2011).

2.5.4 Standard Installation

Advancements in theories of soil mechanics as well as structural design have led to improvements in the design of RCP. The improvements came in the form of a research program initiated by the American Concrete Pipe Association (ACPA) in 1970 to understand the interaction between the buried concrete pipe and soil envelope. The ACPA introduced four new standard installations and the Heger earth pressure distribution along with the direct design method. These were incorporated into the ASCE standards "Standards Practice for Direct Design of Buried Precast Concrete Pipe Using Standards Installations (SIDD)" (American Society of Civil Engineers, 15-98). The standard installations (beddings) were incorporated into the indirect design method, replacing the historical A, B, C, D beddings established by Marston and Spangler and thus presenting a state-of-the-art method for the determination of the bedding factor.

The four standard installations provide an optimum range of soil-pipe interaction conditions. Each standard installation type identifies the bedding thickness as a function of the outer diameter of the pipe. Furthermore, the compaction level and quality of the soil envelope according to USCS and AASHTO soil classification is defined for each type as shown in **Table 2.2** and **Table 2.3** (American Concrete Pipe Association, 2011)**.**

Table 2.2-Standard Installations Soil and Minimum Compaction Requirements

Installation Type	Bedding Thickness	Haunch and Outer Bedding	Lower Side
Type 1	D_o/24 minimum, not less than 75 mm (3”). If rock foundation, use D_o/12 minimum, not less than 150 mm (6”).	95% Category l	90% Category l, 95% Category ll, or 100% Category lll
Type 2	D_o/24 minimum, not less than 75mm (3”). If rock foundation, use D_o/12 minimum, not less than 150mm (6”).	90% Category l or 95% Category ll	85% Category l, 90% Category ll, or 95% Category lll
Type 3	D_o/24 minimum, not less than 75mm (3”). If rock foundation, use D_o/12 minimum, not less than 150mm (6”).	85% Category l, 90% Category ll, or 95% Category lll	85% Category l, 90% Category ll, or 95% Category lll
Type 4	No bedding required, except, if rock foundation, use D_o/12 minimum, not less than 150mm (6”).	No compaction required, except if Category lll, use 85% Category lll	No compaction required, except if Category lll, use 85% Category lll

Table 2.3-USCS and AASHTO Soil Classifications

	Representative Soil Type		Percent Compaction	
SIDD Soil	**USCS**	**Standard AASHTO**	**Standard Proctor**	**Modified Proctor**
Gravelly Sand (Category l)	SW, SP, GW, GP	A1, A3	100	95
			95	90
			90	85
			85	80
			80	75
			61	59
Sandy Silt (Category ll)	GM, SM, ML, Also GC, SC with less than 20% passing #200 sieve	A2, A4	100	95
			95	90
			90	85
			85	80
			80	75
			49	46
Silty Clay (Category lll)	CL. MH, GC, SC	A5, A6	100	90
			95	85
			90	80
			85	75
			80	70
			45	45

Type 1 is the most rigorous in terms of quality requirements, thus, a pipe with lower load capacity can be used. Conversely, Type 4 is the most lenient in terms of quality requirements, and thus requires a higher strength pipe for the same depth of installation. The choice of installation type depends on the quality of the construction and anticipated inspection. **Figures 2.6** and **2.7** display standard pipe terminology and a buried pipe in trench/embankment condition respectively.

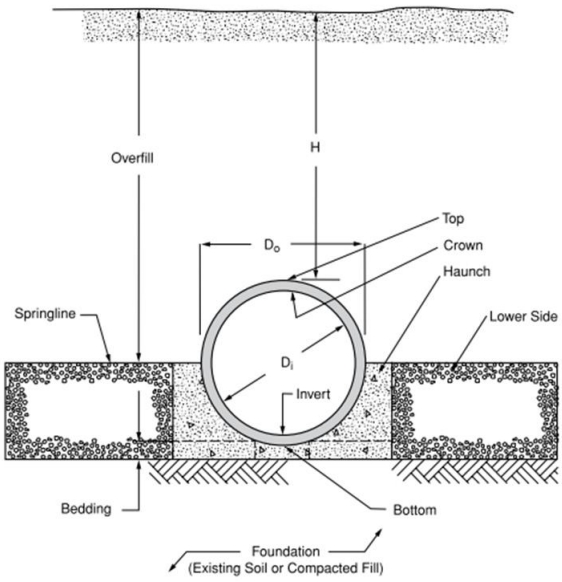

Figure 2.6-Standard Pipe Terminology (ACPA, 2011).

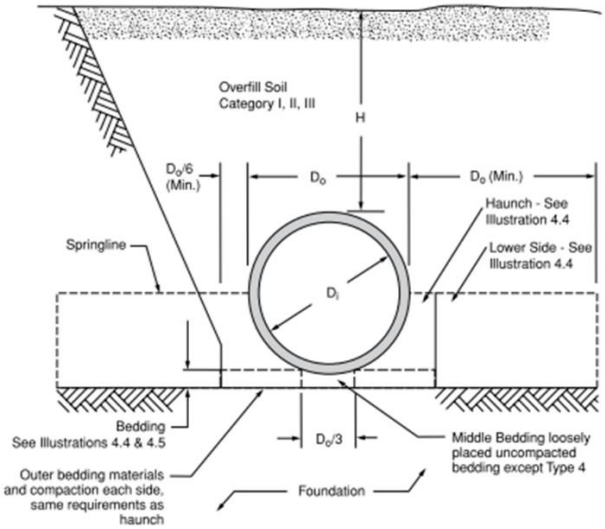

Figure 2.7-Standard Trench/Embankment Installations (ACPA 2011).

2.6 Indirect Design Method

In the indirect design method, the required supporting strength of the pipe is dependant on total load calculated, the bedding factor, and the factor of safety applied (Erdogmus et al., 2010). The D_{ult} load obtained can be validated through the TEBT load, which is the ratio of the total load to the bedding factor. Setting the factor of safety to 1.0 yields the $D_{0.3}$. With the wall thickness and internal diameter of the pipe known, the required area of steel can be determined using the design Tables in CSA A257.2 and ASTM C76.

The ACPA design manual outlines a six-step procedure for the indirect design of RCP (American Concrete Pipe Association, 2011):

1. Determination of the geometric requirements of the pipe
2. Determination of the earth and live load acting on the pipe
3. Selection of standard installation type
4. Determination of bedding factor
5. Application of factor of safety
6. Selection of pipe strength

Determining the diameter of the pipe requires the calculation of the design flow. The slope and pipe roughness coefficient are then determined to solve Mannings formula and compute the pipe diameter. The wall thickness of the pipe is a function of the internal diameter of the pipe. Standards specify the minimum designated wall thickness and the wall thickness for each diameter of pipe.

2.6.1 Determination of Earth Load

The results of the ACPA research program established the Heger earth pressure distribution for each standard installation type. The pressure distribution on the pipe due to the earth load was different from the theories developed by Marston and Spangler. As mentioned, the construction method has a significant effect on the distribution of earth pressures

resisted by the rigid pipe. In the positive embankment construction method, the soil along the side of the pipe will settle more than the soil above the rigid pipe structure, thus imposing an additional load to the prism of soil directly above the pipe. The additional load is accounted for by applying a ratio known as the Vertical Arching Factor (VAF) for each standard installation type. VAF is the ratio of the vertical load on the pipe to the weight of the prism of earth directly above the outside diameter of the pipe (Erdogmus et al., 2010). The VAF is then multiplied by the PL to yield the total earth load on the pipe in Newton per meter as shown in **Eq. (2.1).**

$$W_e = VAF \times PL \qquad \textbf{Eq. (2.1)}$$

where: $PL = w\left[H + \left(\frac{D_o(4-\pi)}{8000}\right)\right]\frac{D_o}{1000}$; w=soil unit weight (N/m^3); H=height of fill (m); and D_o=outside diameter of pipe (mm).

The VAF for a trench condition is less that that of an embankment condition since frictional forces will resist a portion of the earth load in trench condition. The earth load on a pipe in the trench condition can be computed using **Eq. (2.2).**

$$W_d = \frac{(C_d w {B_d}^2)}{1000} * \left(\frac{D_o(4-\pi)}{8000}\right) w \qquad \textbf{Eq. (2.2)}$$

where: $C_d = \frac{1-e^{-2Ku\prime\frac{H}{B_d}}}{2Ku\prime}$; C_d =trench load coefficient; B_d =width of trench (m); K=ratio of active lateral unit pressure to vertical unit pressure; u'= tan θ, coefficient of friction between fill material and sides of trench.

2.6.2 Fluid Load and Determination of Live Load

There is no data on pipe failure as a result of neglecting the effect of the fluid load, W_L. Typically, the fluid weight is about the same order of magnitude as the pipe weight. Hence, the fluid weight only represents a significant portion of the total design load for large diameter pipe under shallow fill. The AASHTO Standard Specifications for Highway Bridges states that unless specified, the design fluid weight shall be 1000 kg/m^3.

The AASHTO Standard Specifications for Highway Bridges also specify the design live load needed to determine the supporting strength of the pipe. The live load is dependent on the use of flexible or rigid pavement. Consequently, live loads such as highway truck loads, airport, and railroads can be calculated. Furthermore, construction loads might be considered in a situation where heavy construction equipment travels over the pipe (American Concrete Pipe Association, 2011).

2.6.3 Determination of Bedding Factor

The type of standard installation chosen affects the distribution of the reaction of the pipe to the vertical loads, subsequently affecting the bedding factor. The ACPA research program determined the bedding factors for a range of pipe diameters with different buried depths for both embankment and trench construction methods. The studies showed that the variations for bedding factors were negligible for different wall thicknesses and for different concrete covers. **Table 2.4** shows the bedding factors for embankment condition for different pipe diameters. Bedding factors for pipe diameters other than those listed may be interpolated.

Table 2.4 Bedding Factors for Embankment Conditions (B_{fe})

Pipe Diameter (mm)	Standard Installations			
	Type 1	Type 2	Type 3	Type 4
300	4.4	3.2	2.5	1.7
600	4.2	3.0	2.4	1.7
900	4.0	2.9	2.3	1.7
1800	3.8	2.8	2.2	1.7
3600	3.6	2.8	2.2	1.7

The bedding factors for a trench condition are constant for all pipe diameters for condition of zero vertical load acting on pipe. These bedding factors, shown in **Table 2.5**, are known as minimum bedding factors, B_{f0}, and exist at the interface of the pipe wall and soil. As the trench width increases, the bedding factor becomes variable for different standard installation types.

Table 2.5-Trench Minimum Bedding Factors

Standard Installations	Minimum Bedding Factor, B_{f0}
300	4.4
600	4.2
900	4.0
1800	3.8

Eq. (2.3) shows the variable bedding factor, B_{fv}, for trench conditions. Moreover, a schematic of the variable bedding factor description is shown in **Figure 2.8**.

$$B_{fv} = \frac{[B_{fe} - B_{fo}][B_d - B_c]}{[B_{dt} - B_c]} + B_{fo} \qquad \textbf{Eq. (2.3)}$$

where: B_c=outside horizontal span of pipe (m); B_d=trench width at top of pipe (m); B_{dt}=transition width at top of pipe (m); B_{fe}=bedding factor, embankment; B_{f0}=minimum bedding factor, trench; and B_{fv}=variable bedding factor, trench.

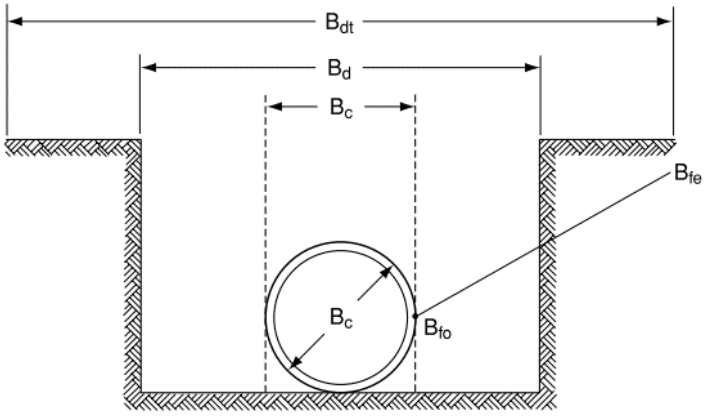

Figure 2.8-Variable Bedding Factors (ACPA, 2011).

The final steps of the indirect design method are the application of the Factor of Safety (F.S.) as per ASTM C76 and CSA A257.2, and the selection of the pipe strength through the calculation of the three-edge bearing strength of RCP, which is expressed in ultimate D-load in **Eq. (2.4):**

$$D - load = \left[\frac{W_e}{B_f} + \frac{W_L}{B_{fLL}}\right]\frac{F.S.}{D} \qquad \textbf{Eq. (2.4)}$$

where B_{fLL} is the live load bedding factor, with values ranging between 2.2 and 1.1 for different depth and pipe diameter (American Concrete Pipe Association, 2011).

2.7 Direct Design

The supporting strength of a pipe in the direct design method is dependent on the determination of moments, thrusts, and shears in the critical sections of the pipe due to the applied loads. Similar to the indirect design method, the direct design method involves the initial determination of the geometric requirements of the pipe. Subsequently, the earth and live load acting on the pipe should be determined as well as the choice of the standard installation type. The direct design method is based on limit state design, with the structural behaviour of the pipe governed by one of the following areas:

1. Flexural Strength
2. Radial Tension
3. Shear (Diagonal Tension)
4. Crack Control

Eqs. (2.5), (2.6), and **(2.7)** are used to calculate the moments (M_i), axial thrusts (N_i), and shear forces (V_i) in the pipe:

$$M_i = C_{mi} W_i \frac{D_m}{2} \qquad \textbf{Eq. (2.5)}$$

$$N_i = C_{ni} W_i \qquad \textbf{Eq. (2.6)}$$

$$V_i = C_{vi} W_i \qquad \textbf{Eq. (2.7)}$$

W_i represents the total load acting on the pipe including earth and live load. C_{mi}, C_{ni}, and C_{vi} are coefficients that depend on the distribution of earth pressures and support reactions and are obtained from the ACPA research program computer analysis. D_m is the mean pipe diameter which is taken as 1 (F. J. Heger & McGrath, 1982).

After the straining actions have been determined, the area of reinforcement for both flexure and shear (ties and stirrups) can be calculated for flexure, radial tension, and diagonal tension ultimate strength, in addition to control of crack width at service load. ASCE standards "Standard Practice for Direct Design of Buried Precast Concrete Pipe Using Standard Installations (SIDD)" outlines the determination of required reinforcement are in more detail (American Society of Civil Engineers, 15-98).

2.8 Previous Research on Reinforced Concrete Pipe

The performance of RCP with conventional DC reinforcement using TEBT was first established by Frank Heger in the 1960s. He evaluated the cracking behaviour, deflection, and ultimate strength of circular concrete pipes under TEBT loading. His study examined the experimental results of various test programs to evaluate the strength and cracking of pipes (F. Heger, 1963). A semi-empirical equation **Eq. (2.8)** was developed to estimate $D_{0.3}$ of a pipe with the pipe size between 1200 mm and 2700 mm and longitudinal wire spacing between 100 mm and 200 mm (F. Heger, 1963). All parameters are in imperial units.

$$(DL)_{0.01} = \frac{(1.15\times10^5)A_{s1}d}{l_o D_i^2} + \frac{0.3 l_o h d\sqrt{f_c'}}{\varphi D_i^2} - \frac{0.72W}{D_i} \qquad \textbf{Eq. (2.8)}$$

where: $(DL)_{0.01}$ = imperial equivalent to $D_{0.3}$ (lb/in^2.); A_{s1} = steel area of inner reinforcement (in^2/ft of length); D_i = inside diameter of pipe (ft); l_o = spacing of longitudinal wires (in.); h = pipe wall thickness (in.); d = depth of the section from extreme compressive fibre to center of tensile reinforcement (in.); φ = diameter of reinforcing wire (in.); fc' = ultimate compressive strength of concrete (psi); and W = weight of the pipe (lb/ft of length).

Furthermore, the flexural ultimate three edge bearing capacity of a circular pipe which has two circular reinforcing cages with outer reinforcement area that is three quarter of the inner cage reinforcement was estimated in **Eq. (2.9)** (F. Heger, 1963)**.**

$$(DL)_u = \frac{7.3M_{p1}}{D_i^2} - \frac{0.5W}{D_i} \qquad \textbf{Eq. (2.9)}$$

where: $M_{p1} = f_s' A_{s1}(d - 0.5a)\left(\frac{1}{12}\right)$ft-lb; and $a = 0.1\frac{f_s' A_{s1}}{f_c'}$; $(DL)_u$ = imperial equivalent to D_{ult} (lb/ft^2); M_{p1} = ultimate bending moment at crown and invert (lb-ft per ft of length); W = weight of the pipe (lb per ft of length); D_i = inside diameter of pipe (ft); d = depth of the section from extreme compressive fibre to center of tensile reinforcement (in.); a= depth of equivalent rectangular stress block at ultimate strength of concrete section (in.); f_s' = ultimate tensile strength of reinforcement (psi); fc' = ultimate compressive strength of concrete (psi); and A_{s1} = steel area of inner reinforcement (in^2/ft of length).

The flexural rigidity of a reinforced concrete flexural section depends on the extent of cracking in the section. Heger specifies that when examining the flexural rigidity of a RCP with two circular cages, the small influence of the second reinforcing steel cage acting as compression steel is neglected, arguing that the cage is situated close to the neutral axis in typical RCP and thus has little influence on the short-time flexural properties (i.e. 0.3-mm crack load) of the section (F. Heger, 1963).

In several recent studies, advanced techniques to monitor the deformation of RCP using Linear Variable Inductive Transducers (LVITs) were reported. Mohamed *et, al.* (Mohamed et al., 2014) investigated the mechanical properties of dry-cast steel fibre-reinforced concrete using LVITs. The vertical deflection of the crown towards the invert at the pipe spigot against the applied load was measured using LVITs positioned against the inner surface of the pipe crown and attached to supports at the bottom end of the pipe. An additional LVIT was used to measure the horizontal deflection of the spring-lines in order to evaluate the mechanical performance of full-scale buried precast fibre-reinforced concrete pipes (Silva et al., 2018).

Various other studies used displacement sensing technology in different configurations to measure the vertical and horizontal deflections of the pipe versus the load. For instance, Abolmaali *et, al.* (Abolmaali et al., 2012) considered the deflection at the spigot end of the pipe. Silva *et, al.* (Silva et al., 2018) studied the displacement of the pipe versus loading to evaluate the performance of ogee-joint pipes and spigot pocket pipes with both single cage reinforcement and double cage reinforcement. LVITs were installed at the bell, midsection, and spigot of the pipe at the inverts, crowns, and spring-lines to capture the complete

displacement of the pipe under loading. LVITs provided reliable and accurate monitoring of pipe deformation during the tests, and therefore it was decided to adopt it in the present study.

2.9 Summary

This chapter presents an in-depth review of RCP standards, testing methods, fabrication and design methods. Furthermore, studies on the structural behaviour of RCP in addition to previous experimental and numerical studies on RCP were presented.

Limited research is available in the open literature to validate the performance of RCP with single elliptical cage reinforcement, which discourages its use in the industry despite the potential for substantial cost savings. The subsequent chapters of the thesis aim at bridging the knowledge gap of the structural performance of the RCP with SE cage reinforcement and increase RCP competitiveness in the industry. An extensive experimental study was performed in order to assess the structural performance of precast concrete pipe with SE cage reinforcement. The pipes were tested following CSA A257 standards under the TEBT and were assessed based on their serviceability performance, vertical deflections, cracking patterns, and failure modes at ultimate load. The experimental data was then used to calibrate and validate a finite element model of RCP with SE cage under the TEBT. The model was used to assess the rotation of the SE cage reinforcement on the structural capacity of the pipe.

2.10 References

Abolmaali, A., Mikhaylova, A., Wilson, A., & Lundy, J. (2012). Performance of steel fiber–reinforced concrete pipes. *Transportation Research Record: Journal of the Transportation Research Board*, *2313*(1), 168–177. https://doi.org/10.3141/2313-18

American Concrete Pipe Association. (2007). *Concrete Pipe and Box Culvert Installation* (No. 01–103).

American Concrete Pipe Association. (2011). *Concrete Pipe Design Manual* (Library of Congress catalog number 78-58624).

American Society of Civil Engineers. (15-98). *Standard Practice for Direct Design of Buried Precast Concrete Pipe Using Standard Installations (SIDD)*.

Arnold, T. E., Barringer, W. L., Basheer, M. P., Bognacki, C., Brenno, G. L., Brown, M. L., Carrasquillo, R. L., Cook, J. E., Cook, J. F., Cook, R. A., Crocker, D. A., Daniel, D. G., Boyle, M. J., de Larrard, F., Dixon, D. E., Dodl, C. L., Elliot, D. F., Gardner, M. R., Guthrie, J. T., … Wing, R. M. (n.d.). *Guide for Selecting Proportions for No-Slump Concrete*. 26.

ASTM A1064/A1064M-18a. (2018). *Specification for Carbon-Steel Wire and Welded Wire Reinforcement, Plain and Deformed, for Concrete*. ASTM International. https://doi.org/10.1520/A1064_A1064M-18A

ASTM C76-16. (2016). *Specification for Reinforced Concrete Culvert, Storm Drain, and Sewer Pipe*. ASTM International. https://doi.org/10.1520/C0076-16

ASTM C469 / C469M-14. (2014). *Standard Test Method for Static Modulus of Elasticity and Poisson's Ratio of Concrete in Compression*. ASTM International.

CSA A257-14. (2014). *Standards for Concrete Pipe and Manhole Sections*. CSA Group.

Erdogmus, E., Skourup, B. N., & Tadros, M. (2010). Recommendations for Design of Reinforced Concrete Pipe. *Journal of Pipeline Systems Engineering and Practice*, *1*(1), 25–32. https://doi.org/10.1061/(ASCE)PS.1949-1204.0000039

Heger, F. (1963). Structural Behavior of Circular Reinforced Concrete Pipe-Development of Theory. *ACI Journal Proceedings*, *60*(11). https://doi.org/10.14359/7905

Heger, F. J., & McGrath, T. J. (1982). *Design Method for Reinforced Concrete Pipe and Box Sections*. Simpson Gumpertz & Heger. https://books.google.ca/books?id=CSoonQEACAAJ

Mohamed, N., Soliman, A. M., & Nehdi, M. L. (2014). Full-scale pipes using dry-cast steel fibre-reinforced concrete. *Construction and Building Materials*, *72*, 411–422. https://doi.org/10.1016/j.conbuildmat.2014.09.025

Silva, J. L. da, El Debs, M. K., & Kataoka, M. N. (2018). A comparative experimental investigation of reinforced-concrete pipes under three-edge-bearing test: Spigot and Pocket and Ogee Joint pipes. *Acta Scientiarum. Technology*, *40*(1), 30860. https://doi.org/10.4025/actascitechnol.v40i1.30860

Wong, L., & Nehdi, M. (2018). Critical Analysis of International Precast Concrete Pipe Standards. *Infrastructures*, *3*(3), 18. https://doi.org/10.3390/infrastructures3030018

Wong, L. S. (2016). *Full Scale Manufacturing of Steel Fibre Reinforced Concrete Pipe*. 2016 Annual Conference of the Canadian Society for Civil Engineering, London, Ontario.

Chapter 3

3 Investigation of Structural Behaviour of Precast Concrete Pipe with Single Elliptical Steel Cage Reinforcement

3.1 Introduction

RCP with single elliptical (SE) cage reinforcement can offer an efficient and cost-effective design compared to conventional pipe with double cage (DC) configuration. Such savings result from positioning the SE cage in favorable tensile zones of the RCP cross-section when subjected to loading. Reinforcing steel located in the compression zone is structurally redundant, thus it is omitted in the SE cage design. The single elliptical cage design eliminates such redundancy by positioning the steel reinforcement on the tensile faces of the pipe to fulfill the tensile sectional capacity for flexure at the invert, obvert, and spring-line**.** The CSA A257.2 (CSA A257-14, 2014) and ASTM C76 (ASTM C76-16, 2016) standards require that the area of steel reinforcement be 10% more when SE reinforcement is used, in comparison to the inner reinforcement in a DC configuration (**Table 3.1)**. Theoretically, the structural performance of SE and DC design should be similar if the flexural strength governs the capacity of the RCP.

There is currently lack of research available to validate the structural behaviour of RCP with SE cage reinforcement, which discourages its use in the industry. Accordingly, this chapter aims to (a) explore the structural performance of RCP reinforced with single elliptical cage, (b) compare its performance with that of RCP reinforced with conventional steel double cage, and (c) assess the applicability of SE-RCP for the industry. Full-scale tests utilizing RCP pipes were conducted using a modified three-edge-bearing test. The test method and associated results are reported and critically analyzed in this chapter. Despite new technology allowing true elliptical shaped cage to be made, challenges of manufacturing full-scale SE-RCP were encountered in this chapter. The findings reveal the

need for updating the reinforcing steel requirement in CSA A257.2 and ASTM C76 for RCP with specific SE reinforcements.

Table 3.1-CSA A257.2 and ASTM C76 Reinforcement Design Requirements

CSA A257.2					
			Reinforcement Area (mm^2/m)		
Internal Diameter (mm)	**Design Class**	**Wall Thickness (mm)**	**Inner Cage**	**Outer Cage**	**Elliptical Cage**
1050	100D	133	420	252	470
	140D	133	760	456	850
1200	100D	127	890	534	990
	140D	127	1550	930	1710
ASTM C76					
			Reinforcement Area (mm^2/m)		
Internal Diameter (mm)	**Design Class**	**Wall Thickness (mm)**	**Inner Cage**	**Outer Cage**	**Elliptical Cage**
1050	IV	133	423	254	445
	V	133	762	445	847
1200	IV	127	889	508	995
	V	127	1545	931	1715

3.2 Experimental Program

3.2.1 Test Specimen Selection and Fabrication

Two pipe sizes with nominal inner diameters of 1050 mm and 1200 mm were selected based on the existing design of DC cage, which ranges from 975 mm to 1500 mm. The size of the cage reinforcement is also limited by the capability of the manufacturing machine. For comparison, similar size control pipes with double cage design were also produced and tested. All test pipes were 2.44 m in lay length with uniform outside diameter. The wall thickness of the 1050 mm and 1200 mm were 133 mm and 127 mm, respectively. The selected design classes are 100D and 140D according to CSA A257.2. A total of 24 full-scale RCP was manufactured, including 20 RCP with SE reinforcement and 4 with DC reinforcement. **Table 3.2** summarizes the experimental details, including the reinforcement configuration, inner area of steel, outer area of steel for DC pipes, compressive strength of

concrete at the time of test, yield strength of steel, and age of the pipe at the time of test (TEBT Reports are presented in **Appendix A**)

Table 3.2-Properties of Tested Reinforced Concrete Pipe Specimen

Nominal Pipe Diameter(mm)	Cage Config.	Pipe Reference	Design Class	*Asi* (mm^2/m)	*Aso* (mm^2/m)	f_c' (MPa)	f_y (MPa)	Age Tested (Days)
1050	SE	E08	100D	581		64.8	630	27
1050	SE	E21	100D	581		60.2	630	11
1050	SE	E23	100D	581		60.2	630	11
1050	SE	E24	140D	903		60.2	630	11
1050	SE	E25	140D	903		60.2	630	11
1050	SE	E26	140D	903		60.2	630	11
1200	SE	E02	100D	821		58.5	630	8
1200	SE	E09	100D	903		64.4	630	25
1200	SE	E10	100D	903		64.4	630	25
1200	SE	E11	100D	903		64.4	630	25
1200	SE	E12	100D	993		65.7	640	32
1200	SE	E13	100D	993		65.7	640	32
1200	SE	E14	100D	993		65.7	640	32
1200	SE	E18	100D	1290		60.6	640	12
1200	SE	E19	100D	1290		60.6	640	12
1200	SE	E20	100D	1290		60.6	640	12
1200	SE	E01	140D	1548		57.8	620	7
1200	SE	E15	140D	1936		59.1	620	9
1200	SE	E16	140D	1936		59.1	620	9
1200	SE	E17	140D	1936		59.1	620	9
1050	DC	T44	100D	581	290	60.2	630	11
1050	DC	T43	140D	1129	452	70.6	630	782
1200	DC	T23	100D	821	645	57.8	630	7
1200	DC	T22	140D	1548	645	57.0	620	6

Full-scale RCP were fabricated at a precast concrete plant located in Ontario, Canada. The concrete for all RCP specimens was a dry-cast mixture with a water-cement ratio of 0.38. High-early strength Portland cement and ground granulated blast furnace slag were used as binder. Gravel with maximum nominal size of 13 mm and natural sand with a fineness modulus of 2.82, respectively were used. Polycarboxylate superplasticizer was added at a rate of 0.16% by mass of cementitious materials. A dispersing admixture and non-ionic surfactant were added at a dosage of 0.20% by mass of cementitious material (Mohamed et al., 2015). The RCP specimens were fabricated and tested on separate days throughout the experimental program. Standard 100 mm x 200 mm cylinders were cast for 7, 28, and 120 days compressive strength measurement, in accordance with ASTM C39 (ASTM

C39/C39M − 16b, 2016). The cylinders were used to estimate the pipe compressive strength based on testing age. The primary reinforcement was made from deformed cold-drawn steel wires having yield strength ranging from 620 MPa to 640 MPa. The SE reinforcing cage consisted of 24 longitudinal steel wires with equal spacing, while the circular cage for DC reinforcement consisted of 12 longitudinal wires.

3.2.2 Elliptical Steel Cage Reinforcement Design and Fabrication

Figure 3.1 (Left) illustrates the orientation of SE reinforcement. The design of elliptical steel cage was to fulfill the sectional flexural tensile capacity at the obvert (12 o'clock) and invert (6 o'clock). Thus, the reinforcement was positioned in the tension (shaded) zone in **Figure 3.1** (Left). The vertical inner dimension of the cage is set to the sum of inner diameter of the pipe and two times of the required clear concrete cover. The horizontal outer dimension of the cage at the spring-line was set to the outer diameter of the pipe less two times of the clear cover. Under loading, the inside faces of the invert and obvert of the pipe in tension were shaded in grey, while the outside faces of the spring-lines are in tension. In the conventional DC reinforcement design illustrated in **Figure 3.1** (Right), the inner reinforcement at the spring-line and the outer reinforcement at the invert and obvert are in compression, therefore can be considered redundant. In the testing program, few tests such as 1050 mm 100D and 1200 mm 100D purposely had similar area of steel in its SE design as that of the steel of the inner cage in the DC cage design.

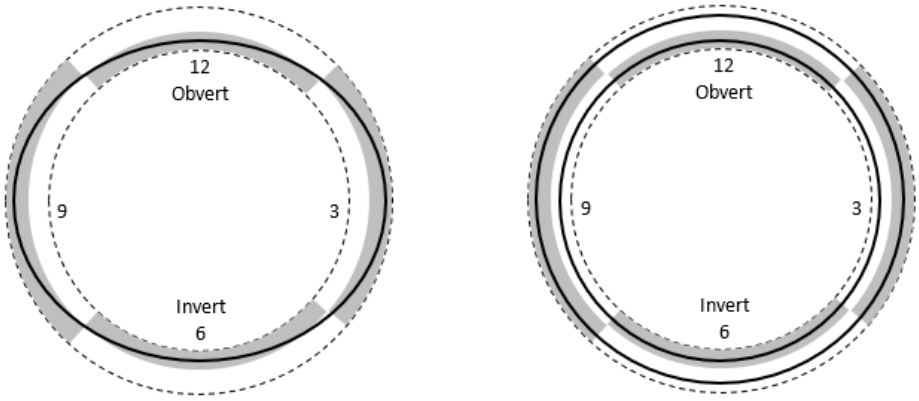

Figure 3.1-Single Elliptical (left), and Double Circular (right) Cage Orientation.

Ideally, true elliptical shape of the cage shall be maintained through the fabrication process along the pipe axis. However, the cage shape is required to transition into circular shape at the spigot and the bell of the pipe to accommodate the pipe joint profile, as illustrated in **Figure. 3.2**. The circular-elliptical-circular shape requires approximately 200 mm transition zones in between each shape due to the fabrication limitation. At the spigot end, the circular shape had the outside diameter equaling the minor outer dimension of the SE cage. At the bell end, the circular shape had the outside diameter equaling the major outer dimension of the SE cage. During the fabrication process at the transition zones, the spacing between the circumferential wires reduced by half to counter the effect of the induced stresses from the bending of the longitudinal wires. Thus, the section with the true elliptical shape was approximately 80% of the pipe length, which could affect the expected load capacity of the pipe.

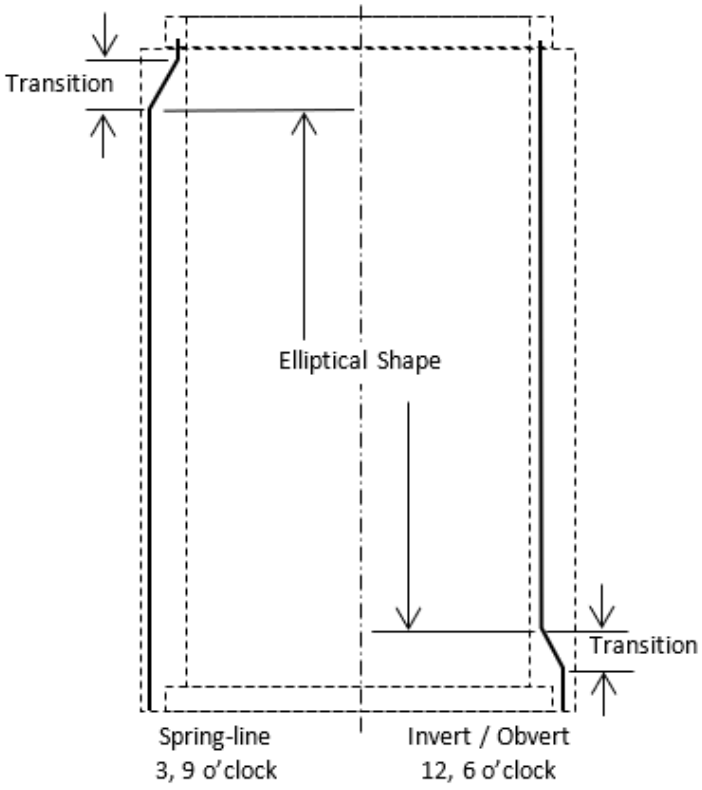

Figure 3.2-Profile of Elliptical Shape Cage Along Pipe.

A further fabrication challenge was faced when producing the first few samples. The position and orientation of the elliptical cage were affected by the vibration process of the

mould. The high amplitude vibration rotated the cage from its intended orientation on the tensile faces of the pipe, thus reducing the effectiveness of the steel reinforcement for flexural resistance. This is not an issue with conventional DC reinforcement since the reinforcement is radially symmetric, thus any rotation in orientation will not influence the effectiveness of the reinforcement. **Figure 3.3** shows the concrete cover meter measurements at 600 mm from the spigot end, 600 mm from the bell end and at the mid-section for a 1050 mm diameter pipe (Test E24). The peak of curves indicates the minimum cover and should appear at the invert (0 degree) and obvert (180 degree). The maximum cover should appear at the spring-line (90 degree and 270 degree). The actual measurement clearly showed an approximate 40-degree rotation of the cage with respect to the intended orientation. Further discussion will be provided in subsequent section. In order to address this, two circular steel hoops were welded to the cage at the location of the lifting pins with additional spacers. The circular steel hoops restrained rotation, while the spacers restrained translation; thus, the problem was resolved for subsequent pipe specimens.

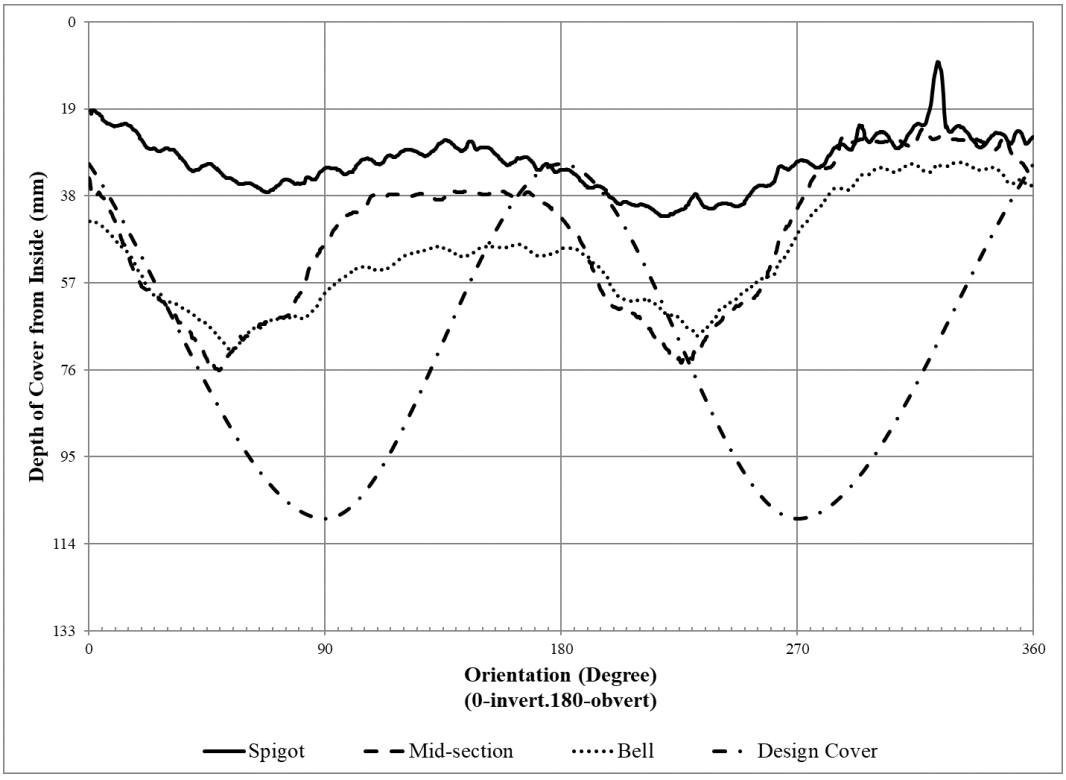

Figure 3.3-Reinforcement Cover Meter Profile *Di*=1050 mm Sample E24.

3.2.3 Testing Instrumentation and Procedure

To monitor vertical deflection of the pipe during testing, a pair of LVITs were mounted on the standard TEBT testing frame and positioned inside the pipe to measure vertical displacements at the invert and obvert of the RCP specimen. **Figure 3.4** shows a schematic diagram of the instrumentational setup.

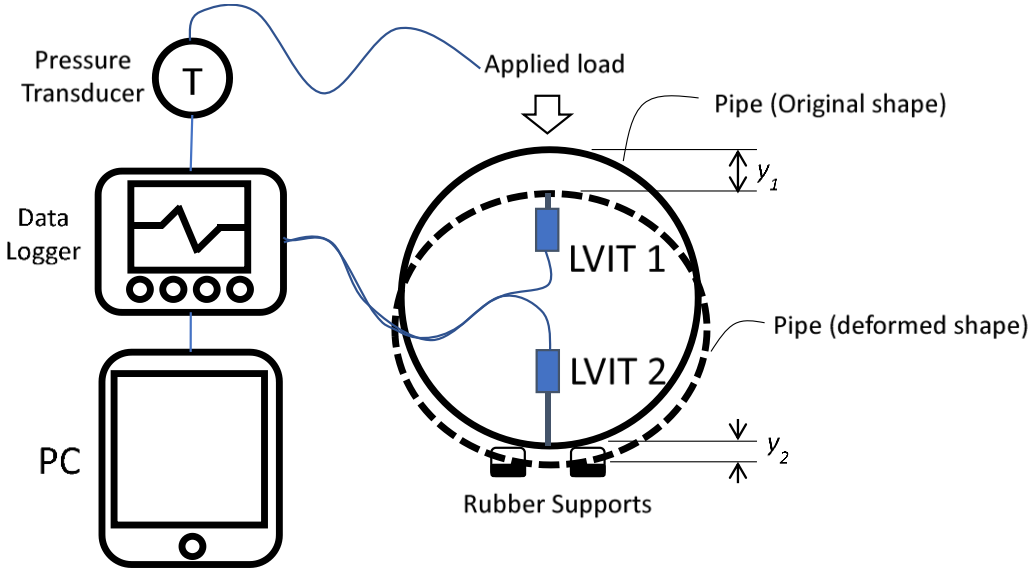

Figure 3.4-Instrumentation Setup.

The loading beam powered by a hydraulic press can exert a load of up to 560-kN. The LVITs, manufactured by Alliance Sensor Group, had a stroke of 50.8 mm with linearity error of ±0.15%. Both displacement and pressure transducers from the loading machine were connected to a data logger module supplied by ICP DAS. The load and displacement were simultaneously recorded at a rate of 1-Hz. The output measurements were also displayed on a tablet computer during the loading process. The LVIT positioned to measure the displacement at the obvert of the pipe will compress during the loading process, indicating a downward movement of the pipe. The LVIT positioned to measure the displacement at the invert will extend as the rubber supports are being compressed. The deflection of the pipe, δ, is calculated using **Eq. (3.1)** and subsequently plotted against the actual load.

$$\delta = y_1 - y_2 \qquad \textbf{Eq. (3.1)}$$

where, δ = vertical deflection of RCP in millimeter; y_1 = vertical displacement at pipe obvert in millimeter and should be positive indicating downward movement; y_2 = vertical displacement at the pipe invert in millimeter, and should be negative, indicating upward movement.

Load testing was carried out as per the CSA A257.0 discussed earlier. The pipe is first positioned onto the hydraulic press, after which a pair of LVITs are positioned at approximately 610 mm into the pipe against the inside face of the obvert and invert near the pipe spigot. Prior to testing, cover meter checks were performed to verify that the orientation of the as-built steel cage matches the design. One operator controlled and maintained constant load rate, while a second operator monitored the crack development on the surface of the concrete in the RCP specimen. **Figure 3.5** shows the test RCP loaded in the TEBT machine (Left) and the instrumentation inside the pipe (Right).

Figure 3.5-TEBT Setup (Left) and LVIT Setup (Right).

3.2.4 Data Collection

During testing, several critical crack events were reported by the second operator indicating the load for appearance of the first visible crack, known as hairline crack D_{HL}; the load for the appearance of the second visible hairline crack, D_{MHL}; and the load when the crack width having minimum length of 300 mm that reached 0.3 mm, $D_{0.3}$. The datalogger recorded the applied load in kilonewton from a pressure transducer and the vertical displacements in millimeters from LVITs. Load-displacement curves were plotted for each specimen from which D_{peak}, the first maximum load value at the end of the linear behaviour of the curve, was obtained. Furthermore, D_{ult}, the maximum load recorded was identified. **Table 3.3** summarizes the critical loads reported for each test. **Figure 3.6** shows typical load-deflection curve plotted using the collected data. Each of the critical load values was marked as deflection increased under increasing applied load. The reported critical loads were compared to the load-deflection data collected by the data logger and the structural behaviour was assessed considering the following parameters: reinforcement design (SE or DC), area of steel, concrete compressive strength, wall thickness, and position of the reinforcement.

Table 3.3-Testing Data Collection Points and Method of Identification

Abbreviation	Description of Normalized load (N/m/mm)	Method of Identification
$\mathbf{D_{HL}}$	Load when the first visible hairline crack appears	Visual inspection
$\mathbf{D_{MHL}}$	Load when the second visible hairline crack appears	Visual inspection
$\mathbf{D_{0.3}}$	Load when the crack width reaches 0.3 mm width with minimum length of 300 mm	Measured using leaf gauge
$\mathbf{D_{peak}}$	First maximum linear value followed by a declined in loads.	Obtained from the load-deflection curve
$\mathbf{D_{ult}}$	Maximum load the pipe can withstand	Obtained from the maximum load value from the instrumentation

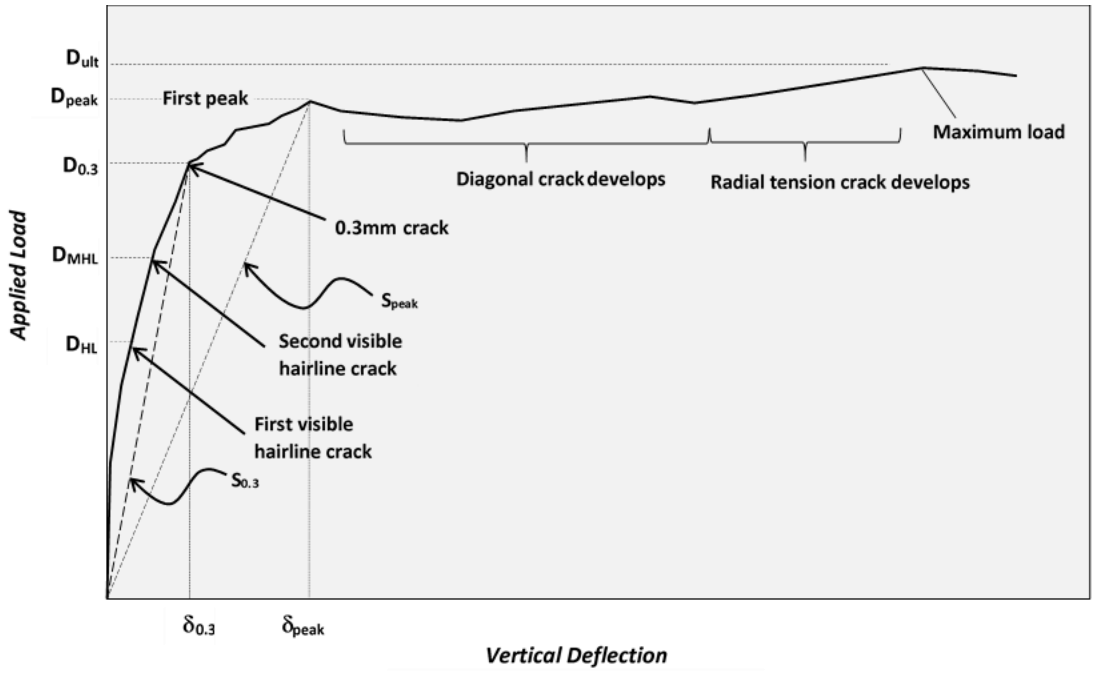

Figure 3.6-Typical RCP Load Deflection Curve.

3.3 Experimental Test Results

3.3.1 Load Data Measurements

Table 3.4 summarizes the TEBT test results reporting the load observation at first visible crack, second visible crack, 0.3-mm crack, the first peak load, and the ultimate load. All loads were normalized in newton per meter lay length per millimeter internal pipe diameter for ease of comparison between different pipe diameters. Multiple hairline cracks were not observed in most pipes made with SE reinforcement; thus, such load values were not reported. In addition, the post-crack load ratio ($R_{0.3}$), the post-peak load ratio (R_{peak}) and equivalent class (EC) are computed using **Eqs. (3.2), (3.3) and (3.4),** respectively.

$$R_{0.3} = \frac{D_{ult}}{D_{0.3}} \qquad \textbf{Eq. (3.2)}$$

$$R_{peak} = \frac{D_{ult}}{D_{peak}} \qquad \textbf{Eq. (3.3)}$$

$$EC = min.\begin{cases} D_{0.3} \\ \frac{D_{ult}}{\text{FS}} \end{cases} \qquad \textbf{Eq. (3.4)}$$

Where: FS = 1.25 when D_{ult} >175; FS = 1.5 when $D_{ult} \leq 150$; and FS = $1.5 - 0.25\left(\frac{D_{ult}-150}{25}\right)$ when $150 < D_{ult} \leq 175$.

Table 3.4-Critical Loads Obtained From the TEBT (All D-Load Values in N/m/mm)

Nominal Pipe Size (mm)	D_{HL}	D_{MHL}	$D_{0.3}$	D_{peak}	D_{ult}	$R_{0.3}$	R_{peak}	Equivalent Class (*D*)	Governing Factor
E08-1050	101.5		157.6	179.9	188.9	1.20	1.05	151	D_{ult}
E21-1050	79.2		114.2	114.8	145.3	1.27	1.27	97	D_{ult}
E23-1050	61.9		90.0	102.5	128.9	1.43	1.26	86	D_{ult}
E24-1050	70.0		113.8	113.8	113.9	1.00	1.00	76	D_{ult}
E25-1050	79.6	135.0	135.0	135.3	154.1	1.14	1.14	106	D_{ult}
E26-1050	72.7		123.4	124.3	150.4	1.22	1.21	101	D_{ult}
E02-1200	69.3		87.8	88.1	115.0	1.31	1.31	77	D_{ult}
E09-1200	79.4		118.1	125.4	146.2	1.24	1.17	97	D_{ult}
E10-1200	78.4		120.8	136.2	136.2	1.13	1.00	91	D_{ult}
E11-1200	68.0		118.1	147.8	147.8	1.25	1.00	99	D_{ult}
E12-1200	76.4		123.8	134.7	139.8	1.13	1.04	93	D_{ult}
E13-1200	59.2		115.1	136.2	136.2	1.18	1.00	91	D_{ult}
E14-1200	56.5		115.7	143.7	149.0	1.29	1.04	99	D_{ult}
E18-1200	56.2		124.1	143.6	143.6	1.16	1.00	96	D_{ult}
E19-1200	49.5		101.6	124.4	125.7	1.24	1.01	84	D_{ult}
E20-1200	54.2		110.7	139.8	139.8	1.26	1.00	93	D_{ult}
E01-1200	82.1	128.2	139.3	139.7	149.8	1.08	1.07	100	D_{ult}
E15-1200	79.1		143.0	145.3	192.1	1.34	1.32	143	$D_{0.3}$
E16-1200	67.6		140.6	148.1	183.8	1.31	1.24	141	$D_{0.3}$
E17-1200	55.5		143.0	144.3	186.5	1.30	1.29	143	$D_{0.3}$
T44-1050	72.7	98.0	114.2	114.2	161.2	1.41	1.41	114	$D_{0.3}$
T43-1050	83.8	138.8	163.4	198.9	204.7	1.25	1.03	163	$D_{0.3}$
T23-1200	65.3	74.0	114.7	150.9	167.0	1.46	1.11	115	$D_{0.3}$
T22-1200	80.4	107.0	163.2	182.9	195.9	1.20	1.07	157	D_{ult}

The post-crack load ratio, $R_{0.3,}$ is the ratio between the ultimate load and the 0.3-mm crack load. Higher post-crack ratio indicates larger post-design crack capacity of the pipe and greater ductile behaviour. The post-crack load ratio based on the test result for pipe with SE cage ranged between 1.00 and 1.43 for 1050 mm diameter pipe and between 1.08 and 1.34 for 1200 mm diameter pipe, respectively. For pipes with DC cage, the ratio ranged between 1.20 and 1.46. This indicates that the pipe with DC cage had larger post-crack load capacity. The post-peak load ratio, R_{peak}, is the ratio between the ultimate load and the first peak load. When the post-peak load ratio is greater than one, the pipe had undergone substantial stress transfer into plastic behaviour and re-gained capacity. These ratios are used to appraise the plastic behaviour of the pipe under TEBT load. Several pipe specimens had post-peak loads equal to the post-crack load, indicating that the first peak occurred at time where the 0.3-mm crack was identified. The equivalent RCP class is computed by taking the minimum of the $D_{0.3}$ or D_{ult} divided by the required safety factor stated in CSA A257.2. The safety factor is taken as 1.5 and 1.25 when the 0.3 mm crack load is less or equal to 100 N/m/mm, and greater than 140 N/m/mm, respectively. The safety factor is linearly interpolated between 100 N/m/mm and 140 N/m/mm. The equivalent classes of RCP show that most of pipes with SE did not meet the required design class according to Canadian standard design. Other than tests E08 and E02, which were outliers, the equivalent class ranged between 84D and 99D for 100D design. For 140D design, the equivalent class ranged between 76D and 143D.

3.3.2 Load-Deflection Curves

Figure 3.6 illustrates typical load-deflection curve for RCP under TEBT with critical points identifying the crack propagation at different stages. Load and deflection values were normalized to newton-per-meter-length-per-millimeter (N/m/mm) internal diameter and millimeter-per-meter length-per-millimeter internal diameter (mm/m/mm), respectively. When the pipe was loaded under TEBT, deflection increased in a relatively linear manner. The slope of the curve was somewhat steep, indicating rigid behaviour. When the first hairline crack occurred, the slope of the curve decreased, further reducing when multiple cracks propagated. The load measured when 0.3-mm crack width occurred was used as a threshold to classify the pipe. At this point, the linear elastic behaviour

usually approached conclusion and was followed by a non-linear plastic behaviour. The pipe stiffness at the crack load, $S_{0.3}$, was computed via dividing the 0.3-mm crack load by the corresponding deflection, $\delta_{0.3}$, defined in **Eq. (3.5)**. The pipe stiffness at the first peak load, S_{peak}, was computed via dividing the first peak load by the corresponding deflection, δ_{peak}, defined in **Eq. (3.6)**. The unit of the pipe stiffness is in newton per millimeter.

$$S_{0.3} = \frac{D_{0.3}}{\delta_{0.3}} \qquad \textbf{Eq. (3.5)}$$

$$S_{peak} = \frac{D_{peak}}{\delta_{peak}} \qquad \textbf{Eq. (3.6)}$$

Figures 3.7 and 3.8 show the load-deflection curves for the pipe with DC and SE reinforcement, respectively. In the case of pipe with DC reinforcement, typical elastic and plastic behaviour were observed. All DC reinforced pipes regained full capacity in the plastic phase, surpassing their elastic load and exhibiting large deformations until failure. This was also reflected in their 0.3-mm crack load to ultimate load, $R_{0.3}$ ratio. In some tests on 1200 mm diameter pipes with SE reinforcement (E10 - E14 and E18 - E20), the load reached the first peak followed by an abrupt decrease in load carrying capacity without re-gaining strength or regaining slightly higher strength. The R_{peak} for those tests ranged between 1.00 and 1.04, indicating close to no residual post first-peak load capacity. The load-deflection profiles for the specimens with SE reinforcement demonstrated greater decrease in strength following the 0.3-mm crack load in comparison with the DC reinforced pipe. All SE-RCP specimens surpassed the elastic crack load in the plastic phase, except for one 1050 mm 140D specimen, E24, which did not regain its strength in the plastic phase. It was observed that the DC configuration pipes experienced greater deflections, i.e. had more ductile behaviour in the plastic phase than that of the SE reinforced pipes.

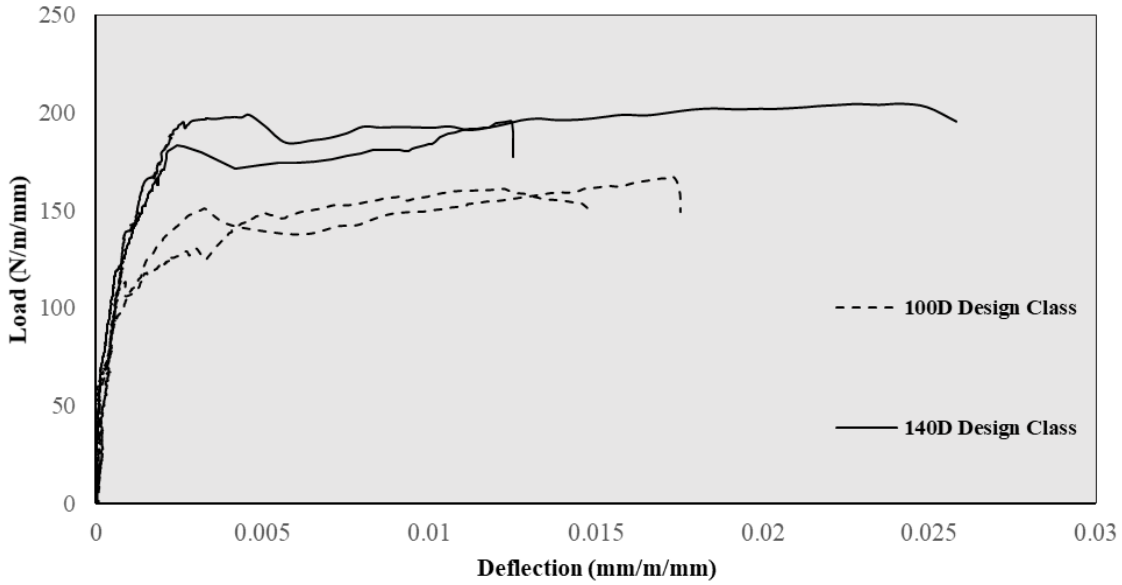

Figure 3.7-Normalized Load-Deflection Curves for DC RCP.

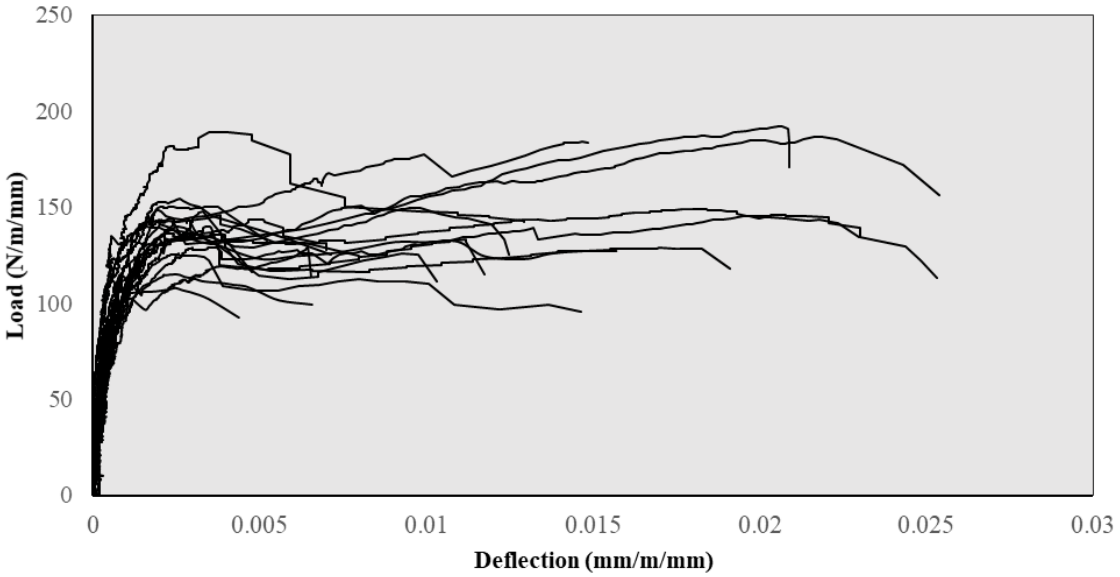

Figure 3.8-Normalized Load-Deflection Curves for SE RCP.

3.3.3 Plastic Behaviour

After first peak load, deflection increased much more substantially than in the previous stage. Diagonal cracks developed from the top, where the load was applied, and from the bottom where the rubber supports were located (**Figure 3.9)**. Upon the plastic stage, radial tension in some cases governed the maximum load that the pipe could withstand. Large vertical deflections observed in the plastic stage resulted from the inability of the circular cage to sustain the load due to the diagonal shear and radial tension stresses. Multiple longitudinal spring-line cracks were also observed at this stage. Crack propagation allowed the pipe to gain further capacity until its ultimate load capacity was reached.

Figure 3.9-Diagonal Tension Cracks at Applied Load (Left) and Support (Right).

Three RCP failure modes under TEBT, namely flexure, diagonal tension, and radial tension were observed during the tests, as per Heger's earlier research ((F. Heger, 1963), (F.J. Heger & McGrath, 1982)). For pipes with DC reinforcement, the pipe failed under diagonal tension cracks that developed at the applied load and at the rubber support (**Figure 3.9**). Multiple longitudinal cracks were distinct in DC-RCP specimens, forming along the invert of the pipe; however, none governed the ultimate capacity. Flexural cracks were also observed along the spring-line at failure, forming a plastic hinge (**Figure 3.10**), which contributed to larger deformation of the pipe.

Figure 3.10-Flexural Cracking Causing Plastic Hinge in DC RCP.

Similar to pipe specimens with DC reinforcement, pipes with SE reinforcement exhibited radial tension and diagonal tension cracking during its plastic stage. However, at the time of failure, a large concrete section on the outside layer where the radial tension was developed separated from the pipe (**Figure 3.11 Right Bottom**). The dashed line represents the reinforcing cage shape, the solid lines represent major cracks, while the hatched area represents concrete slabbing as a result of radial tension. The governing mode of failure of RCP with SE reinforcement was radial tension followed by slabbing failure. Radial tension was characterized by tension forces within the radial reinforcement that acted to straighten out curved steel, causing the reinforcement to separate from the concrete (F. Heger, 1963). The failure of RCP with SE steel reinforcement was characterized by the slabbing of the concrete cover from the outside faces of the upper and lower haunches where radial tension occurred. However, this may only occur in the testing environment, and is unlikely to occur in field condition where the pipe is normally fully confined in the soil. Slabbing was observed in every RCP specimen made with a SE reinforcement configuration. In addition, a 45° rotation of the plastic hinge was observed in the SE configuration pipes towards the upper and lower haunches causing large deformations. Unlike DC RCP specimens, multiple hairline cracks at the spigot inner face of the invert of the pipe were not common in SE-RCP specimens. Rather, SE-RCP specimens exhibited a single major crack that propagated as the load increased. Furthermore, it was observed that the failure was considerably more brittle in the SE configuration compared to the more ductile failure in the DC configuration.

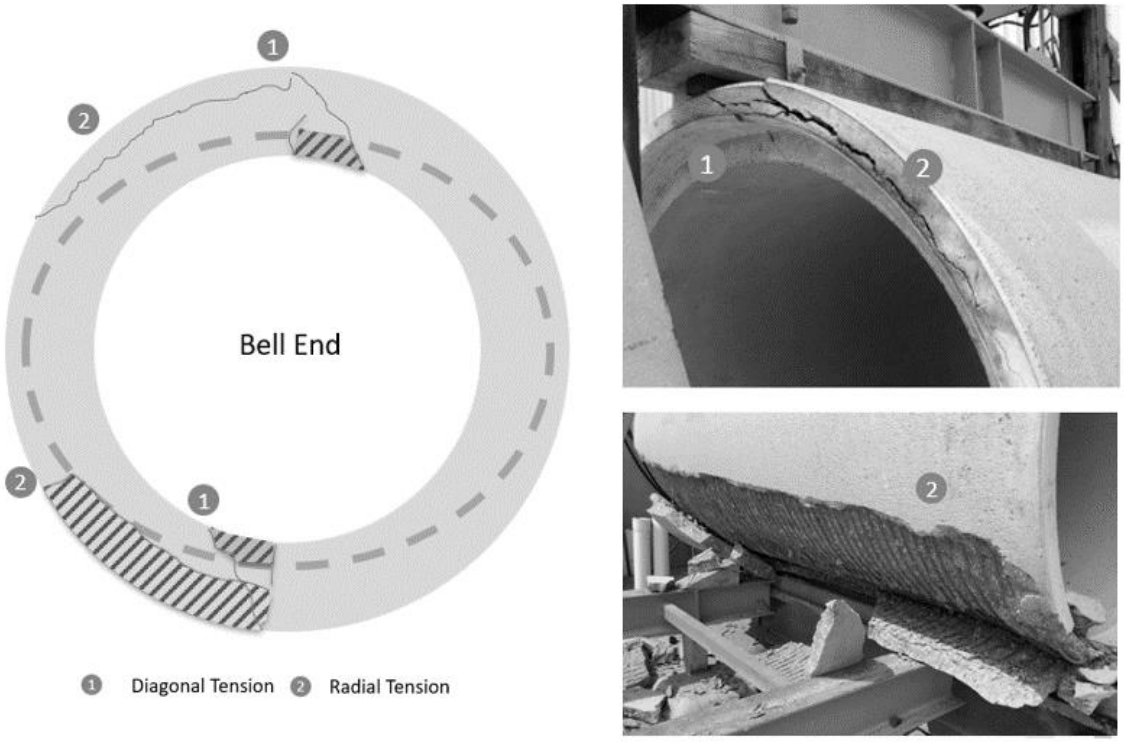

Figure 3.11-Single Elliptical RCP Failure Mode Cracks.

3.4 Discussion

3.4.1 Pipe Stiffness

Table 3.5 shows the calculated pipe stiffness values at 0.3-mm crack load and at the first peak load defined earlier in **Eqs. (3.5)** and **(3.6),** respectively. The pipe stiffness $S_{0.3}$ (Top) and S_{peak} (Bottom) are plotted against the area of reinforcing steel in **Figure 3.12**. By excluding the two outliers, stiffness of pipes made with SE reinforcement at 0.3-mm crack load ranged between 100 kN/mm and 137 kN/mm and 70 kN/mm and 100 kN/mm for 1050 mm and 1200 mm diameter, respectively. The stiffness at first peak load of pipes with SE reinforcement ranged between 71 kN/mm and 137 kN/mm, and from 21 kN/mm to 88 kN/mm, for 1050 mm and 1200 mm diameter pipe, respectively. Although the stiffness at first peak load was lower than that at the 0.3-mm crack load, values at first peak load were

obtained by a clearly defined measurement, while those at 0.3-mm crack load relied on the operator perception and experience.

Table 3.5-Deflections and Pipe Stiffness of Test Pipe Samples

Nominal Pipe Size (mm)	δ_{HL} (mm/m/mm)	$\delta_{0.3}$ (mm/m/mm)	δ_{peak} (mm/m/mm)	δ_{ult} (mm/m/mm)	$S_{HL}= D_{HL}/\delta_{HL}$	$S_{0.3}=D_{0.3}/\delta_{0.3}$	S_{peak} D_{peak}/δ_{peak}
E08-1050	0.00068	0.00154	0.00254	0.00349	149314	102576	70958
E21-1050	0.00039	0.00085	0.00085	0.01968	201554	134094	134434
E23-1050	0.00043	0.0009	0.00117	0.00645	144778	99523	87636
E24-1050	0.00033	0.00083	0.00083	0.00083	209505	136773	136773
E25-1050	0.00022	0.00056	0.00056	0.00261	357562	240820	241355
E26-1050	0.00019	0.00094	0.00097	0.00355	383534	131320	128288
E02-1200	0.00019	0.00046	0.00047	0.00245	371819	190217	185987
E09-1200	0.00044	0.00139	0.00144	0.00381	180850	84936	86987
E10-1200	0.00066	0.00149	0.00219	0.00219	119445	81090	62226
E11-1200	0.00044	0.00166	0.00331	0.00331	153706	71335	44592
E12-1200	0.00052	0.00161	0.00203	0.00336	145572	76856	66355
E13-1200	0.00032	0.00128	0.00286	0.00286	187798	89632	47634
E14-1200	0.00041	0.00136	0.00492	0.018	139139	85126	29232
E18-1200	0.00028	0.00143	0.00287	0.00287	201751	86958	50016
E19-1200	0.00028	0.00119	0.00335	0.00258	178778	85286	37081
E20-1200	0.00022	0.00111	0.00256	0.00256	245586	99470	54669
E01-1200	0.00018	0.00153	0.00159	0.00984	445319	90782	88088
E15-1200	0.00037	0.00657	0.00686	0.02069	214328	21772	21196
E16-1200	0.00023	0.0016	0.00199	0.01467	295492	87633	74448
E17-1200	0.00017	0.002	0.0023	0.02161	321576	71642	62772
T44-1050	0.00036	0.0007	0.0007	0.01216	203314	163737	163737
T43-1050	0.00046	0.00144	0.00461	0.02415	182539	113661	43113
T23-1200	0.00025	0.00129	0.00327	0.01732	258110	89017	46132
T22-1200	0.00027	0.00171	0.00263	0.01243	292511	95699	69492

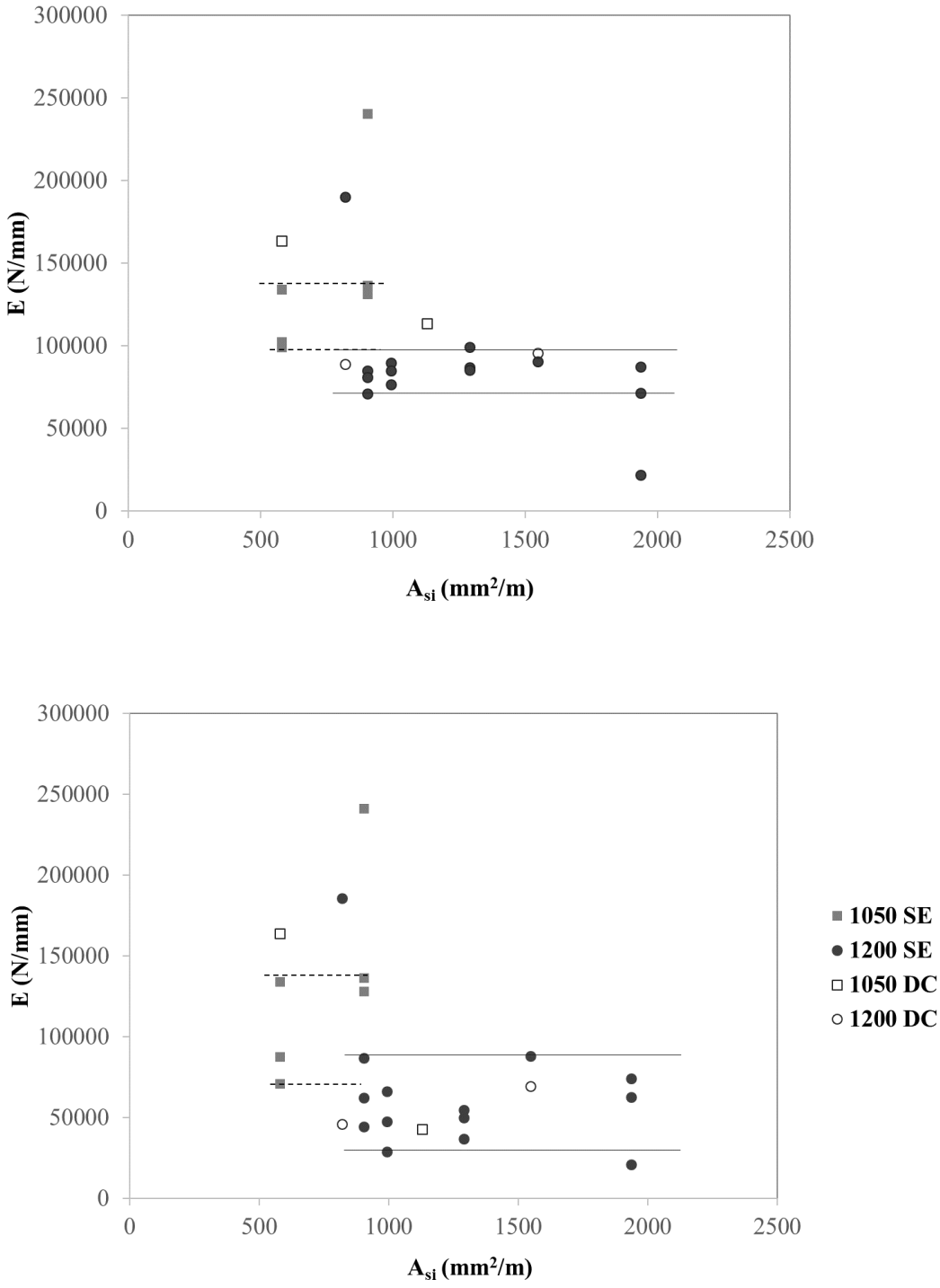

Figure 3.12-Pipe Stiffness (Top) at 0.3-mm Crack Load, and (Bottom) at the First Peak Load

3.4.2 Load-Deflection Curves

For comparison, **Figures 3.13** and **3.14** show the elastic phase response with deflection up to 0.005 mm/m/mm, corresponding to **Figures 3.7** and **3.8** for RCP with DC and SE reinforcement, respectively. In the case of DC reinforcement, the pipe stiffness (PS), characterized by the slope of the load-deflection curve, had a consistent increase until 50 N/m/mm, followed by a slight reduction in PS up to 100 N/m/mm. The reduction tended to increase in variability after the load exceeded 100 N/m/mm. All specimens reached their first peak before 0.005 mm/m/mm deflection, followed by a plastic phase response. For pipes with SE reinforcement, the PS showed a much larger variance between 0 and 50 N/m/mm, and 50 and 100 N/m/mm. Similar behaviour to the DC reinforced RCP was observed after 100 N/m/mm. The reduction in PS resulted from an increase in bending moment at the invert and obvert of the pipe. Hairline cracks (first visible cracks) were observed between 50 N/m/mm and 84 N/m/mm. Slight variation was observed between pipes made with SE and DC reinforcement (**Table 3.6**).

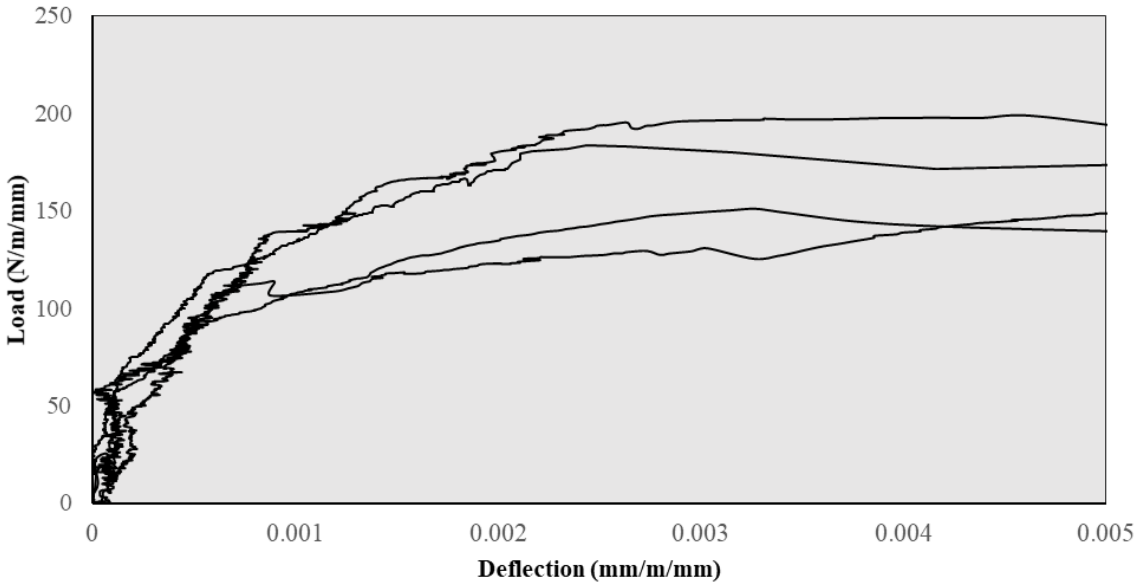

Figure 3.13-Elastic Phase Response of DC RCP.

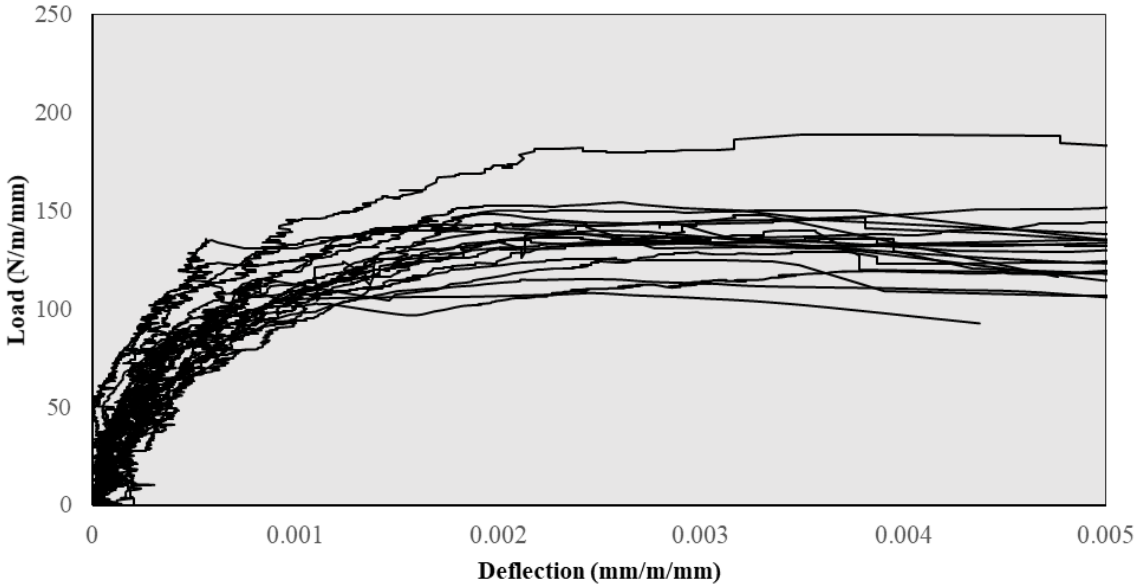

Figure 3.14-Elastic Phase Response of SE RCP.

Table 3.6-Load at First Visible Crack (D_{HL}) Measured in N/m/mm

Cage Config.	Min.	Average	Max	Std. Dev.	Sample Number
SE RCP	49.5	68.1	82.1	10.2	20
DC RCP	65.3	75.6	83.8	7.2	4

The development of cracking reduced the compression zone of the reinforced concrete stress block; hence reducing its sectional properties for flexure resulting in an increased rate of deflection. In addition, the occurrence of the first crack did not seem to be related to the existence of the second cage and was likely attributed to the tensile strength of the concrete. The multiple cracks which developed in RCP with DC reinforcement enhanced the deflection response. However, RCP with SE reinforcement did not develop a second crack, except two specimens prior first peak. The first crack developed usually along the invert and obvert along the pipe axis, while the second crack usually developed parallel to the first crack at 300 mm to 400 mm. In the SE shaped reinforcement, the concrete cover increased in sections further from the invert and obvert of the pipe, which seemed to delay the occurrence of a second crack before the non-elastic behaviour occurred, while also contributing to low first peak load.

3.4.3 Significance of Outer Cage in Double Cage Reinforced Pipe

Significant difference in failure mode was observed between the DC and SE reinforced pipe under TEBT loading. In SE reinforced pipes, large concrete slabbing was observed at the pipe haunches at the end of each test (**Figure 3.15**). In the plastic phase, and with absence of stirrups, concrete was the only material resisting diagonal shear stresses. The diagonal crack begun at the support, running approximately 45° inwards. In the case of the DC reinforced pipes, the crack reached the outer layer of reinforcement and propagated for a distance followed by continuation of the diagonal crack further inwards. For SE reinforced pipes, the first layer of steel was the inner steel where the crack developed along the inner layer resisting tensile stresses. The crack did not pass through the inner layer, as opposed to the outer layer of steel in the DC reinforced pipe. The radial tension from the inner layer steel further separated the concrete and steel, causing substantial slabbing at failure. The double layer of steel reinforcement seemed to play an important role in controlling the end behaviour of the pipe at failure

Figure 3.15-Major Concrete Slabbing in Sample E24.

3.4.4 Influence of Reinforcing Steel

An increase in the area of reinforcing steel for the SE reinforced pipes improved the D_{HL}, $D_{0.3}$ and D_{ult} up to a certain degree. However, this improvement was not proportional to the added amount of steel. **Figure 3.16** illustrates the effect of area of steel on $D_{0.3}$ and D_{ult} for Di=1200 mm SE RCP specimens. It can be observed that the increase in steel area did not yield the expected increase in $D_{0.3}$ and D_{ult}, except for specimens E15, E16, and E17, which had 12% greater steel area than what is required by CSA A257.2. The average $D_{0.3}$ and D_{ult} values for 1290 mm^2/m pipes decreased relative to the 903 mm^2/m and 993 mm^2/m pipes (**Table 3.7**). Other than the outlier E02, specimens with 903 mm^2/m, 993 mm^2/m, and 1290 mm^2/m, all showed 18%-19% increase in $D_{0.3}$ to D_{ult}. This indicates that the increase in reinforcement area did not yield significant improvement in the ultimate capacity of SE reinforced pipes. This can be attributed to the radial tension mode of failure for SE RCP specimens. Studies from Heger demonstrate that the addition of circumferential inner steel area significantly improved flexural capacity compared to radial and diagonal tension capacity (F. Heger, 1963). Radial tension depends on the concrete strength and reduction of the concrete wall thickness without reinforcement. Thus, increasing the area of steel alone improved D_{ult} up to a certain point, after which it was not effective in improving radial tension strength.

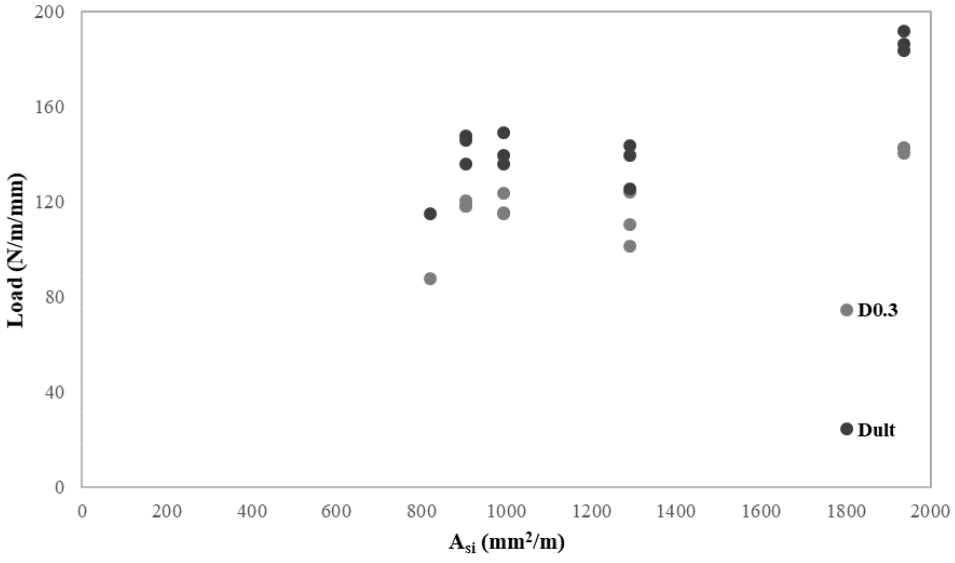

Figure 3.16-Load vs Inner Reinforcement Area for *Di*=1200mm SE Reinforced Pipe.

Table 3.7-Average $D_{0.3}$ and D_{ult} for 1200 SE Reinforced Pipes Measured in N/m/mm

Reinforcement Area	Average $D_{0.3}$	Average D_{ult}	Percent Difference	Sample Number
903 mm^2/m	119.0	143.3	18.6%	3
993 mm^2/m	118.2	141.7	18.1%	3
1290 mm^2/m	112.1	136.4	19.5%	3

Figure 3.17 compares the experimental $D_{0.3}$ to the calculated ultimate moment capacity at invert and crown of tested RCP. A sample calculation for the moment capacity is presented in **Appendix B**. The moment capacity of RCP is related to the 0.3-mm crack load. Typically, the higher the ultimate moment capacity of the pipe, the higher the 0.3-mm crack load. The moment was calculated from Heger's relationship (F. Heger, 1963). Generally, steel used for higher design class RCP results in under reinforced sections, such that the bending moments produce yielding of the circumferential steel prior to failure (F. Heger, 1963). Steel fracture was detected for the DC RCP specimens (**Figure. 3.18**). No steel fracture was observed in the steel reinforcement for the SE RCP specimens. This implies that the full tensile capacity of the steel was not utilized in resisting the TEBT load. Furthermore, the lack of steel yielding explains the radial tension failure for the SE reinforcement configuration. Adding more steel would not have improved D_{ult} since the reinforcement tensile strength was not being fully utilized.

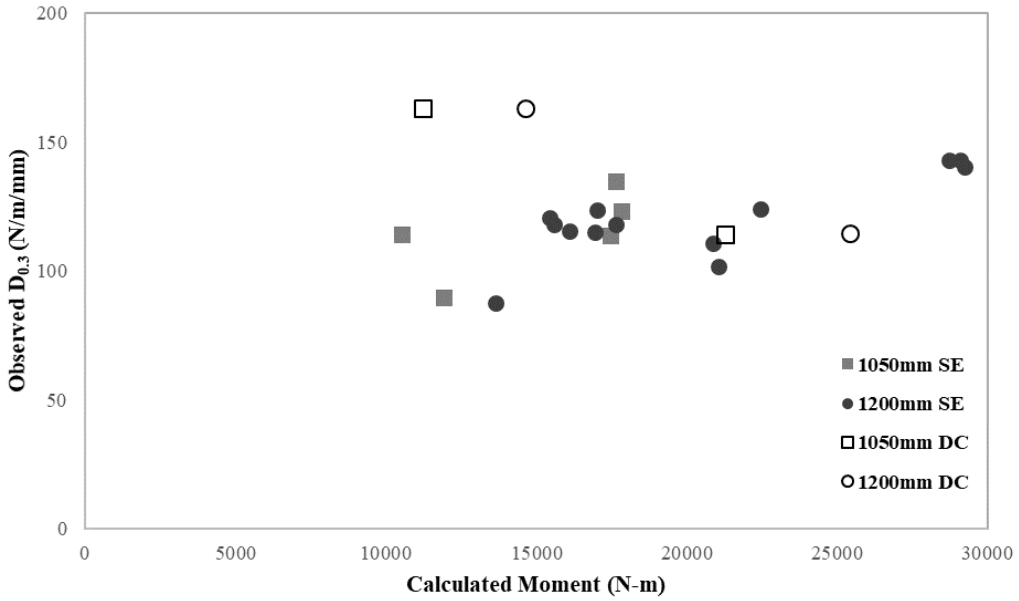

Figure 3.17-Obserevd $D_{0.3}$ vs. Ultimate Moment Capacity.

Figure 3.18-Evidence of Steel Fracture in DC RCP Specimen.

A shift of the plastic hinge under loading from the invert, obvert, and spring-lines of the pipe towards the upper and lower haunches was observed in SE RCP specimens. The plastic hinge was characterized by maximum rotation in the pipe to start deformation as a plastic mechanism, with the assumption that the pipe behaved elastically between plastic hinges (F. Heger, 1963). Once the plastic hinges formed, the pipe experienced large deformations at constant plastic moment. The development of the plastic hinge depended on the ductility of the pipe and was limited by the compressive strain of the concrete and the amount of tension steel (Frank Joseph Heger, 1962). SE RCP had less reinforcing tension steel limiting the ductility and rotational capacity of the pipe, leading to earlier development of plastic hinges at the upper and lower haunches, which had the least reinforcement.

3.4.5 Reinforcement Orientation

Previous findings demonstrate that the depth of inner reinforcement had an effect on $D_{0.3}$ and D_{ult} (F. Heger, 1963). The first pipe (E24) made with mis-aligned SE cage incurred a

mis-orientation close to 40° (**Figure. 3.3**). As discussed earlier, the mis-orientation was due to heavy vibration combined with non-restrained cage during the manufacturing process. The equivalent class of this pipe was computed as 76D. With the same amount of steel, the pipe with no mis-orientation (E25) reached equivalent class of 106D, with a 30% increase in ultimate capacity. Measurement of the concrete clear cover profile of the pipe specimen (E25) showed less than 1% difference between the as-built cage and design cage, indicating no mis-orientation in the manufacturing process. The first cracks appeared in both cases at 70 and 79.6 N/m/mm, respectively indicating that it was not influenced by mis-orientation. The specimen with mis-orientation did not exhibit multiple cracks before the 0.3-mm crack threshold was reached. The 0.3-mm crack load was found to be 113.8 N/m/mm, which was 21.2 N/m/mm less than that of the pipe with no mis-orientation. The crack load was severely compromised by the mis-orientation due to the reduction of the principle steel depth at the critical section (invert and obvert) where the flexural stress was most severe.

3.4.6 Pipe Load Capacity vs. Heger Calculated Load Capacity

Calculation of the 0.3-mm crack load was performed on the test RCP using the semi-empirical **Eq. (2.8)** developed by Heger (F. Heger, 1963). Although the parameters for the relationship encompass pipe diameters between 1200 mm and 2700 mm with a longitudinal wire spacing between 100-200 mm in Heger's study (F. Heger, 1963), comparison between the test results and the calculated crack load was made to provide insight into the prediction. **Figure 3.19** correlates the observed and calculated $D_{0.3}$. The load calculated using Heger's equation overestimated $D_{0.3}$ for most experimental results. The average observed $D_{0.3}$ for SE and DC RCP was 118.8 N/m/mm and 138.9 N/m/mm, respectively, while the average calculated $D_{0.3}$ for SE and DC RCP was 139.1 N/m/mm and 146.2 N/m/mm, respectively. The DC RCP exhibited slightly steeper slope of the trendline than that of SE RCP, indicating closer agreement between the observed and calculated value. The calculated $D_{0.3}$ had high coefficient of variance for both the SE and DC RCP of 21.2 and 25.9, respectively. The results indicate that reduction factors of 0.83 and 0.89 be applied for the SE and DC RCP, respectively, to compensate for the overestimation of Heger's semi-empirical equations.

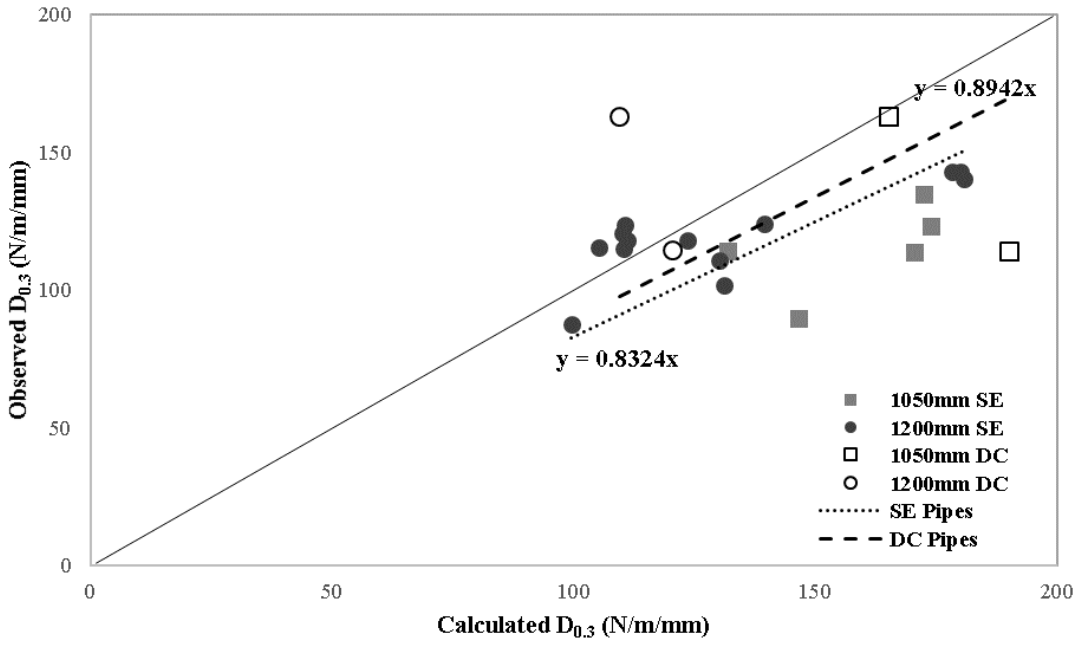

Figure 3.19- Observed $D_{0.3}$ vs. Calculated Heger $D_{0.3}$.

The calculated $D_{0.3}$ was dependent on the area of inner steel cage, the depth of inner cage, pipe diameter, and longitudinal wire spacing. The DC RCP specimens had a longitudinal wire spacing of 300 mm on average (12 longitudinal steel wires), which was the main reason for the overestimated calculated $D_{0.3}$ results. The 1200 mm RCP for both SE and DC reinforcement had lower calculated $D_{0.3}$ than the observed $D_{0.3}$ relative to the 1050 mm RCP specimens. This was due to both sets of RCP diameters using the same number of longitudinal steel wires, resulting in smaller longitudinal wire spacing for the smaller diameter 1050 mm RCP specimens, which increased the calculated crack load. The longitudinal wire spacing for the SE RCP specimens was 150 mm on average (24 longitudinal steel wires), within the parameter requirements. However, the observed $D_{0.3}$ for the SE specimens was lower than the intended design class according to CSA A257.2.

Calculation of the ultimate load capacity was also performed on the test RCP using Heger's semi-empirical **Eq. (2.9)** (F. Heger, 1963). The relationship estimates the ultimate capacity of a circular pipe having two circular reinforcing cages with outer reinforcement area that is three quarter of the inner cage reinforcement. **Figure 3.20** correlates the observed ultimate load from the test specimens and the calculated D_{ult}. Similar to $D_{0.3}$, Heger's

relationship overestimated D_{ult} for all experimental results. Both the SE and DC RCP were not within the parameters, which explains the overestimated results. The average observed D_{ult} for SE and DC RCP was 146.4 N/m/mm and 182.2 N/m/mm, respectively, while the average calculated $D_{0.3}$ for SE and DC RCP was 318.2 N/m/mm and 326.3 N/m/mm, respectively. The calculated $D_{0.3}$ had high coefficient of variance for both the SE and DC RCP of 15.1 and 11.7, respectively. The results indicate that reduction factors of 0.44 and 0.52 be applied for the SE and DC RCP, respectively, to compensate for the overestimation of Heger's semi-empirical equations. Sample calculations of the calculated $D_{0.3}$ and D_{ult} are presented in **Appendix B**

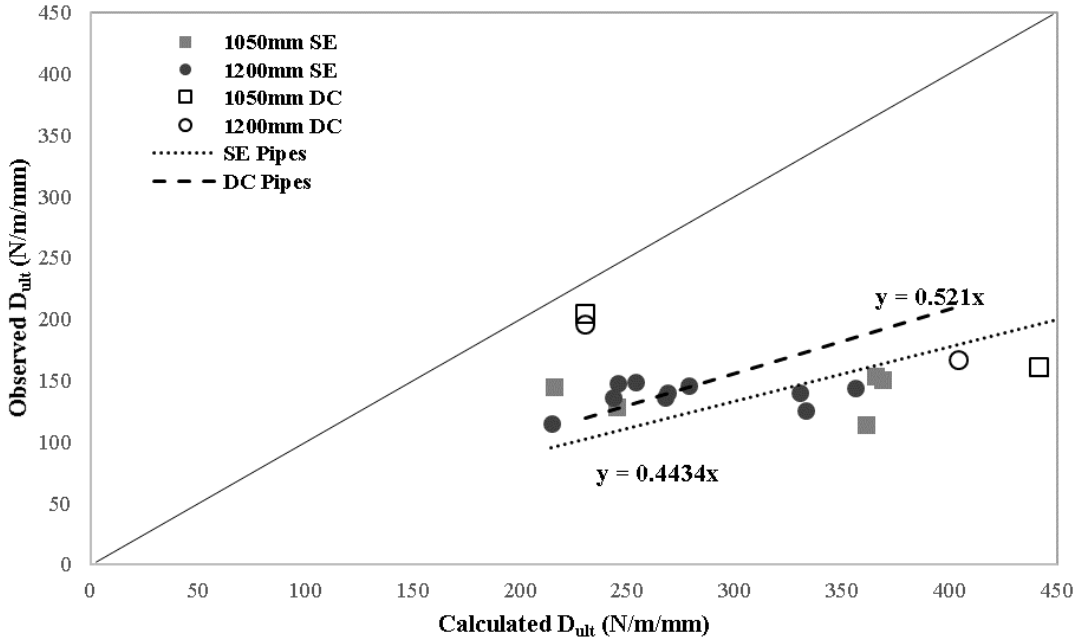

Figure 3.20- Observed D_{ult} vs. Calculated Heger D_{ult}.

3.4.7 Cost Effectiveness of Single Elliptical RCP

Table 3.8 shows a comparison of the $D_{0.3}$ and D_{ult} load capacities of the SE and DC RCP compared to the total area of reinforcement of the pipe per meter length. The total area of reinforcement for the DC RCP considers both the inner and outer steel layers. For 1050 mm pipes, the comparison indicates that increasing the total reinforcement area of the SE RCP by 3.6% relative to the DC RCP improved the $D_{0.3}$ capacity by 12.3%. Conversely,

the D_{ult} capacity was reduced by 6.3%. For the 1200 mm pipes, 12.5% reduction in the total reinforcement area of the SE RCP reduced the $D_{0.3}$ and D_{ult} capacities by 13.8% and 4.4% respectively.

Table 3.8- Total Area of Steel Reinforcement compared to $D_{0.3}$ and D_{ult} Measured in N/m/mm for SE and DC RCP

1500 mm Nominal Diameter				
Cage Config.	**Total Steel Reinforcement Area (mm^2/m)**	**Average $D_{0.3}$**	**Average D_{ult}**	**Sample Size**
SE RCP	903	129.2	152.3	2
DC RCP	871	114.2	162.2	1
Percent Difference	3.6%	12.3%	6.3%	
1200 mm Nominal Diameter				
Cage Config.	**Total Steel Reinforcement Area (mm^2/m)**	**Average $D_{0.3}$**	**Average D_{ult}**	**Sample Size**
SE RCP	1936	142.2	187.5	3
DC RCP	2194	163.2	195.9	1
Percent Difference	12.5%	13.8%	4.4%	

Utilizing SE steel reinforcement design can be advantageous to the industry, with potential cost savings in material and labor. However, **Table 3.8** signifies that although there is cost savings associated with SE RCP, the structural load capacity of the pipe is reduced compared to DC RCP. Thus, there is a tradeoff between cost savings and reduction of load capacity of the pipe when considering SE RCP as an alternative to the DC RCP in full-scale practical applications.

3.5 Conclusions

This chapter explored the structural behaviour of RCP with SE reinforcement under TEBT loading as compared to control RCP with traditional DC reinforcement and the design requirements of CSA A257.2. The progression of cracks and failure modes were discussed. The structural behaviour and comparison to traditional DC reinforcement were analyzed through experimental deflection data. Moreover, prediction of the crack load using the semi-empirical equation developed by Heger (F. Heger, 1963) was made and compared

against actual experimental measurements. From the experimental testing program, the following conclusions can be drawn:

1. A single elliptical pipe reinforcing cage can be fabricated. However, restraining the rotation of the cage during the pipe casting process is important. Rotational mis-orientation may substantially compromise the pipe flexural capacity due to reduction in the distance between the steel cage and the neutral axis.

2. Although true elliptical shape of the reinforcing cage can be made, the shape may need to be transitioned into circular at both ends of the pipe to account for the joint design. This may affect the effectiveness of the elliptical shape.

3. RCP with SE reinforcement had lower equivalent design class (20%-45% reduction) compared to that of RCP with DC reinforcement and similar area of reinforcing steel.

4. The elastic behaviour of RCP with SE reinforcement was comparable to that with DC reinforcement. However, it was not characterized by the appearance of multiple hairline cracks before reaching the 0.3-mm crack threshold.

5. Multiple hairline cracks were observed at the spigot inner face of the invert RCP with DC reinforcement but were not common in RCP with SE reinforcement. Therefore, RCP with SE cage exhibited a single major crack propagation as the load increased.

6. The governing design criterion for RCP with SE reinforcement was the ultimate load capacity due to radial tension.

7. The radial tension stress and development of plastic hinges led to separation of a large section of concrete from the steel at the upper and lower outside haunch of the SE pipe. This was attributed to the absence of a second layer of reinforcement, thus creating unstable condition.

8. The failure of RCP with SE reinforcement was relatively more brittle than that with DC reinforcement due to the absence of a second layer of reinforcement.

9. RCP with DC cage exhibited greater deformations in the plastic phase of loading, indicating higher ductility.

10. Increasing the steel reinforcement area in SE RCP improved the 0.3-mm crack and ultimate load capacity up to a certain limit, after which increasing the reinforcement area did not yield significant improvement.

11. Though there are material and labor cost savings when utilizing SE RCP, a trade-off with the reduced 0.3-mm crack and ultimate load capacity needs to be considered.

12. RCP with SE reinforcement designed per current standards did not meet the specified load capacities. Hence, pertinent provisions in CSA A257.2 and ASTM C76 for RCP need to be updated with specific and more suitable guidance for single elliptical cage RCP

3.6 References

ASTM C39/C39M − 16b. (2016). *Test Method for Compressive Strength of Cylindrical Concrete Specimens*. ASTM International. https://doi.org/10.1520/C0039_C0039M-16B

ASTM C76-16. (2016). *Specification for Reinforced Concrete Culvert, Storm Drain, and Sewer Pipe*. ASTM International. https://doi.org/10.1520/C0076-16

CSA A257-14. (2014). *Standards for Concrete Pipe and Manhole Sections*. CSA Group.

Heger, F. (1963). Structural Behavior of Circular Reinforced Concrete Pipe-Development of Theory. *ACI Journal Proceedings*, *60*(11). https://doi.org/10.14359/7905

Heger, F.J., & McGrath, T. J. (1982). *Design Method for Reinforced Concrete Pipe and Box Sections*. Simpson Gumpertz & Heger. https://books.google.ca/books?id=CSoonQEACAAJ

Heger, Frank Joseph. (1962). *A Theory for the Structural Behaviour of Reinforced Concrete Pipe*. Massachusetts Institute of Technology.

Mohamed, N., Soliman, A. M., & Nehdi, M. L. (2015). Mechanical performance of full-scale precast steel fibre-reinforced concrete pipes. *Engineering Structures*, *84*, 287–299. https://doi.org/10.1016/j.engstruct.2014.11.033

Chapter 4

4 Modelling Structural Behaviour of Precast Concrete Pipe with Single Elliptical Cage Reinforcement

4.1 Introduction

Using single elliptical cage reinforcement in RCP can reduce both the needed reinforcing steel and labor for manufacturing compared to the double steel reinforcing cages. However, there is currently no robust tools to predict the structural behaviour of RCP with SE reinforcement. Finite element modelling (FEM) offers an inexpensive alternative to optimize RCP without undergoing expensive and time-consuming experimental programs. The present chapter aims at developing and validating 3-D finite element model of 1050 mm and 1200 mm diameter RCP with SE steel cage reinforcement under the TEBT. Model ability to assess the sensitivity of the RCP structural behaviour to rotation of the SE reinforcement cage is of paramount importance. Furthermore, the model should accurately capture the effect of non-symmetrical shape of the SE cage and the associated serviceability performance. From Heger's semi-empirical relationships for $D_{0.3}$ and D_{ult} shown in **Eq. (2.8)** and **Eq. (2.9)**, respectively (Heger, 1963), it can be concluded that the depth or cover of the inner reinforcing cage in a double cage configuration has an effect on crack and ultimate load values. Thus, a change of depth of the reinforcing affects both load capacities. Accordingly, the rotation of the cage was evaluated since it could induce change of depth of the reinforcement at the invert of the pipe.

It is critical to maintain the orientation of the SE cage during the RCP casting process. The pressure induced by pouring concrete and high amplitude vibration during concrete consolidation can shift the SE cage from the intended orientation on the tensile faces of the pipe, hence reducing the flexural capacity of the RCP. This is not an issue with conventional DC cage reinforcement due to its radial symmetry. Orientational shift of the

pipe during RCP field installation can also rotate the SE cage from its intended position. This can be mitigated by installing lifting pins, indicating the location of pipe crown for installation. The shift in SE cage can compromise the RCP flexural capacity and thus needs to be monitored and managed.

There have been previous attempts to numerically model the structural behaviour of RCP and obtain optimum reinforcing steel content. For instance, Mohamed *et al.* (Mohamed & Nehdi, 2016) developed a rational design process for steel fibre-reinforced concrete pipes via a non-linear 3D FEM simulating the pipe under TEBT. They also performed a parametric study to investigate the effect of varying six independent variables adjusted within the range of ASTM standard specifications. The model achieved an average error of 6.5%, which was on the conservative side for the predicted ultimate capacity of the pipe. De La Fuente *et al.* (de la Fuente et al., 2012) conducted both experimental and numerical studies on steel fibre-reinforced concrete pipes. They verified that their numerical model simulating TEBT could be used to determine the optimal steel fibre dosage. Moreover, Kataoka *et al.* (Kataoka et al., 2017) performed 3D finite element analysis on RCP with conventional steel reinforcement under TEBT to analyze strength and stiffness. The models satisfactorily represented the behaviour RCP (Kataoka et al., 2017). However, modelling of RCP with elliptical steel cage reinforcement was not accessible in the open literature.

4.2 Experimental Program

Experimental information from Chapter 3 useful to develop and validate the model is summarized in this section. The experimental program included two pipe sizes with nominal diameters of 1050 mm and 1200 mm. The calibration and validation focused on pipes with a design class of 100D having different area of steel reinforcement to satisfy crack and ultimate load capacity requirements. **Table 4.1** provides the RCP specimens considered in the present chapter and the corresponding area of steel reinforcement. All pipes were tested using the TEBT as per CSA A257.0. (CSA A257-14, 2014). To obtain load-deflection curves of the tested pipes for calibration and validation purposes, LVITs were utilized to measure the vertical deflection of tested pipes. Further detail of the pipe manufacturing, testing, and observations can be found in Chapter 3.

Table 4.1-Experimental and Numerical Results of Pipes for Model Validation

Nominal Pipe Diameter (mm)	Pipe Reference	*Asi* (mm^2/m)	$D_{\delta=0.36\%}$ (N/m/mm)			D_{10mm} (N/m/mm)		
			Experimental	FEM	% Error	Experimental	FEM	% Error
1050	E08	581	156.9	115.4	-26.4	188.9	143.7	-23.9
1050	E21	581	104.3		+10.6	129.1		+11.3
1050	E23	581	96.7		+19.3	119.1		+20.7
1200	E09	903	125.4	118.2	-5.7	144.3	139.7	-3.2
1200	E10	903	120.2		-1.7	134.8		3.6
1200	E11	903	112.7		-4.9	147.8		-5.5
1200	E18	1290	125.6	114.6	-8.6	134.8	135.2	+0.4
1200	E19	1290	114.1		-0.5	125.7		+7.6
1200	E20	1290	128.5		-10.8	129.5		-4.8

Table 4.1 also presents the load results $D_{\delta=0.36\%}$ and D_{10mm} recorded from the tests and used for the purpose of this chapter. $D_{\delta=0.36\%}$ denotes the load when the pipe deflects 0.36% of the internal diameter. For 1050 mm pipe, $D_{\delta=0.36\%}$ represents the load that induces 3.84 mm deflection and was considered after Younis *et al.* (Younis et al., 2020) who suggested 0.36% to be an indicator of RCP serviceability performance. The load value can be easily indicated from the load-deflection curve and used as an alternate criterion in lieu of the $D_{0.3}$ design crack load since the 0.3 mm crack cannot be detected from the model. D_{10mm} is the load capacity of RCP at 10 mm deflection, which represents a limit of plastic analysis in this chapter.

4.3 Finite Element Modelling of RCP

4.3.1 Modelling Approach and Geometric Properties

Finite element analysis of SE reinforced RCP was performed using the commercially available software ABAQUS. Two 3D models: 1050 mm diameter and 1200 mm diameter RCPs were constructed to simulate test specimens under TEBT load. The models included the upper and lower rubber bearing strips, the concrete pipe, and the longitudinal and circumferential steel reinforcements. The upper and lower bearing strips had dimensions of 30 x 50 mm. The cage transitioned from elliptical into circular shape when approaching the RCP end to accommodate the bell and spigot, requiring 3D instead of 2D modelling (**Figure 4.1**). A separate iso-symmetric cage model was built to evaluate the effect of non-iso-symmetricity. The longitudinal steel reinforcement consisted of 24 equally spaced cold

drawn wires. The model length was maintained at 2.438 m. **Table 4.2** reports geometric properties used in modelling. The model was calibrated by performing a sensitivity analysis on the material properties and was subsequently validated with comparable experimental results. The effect of rotation of the cage reinforcement was assessed on the 1050 mm diameter model.

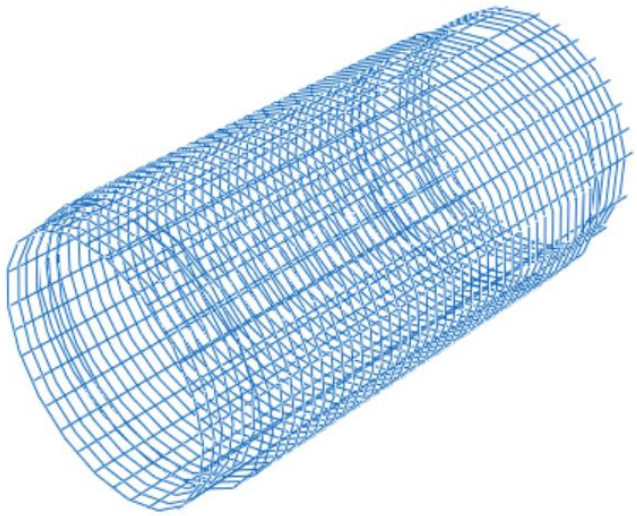

Figure 4.1-Non-Iso Symmetrical SE Cage from FEM.

Table 4.2-Geometric Properties of FE Models

Actual Pipe Diameter (mm)	Spacing Between Lower Strips (mm)	Longitudinal Wire Cross-Sectional Area (mm^2)	Circumferential Wire Cross-Sectional Area (mm^2)	Circumferential Wire Spacing (mm)
1067	88	28.94	28.94	50
1219	100	28.94	45.16	50
1219	100	28.94	64.52	50

The concrete pipe and bearings were modelled as hexahedral (8-node brick) isotropic linear solid elements with reduced integration and hourglass control, while the steel reinforcement was modelled as 2-node linear displacement truss line element. The reduced integration solid element was selected to avoid the effect of shear and volumetric locking under bending that occurs in the fully integrated element. Furthermore, the hourglass control option was chosen to eliminate hour-glassing phenomenon that occurs in reduced integration elements, where extreme distortion of the element under bending leads to unreasonable displacement values. An element mesh size of 25 mm was used in the model

for the meshing the pipe in order to maintain reasonable execution time. **Figure 4.2** shows the finite element model of the setup. The interaction between concrete pipe and steel reinforcement was modelled using a truss-in-solid embedded region constraint, where the steel reinforcement acted as the embedded region, while the concrete pipe was the host region. An embedded region constraint assumes a perfect bond between the concrete and steel, where the concrete elements constraints the translational degrees of freedom of the steel elements at the nodes. Moreover, interaction between the bearing strips (upper and lower) at their face and concrete pipe was modelled using a tie constraint. The two lower bearing strips were pinned, preventing translational degrees of freedom in all directions. Static non-linear analysis was performed via distributed 40 mm downward ramping displacement at the upper bearing strip to achieve displacement-controlled loading.

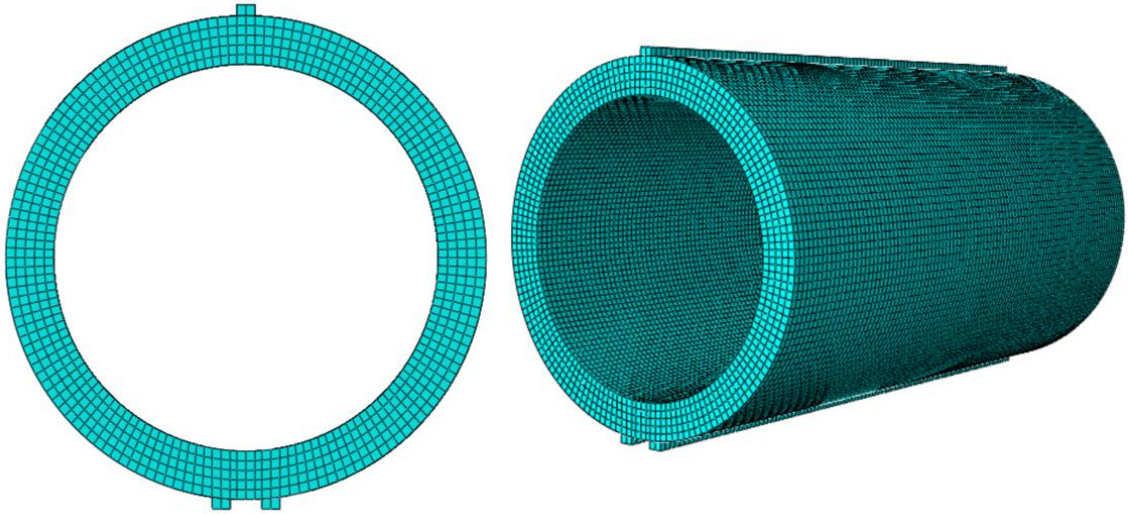

Figure 4.2-Finite Element Model of RCP.

4.3.2 Material Property

4.3.2.1 General Considerations

Concrete exhibits different behaviour under compression and tension. The two main failure mechanisms for concrete are compressive crushing and tensile cracking (Tehrani, 2016). Under uniaxial tension, concrete displays linear elastic stress-strain relationship until the

yield tensile stress(σ_{t0}), **Figure 4.3 (Top),** after which microcracks start to form and are characterized by strain softening in the stress-strain behaviour beyond the peak tensile stress. In compression, the stress-strain relationship to uniaxial compression is linear only up until yield compressive stress , σ_{c0}, **Figure 4.3 (Bottom).** The plastic behaviour under uniaxial compression is characterized by strain hardening until the ultimate compressive stress, σ_{cu} , followed by strain softening beyond the ultimate stress (Smith, Michael, 2009).

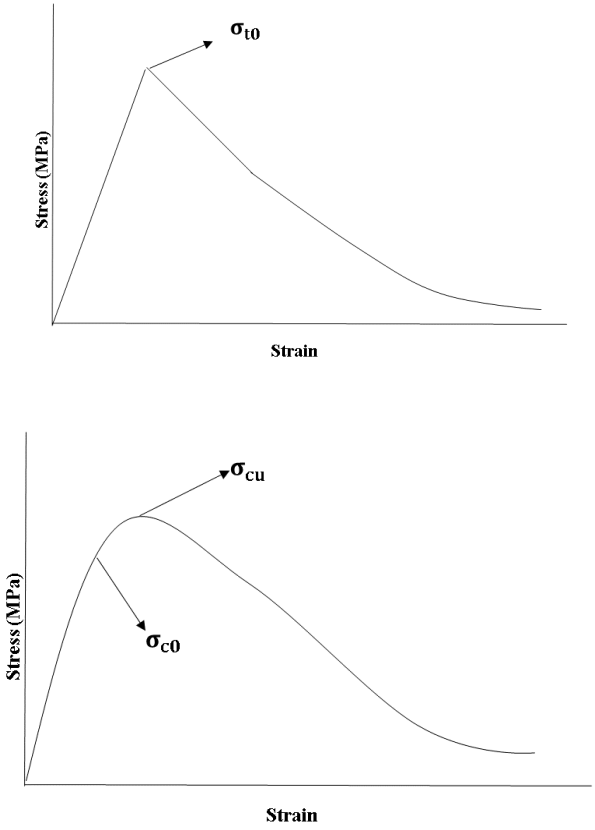

Figure 4.3-Concrete Tensile (Top), and Compressive (Bottom) Stress-Strain Relationship Under Uniaxial Loading (Modified after ABAQUS/Standard User's Manual, Version 6.9).

Constitutive models to analyze concrete are available in ABAQUS/Standard, including concrete smeared cracking (CSC) and concrete damaged plasticity (CDP). CSC is known to have convergence issues after steel yielding. Thus, the CDP model was used (Mohamed & Nehdi, 2016). CDP is generally designed for concrete subjected to monotonic, cyclic, and/or dynamic loading under low confining pressure. It employs both tensile cracking and

compressive crushing of concrete, in addition to degradation mechanisms to represent inelastic behaviour of plain or reinforced concrete (Smith, Michael, 2009). The model considers both the damage model of brittle concrete and plasticity model of ductile steel.

The concrete tensile behaviour in the CDP model was considered by introducing tension stiffening, which accounts for strain softening in the uniaxial tension behaviour. Tension stiffening can be defined either by post-failure stress-strain relationship or by fracture energy cracking criterion (G_f). However, stress-strain relationship introduces unreasonable mesh sensitivity into the results in areas where steel reinforcement does not exist, as is the case in RCP where there are significant regions with no reinforcement. As such, the fracture energy cracking criterion was implemented to define tension stiffening characterized by a stress-displacement relationship developed by Hillerborg *et al.* (Smith, Michael, 2009) (Hillerborg et al., 1976). Under tension, concrete will crack across its critical section. After concrete has been pulled apart sufficiently for most of the stresses to be removed so that the undamaged elastic strain is minimal, its length will be primarily influenced by the opening at the crack. The crack opening is not dependent on the length of the specimen (Smith, Michael, 2009). The fracture energy cracking criterion is represented by determining the post-failure stress as a function of the cracking displacement (u_t^{ck})**.** The cracking displacement is defined by ($u_t^{ck} = 2G_f/\sigma_{t0}$) where ($\sigma_{to}$) is the tensile stress and (G_f) is fracture energy ranging from 40 N/m to 120 N/m for concrete compressive strength of 20 MPa to 40 MPa, respectively.

The stress-strain behaviour of concrete beyond ultimate stress and into strain softening under uniaxial compression can be defined by considering the stress-inelastic strain relationship. The compressive inelastic or crushing strain (ε_c^{in}) can be defined by $\varepsilon_c^{in} = \varepsilon_c - \varepsilon_c^{el}$ where (ε_c) is the total strain and ($\varepsilon_c^{el} = \sigma_c/E_0$) is the elastic strain of the undamaged materials, E_0 is the modulus of elasticity (Smith, Michael, 2009).

The microstructure plasticity of concrete in the CDP model is defined by several parameters including *Kc*, the ratio of the second stress invariant on tensile meridian to that on the compressive meridian, and f_{b0}/f_{c0}, the ratio of the initial equi-biaxial compressive yield stress and the initial uniaxial compressive yield stress (Hamedani & Esfahani, 2012).

The dilation angle (ψ) and eccentricity (e), control the plastic straining behaviour of the material (Blazejowski, 2012). The viscosity parameter (μ) is related to the rate of strain and affects convergence. Convergence difficulties can arise from the strain softening behaviour of concrete. The values of parameters set for the model are shown in **Table 4.3** and were chosen based on successful studies related to CDP model (Mohamed & Nehdi, 2016), (Tehrani, 2016), (Hamedani & Esfahani, 2012), (Blazejowski, 2012), (Alfarah et al., 2017).

Table 4.3-Concrete Plasticity Parameters used in FE Model

Parameters	Value
K_c	0.667
f_{b0}/f_{co}	1.16
Dilation angle (ψ)	36°
Eccentricity (e)	0.1
Viscosity (μ)	0.0001

4.3.2.2 Behaviour of Concrete in Compression

Several researchers have developed numerical equations and analytical approaches to predict the non-linear compressive stress-strain behaviour of concrete under uniaxial compression. The ultimate stress in these analytical approaches is usually a function of several different factors. Alfarah *et .al* (Alfarah et al., 2017) developed a new methodology for calculating damage variables in CDP for reinforced concrete structures. The methodology is based on previous work of Lubliner/Lee/ Fenves (Lubliner et al., 1989) (Lee Jeeho & Fenves Gregory L., 1998), which is the base for the CDP model in ABAQUS. However, no guidelines are provided for the damage variables in the Lubliner/Lee/Fenves approach, which are user-defined. The Alfarah *et .al* (Alfarah et al., 2017) approach modifies the work of Lubliner/Lee/Fenves to develop closed form equations for damage variables in terms of strain and are derived from concrete fracture and crushing energy. This approach is validated for mesh insensitivity by incorporating the mesh size into its equations. Thus, it was used to develop the compression stress-strain behaviour of concrete in this chapter.

Figure 4.4 is a graphical representation of the compressive stress-strain behaviour of concrete under uniaxial compression corresponding to **Figure 4.3 (b)** with the parameters

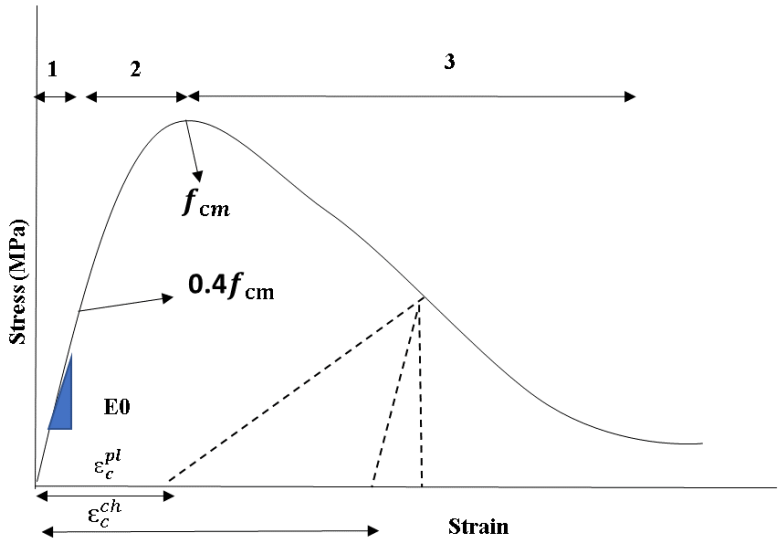

Figure 4.4-Alfarah *et. al* Concrete Compressive Stress-Strain Relationship with Parameters (After Alfarah *et. al.*, 2017).

used in the analytical approach. The input parameters required for concrete compressive stress-strain behaviour are the concrete compressive strength, f_{cm}, which is the peak compressive stress, the mesh size, l_q, and the ratio $b = \varepsilon_c^{pl} / \varepsilon_c^{ch}$, where ε_c^{pl} and ε_c^{ch} are the plastic and crushing components of strain respectively. An initial value of $b = 0.9$ was assumed for the approach. According to the previous study (Alfarah et al., 2017), it is assumed that the value of the corresponding compression strain for the peak compressive stress is $\varepsilon_c = 0.0022$. It is also assumed that the peak tensile stress strength is $f_{tm} = 0.3016 f_{ck}^{2/3}$. Thus, the initial tangent modulus of deformation of concrete, $E_{ci} = 10000\ f_{cm}^{\frac{1}{3}}$, which is the elastic modulus at the peak strain, and the undamaged modulus of deformation, $E_0 = E_{ci}(0.8 + 0.2\frac{f_{cm}}{88})$, can be calculated. Furthermore, the fracture and crushing energy (N/mm) can be calculated by the following relationships, respectively, $G_f = 0.073 f_{cm}^{0.18}$ and $G_{ch} = (\frac{f_{cm}}{f_{tm}})^2 G_f$. Once these values have been obtained, the first, second, and third segments of the concrete uniaxial compressive stress-strain relationship can be built (**Figure 4.4**) using equations developed by Alfarah *et .al* (Alfarah et al., 2017) for each segment. The first segment, σ_{c1}, is linear, reaching $0.4 f_{cm}$. The second segment, σ_{c2} is ascending (between $0.4 f_{cm}$ and f_{cm}), and the third segment, σ_{c3}, is descending. In

the third segment, the strain is bounded, with the condition that the selected upper bound should reach the crushing energy, G_{ch}. The damage parameters are then calculated along with the compressive damage variable, d_c, through relationships developed by Alfarah *et .al* (Alfarah et al., 2017) and incorporate the mesh size, l_q. The final step is to calculate the plastic compressive elastic strain $\varepsilon_c^{pl} = \varepsilon_c^{ch} - \sigma_c d_c/(1-d_c)E_0$ and the ratio of *b*, which must be compared to the initial assumptions and the steps must be repeated until the value of *b* converges. More details on the Alfarah *et .al* analytical approach and equations can be found in (Alfarah et al., 2017). **Figure 4.5** is the stress-strain curve developed for the FEM in the following research for a peak compressive strength of 60 MPa based on the range of concrete strength for the experimental values of the tested SE pipes. The modulus of elasticity of concrete was obtained via the relationship defined by Alfarah *et .al,* while Poisson's ratio (υ) was taken as 0.2.

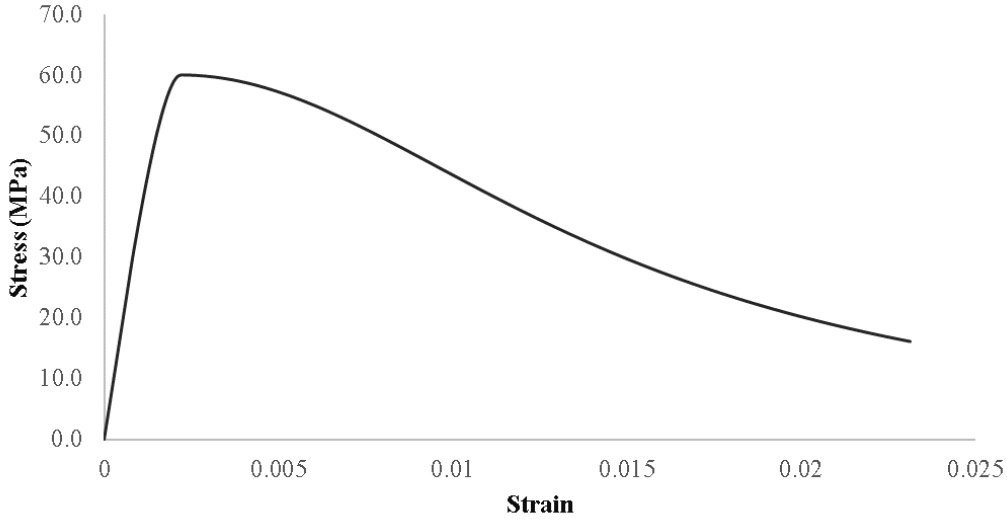

Figure 4.5-Concrete Compressive Stress-Strain Behaviour Used in FEM.

4.3.2.3 Concrete Tensile Behaviour

The concrete uniaxial tensile behaviour was developed using the fracture energy cracking criterion discussed earlier and characterized by the stress-displacement relationship. Although Alfarah *et .al* (Alfarah et al., 2017) define the tensile behaviour by a stress-strain relationship, it is known to introduce unreasonable mesh sensitivity for sections with no

reinforcement. Thus, a stress-displacement relationship was adopted. The peak tensile stress, f_{tm}, and fracture energy, G_f, were calculated from Alfarah *et .al* equations and used to develop the tensile stress-displacement relationship, as shown in **Figure 4.6**.

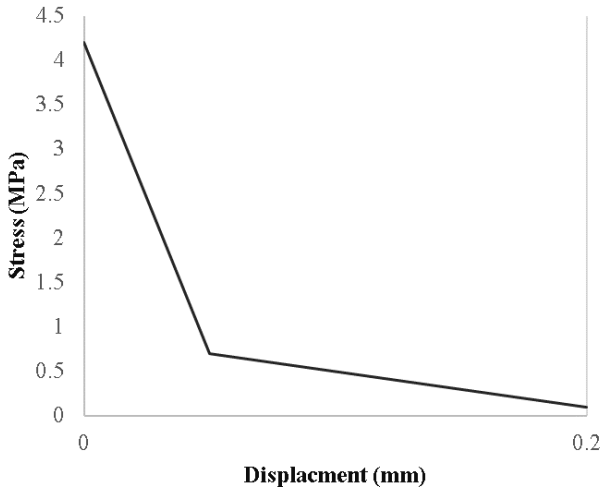

Figure 4.6-Concrete Tensile Stress-Displacement Relationship Used in FEM.

4.3.2.4 Steel Reinforcement and Bearing Strips Material Properties

The steel reinforcement used was deformed cold-drawn steel wires with yield strength, f_y, of 620 MPa as per ASTM A1064 (Standard Specification for Carbon-Steel Wire and Welded Wire Reinforcement, Plain and Deformed, for Concrete) (ASTM A1064/A1064M-18a, 2018). The elastic modulus (E_s) and Poisson's ratio (υ) were taken as 200000 GPa and 0.3, respectively. The upper and lower bearing strips were assumed as infinitely rigidity and assigned enlarged elastic modulus and Poisson's ratio of 0.3.

4.4 Model Calibration and Validation

4.4.1 Model Calibration

The FEM with initial CDP parameters from the material properties mentioned above was calibrated using the equivalent experimental result E21. **Figure 4.7** shows a comparison of the numerical and experimental load deflection curves of the pipe reinforced with SE steel

cage under TEBT. The load-deflection curve of the experimental test exhibited a linear response, followed by an abrupt decease in load carrying capacity. The pipe then regained full capacity in the plastic phase, surpassing its elastic load and exhibiting large deformations until failure. Similarly, the FEM indicated a linear increase in deflection and load. However, the decrease in load carrying capacity was not as distinct as in the experimental curve. Instead, the FEM curve displayed a deflection hardening behaviour until ultimate capacity. The uncalibrated FEM overestimated the D_{ult} load of the experimental result, E21, by 84.2%, thus a sensitivity analysis was performed to adjust the assumed parameters and calibrate the model.

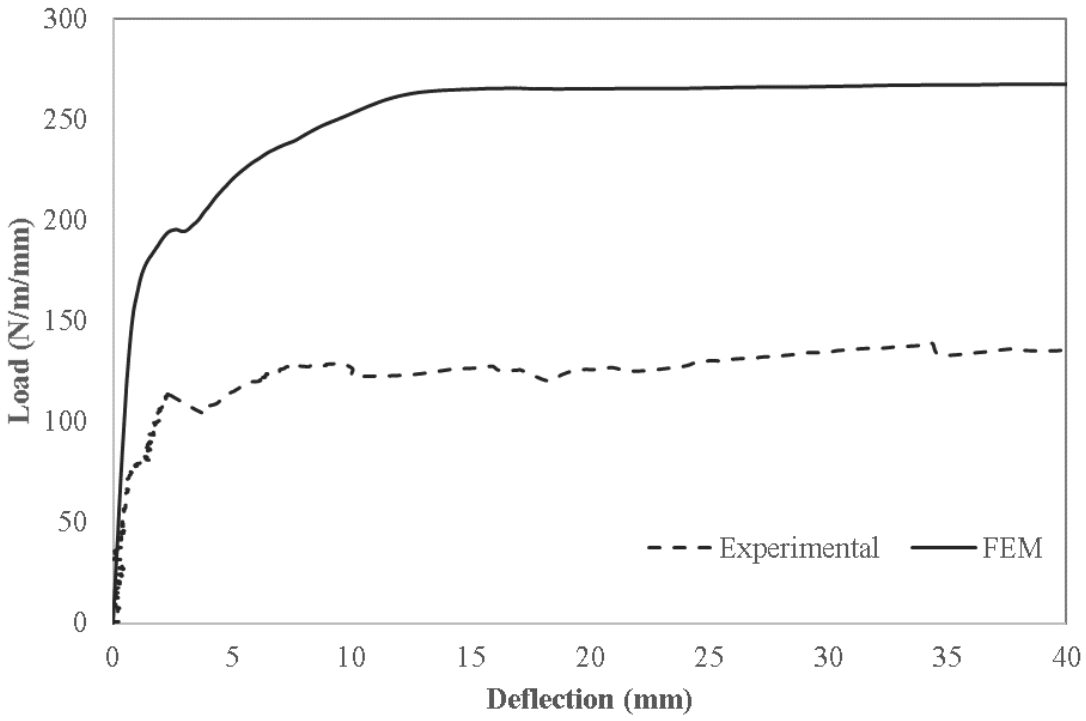

Figure 4.7-Load-Deflection Curve of Numerical Model with Initial CDP Parameters vs. Experimental.

The sensitivity study was performed by varying the material properties to quantify their effects on the numerical model behaviour and output. Blazejowski (Blazejowski, 2012) explored the behaviour of steel fibre-reinforced tunnel linings and indicated that the tension stiffing parameters had a significant effect on the numerical model outputs. Yet, the

compressive stress-strain relationship and Passion's ratio were not as significant. These findings were confirmed in the present chapter through several numerical runs showing that varying the tension stiffening relationship had greater effect on the model output than varying the compressive stress-strain relationship. The effects of varying the concrete plasticity parameters were not investigated since the chosen values of the properties are comparable to that recommended by several other studies with similar applications. Furthermore, the effect of varying the concrete elastic modulus, E_c, was not considered since the FEM showed good agreement with the experimental curve in the linear phase up to 80 N/m/mm where the first hairline crack occurred experimentally, confirming that the Alfarah et al. (Alfarah et al., 2017) assumption was reasonable. As such, the main parameter investigated in this sensitivity analysis was the tensile stiffening parameters.

The tension stiffening parameters used in the FEM were based on the fracture energy cracking criterion and characterized by a peak tensile stress-displacement relationship. The stress-displacement relationship was defined by three points in order to facilitate the calibration and reduce the computational time. In the sensitivity study, the peak tensile stress obtained from the Alfarah model and the corresponding displacements were adjusted, while maintaining a constant fracture energy, G_f, before and after adjustments.

The tension stiffening parameters influence the stress transfer from the cracked concrete section to the steel reinforcement as concrete cracks propagate. The loading pattern of the RCP under the TEBT is characterized by the development of microcracks at the early stage of loading. As the load increases, the cracks propagate, inducing stress transfer from the cracked concrete sections to the steel reinforcement. The steel reinforcement becomes fully effective at the latter stages of loading. Eventually, the steel reinforcement yields and is followed by ultimate failure of the pipe. The elastic phase response is affected by the crack development in the tensile concrete and stress transfer from the cracked concrete section to the steel reinforcement. While the plastic phase response is significantly influenced by steel reinforcement.

4.4.2 Model Validation

An extensive parametric study was conducted to validate the model by adjusting the tensile stiffening parameters. **Figure 4.8** shows the calibrated numerical load-deflection curve with modified tensile stiffening parameters. The experimental and numerical load-deflection curves showed similar response in the elastic phase up to 10 mm deflection. However, the numerical load-deflection curves did not indicate a decrease in load carrying capacity; rather the load increased at a constant rate in the plastic phase until 40 mm deflection. The numerical result showed a 33% error for the ultimate load capacity after calibration compared to the experimental result. Contrarily, **Figure 4.9** displays a comparison between the experimental and numerical load-deflection curves for RCP with conventional double layer steel cage reinforcement. The tensile stiffening parameters used were the same parameters used for the elliptical cage pipe model. For the RCP model with conventional reinforcement, the prediction error for D_{ult} was 4.1% as opposed to 33% for the elliptical cage RCP model.

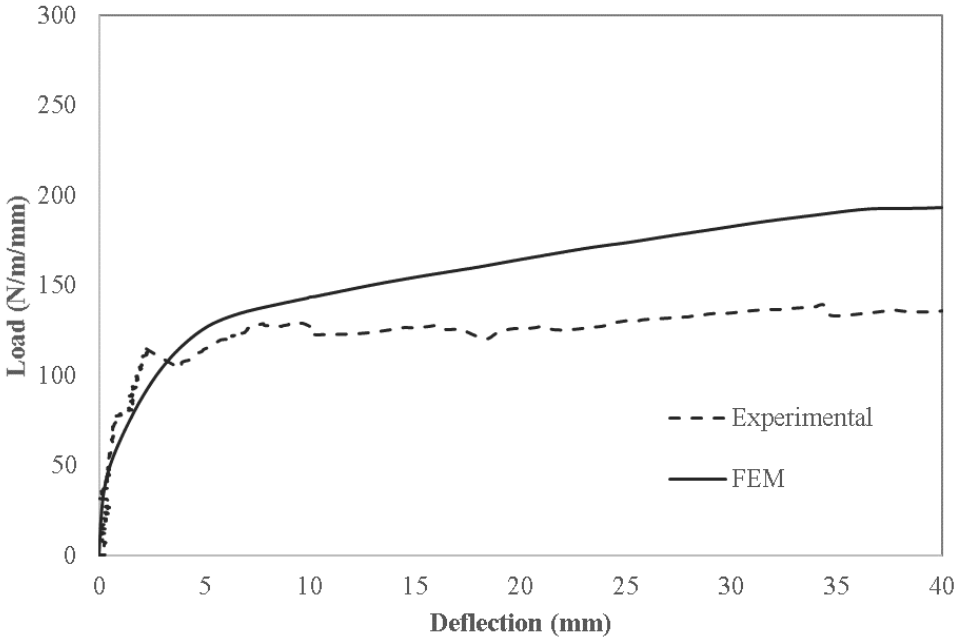

Figure 4.8-Load-Deflection Curve of Single Elliptical RCP Numerical Model with Modified Tensile Stiffening Parameters.

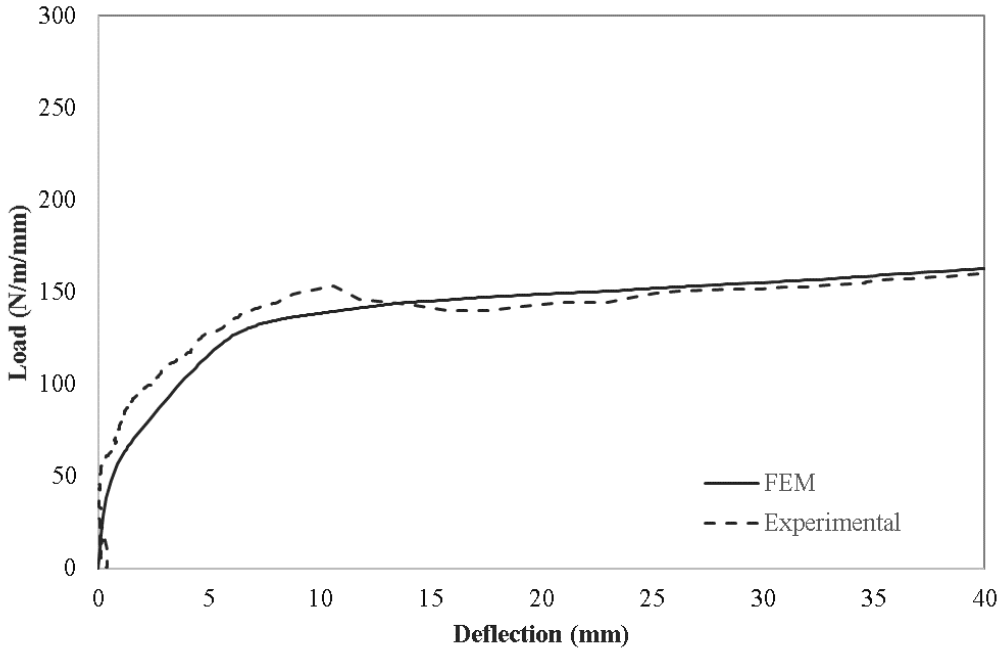

Figure 4.9- Load-Deflection Curve of Double Circular Cage RCP Numerical Model with Modified Tensile Stiffening Parameters.

The relatively high error and variation between experimental and numerical result for the elliptical pipe FEM can be attributed to the significant change of cross-section of the pipe due to the failure mode. Experimentally, the pipe fails in radial tension followed by concrete slabbing (**Figure 4.10**). Radial tension failure is dependent on the concrete strength and the reduction of the wall thickness without reinforcement. Thus, the pipe with elliptical cage reinforcement cannot sustain large load-bearing capacity because the second layer of steel in a double cage configuration plays an important role in the ultimate capacity of the pipe. Most significantly, the experimental observations of RCP with SE cage reinforcement under TEBT revealed that the pipe reached ultimate failure before yielding of the steel. Thus, the steel reinforcement under TEBT did not reach full yielding capacity, which reduced the effectiveness of the steel cage reinforcement. However, the FEM indicated steel yielding towards the end of loading. Furthermore, welding stresses in the steel wire (about 0.35 MPa per weld (Diehl et al., 2017)) and internal stresses that can arise from bending of the steel wires during the RCP manufacturing stage were not accounted for in the FEM.

Figure 4.10-Concrete Slabbing Failure in RCP with SE Cage Reinforcement

It was concluded that the FEM load-deflection curves for the elliptical cage pipes showed good agreement with the corresponding experimental data up to 10 mm deflection, which is beyond the threshold of the load where the 0.3 mm crack occurs. As such, the models were validated with the equivalent experimental results up to 10 mm deflection. The validation of the numerical models was based the load values $D_{\delta=0.36\%}$ and D_{10mm} instead of the load values $D_{0.3}$ and D_{ult} obtained experimentally. These load values were also used to evaluate the effect of the rotation of the cage reinforcement on the load-deflection curve of the SE pipes. The reason for evaluating $D_{\delta=0.36\%}$ as an alternative to $D_{0.3}$ is the fact that the 0.3 mm crack cannot be detected in the FEM due to limitation of the CDP model. Thus, $D_{\delta=0.36\%}$ was used to evaluate the elastic response of the pipe.

Figures 4.11 (a), (b), and (c) show the numerical load-deflection curves with calibrated tension stiffening parameters up to 10 mm deflection. The load-deflection curves indicate good agreement with experimental results. **Table 4.1** shows a comparison between the predicted numerical results and corresponding experimental results for $D_{\delta=0.36\%}$ and D_{10mm}. The numerical results had 9.8% and 9% average error for $D_{\delta=0.36\%}$ and D_{10mm}, respectively. It can be concluded that the finite element model reasonably predicted the experimental results.

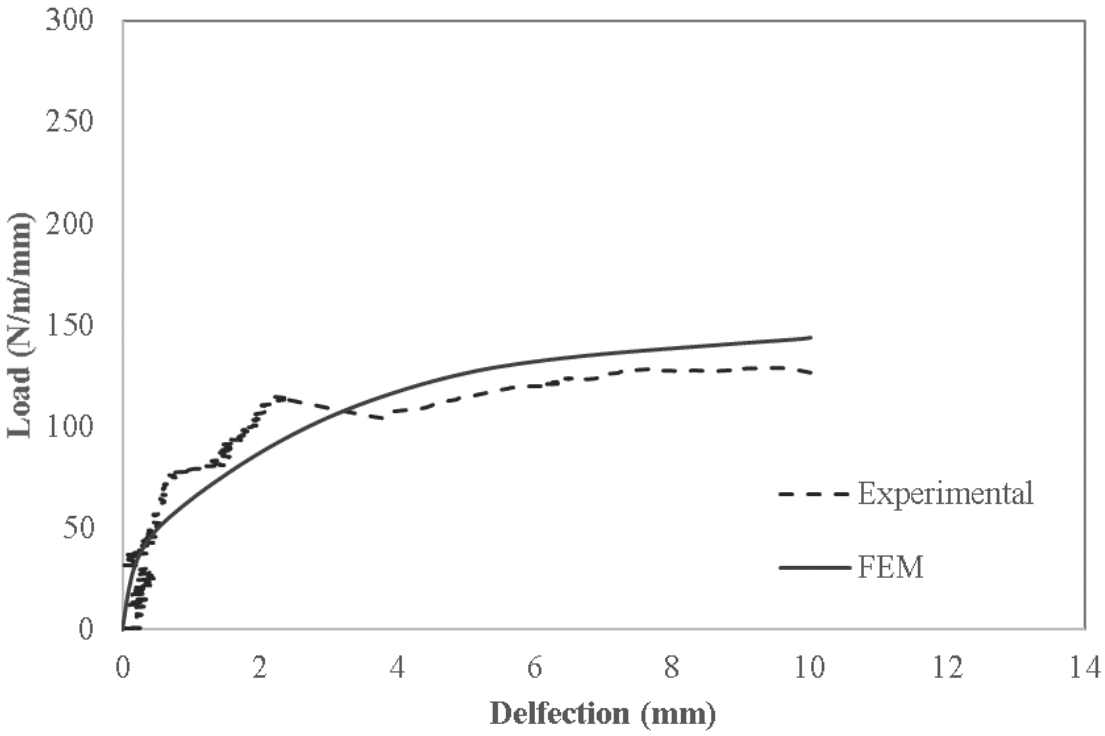

(a) 1050 mm and *Asi*=581 mm^2/m

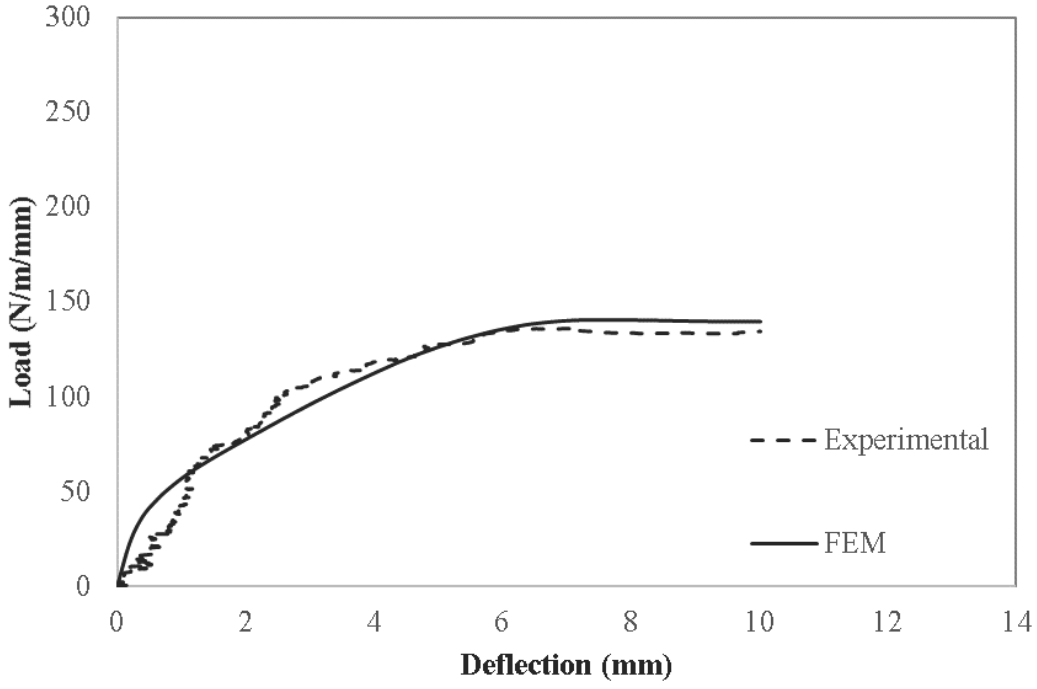

(b) 1200 mm and *Asi*=903 mm^2/m

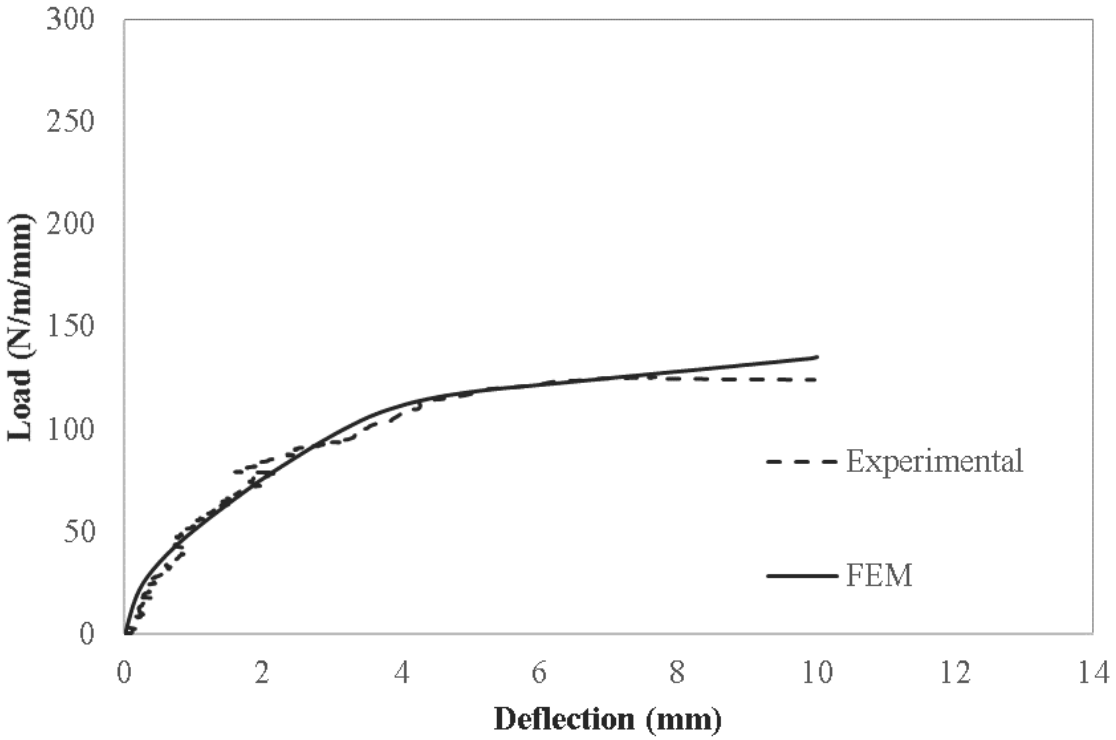

(a) 1200 mm and *Asi*=1290 mm^2/m

Figure 4.11-Comparison between Numerical and Experimental Load-Deflection Curves for SE RCP (a) 1050 mm, (b) 1200 mm, and (c) 1200 mm up to 10 mm Deflection.

The stress distribution of principle stresses in **Figure 4.12** illustrate the propagation of maximum principle stresses in the pipe. Similar to the experimental behaviour of the pipe, the stresses started developing at the inner face of the invert and obvert and the outer face of the spring-lines in the early elastic stages of loading of the pipe prior to reaching $D_{\delta=0.36\%}$ (**Figure 4.12** (**a**))**.** As loading propagated beyond $D_{\delta=0.36\%}$ and cracks begun to form, stresses shifted diagonally towards the bearing supports of the pipe indicative of diagonal shear cracking (**Figure 4.12** (**b**))**.** As the loading developed plastically towards D_{10mm}**,** localized tensile stresses started developing at the upper and

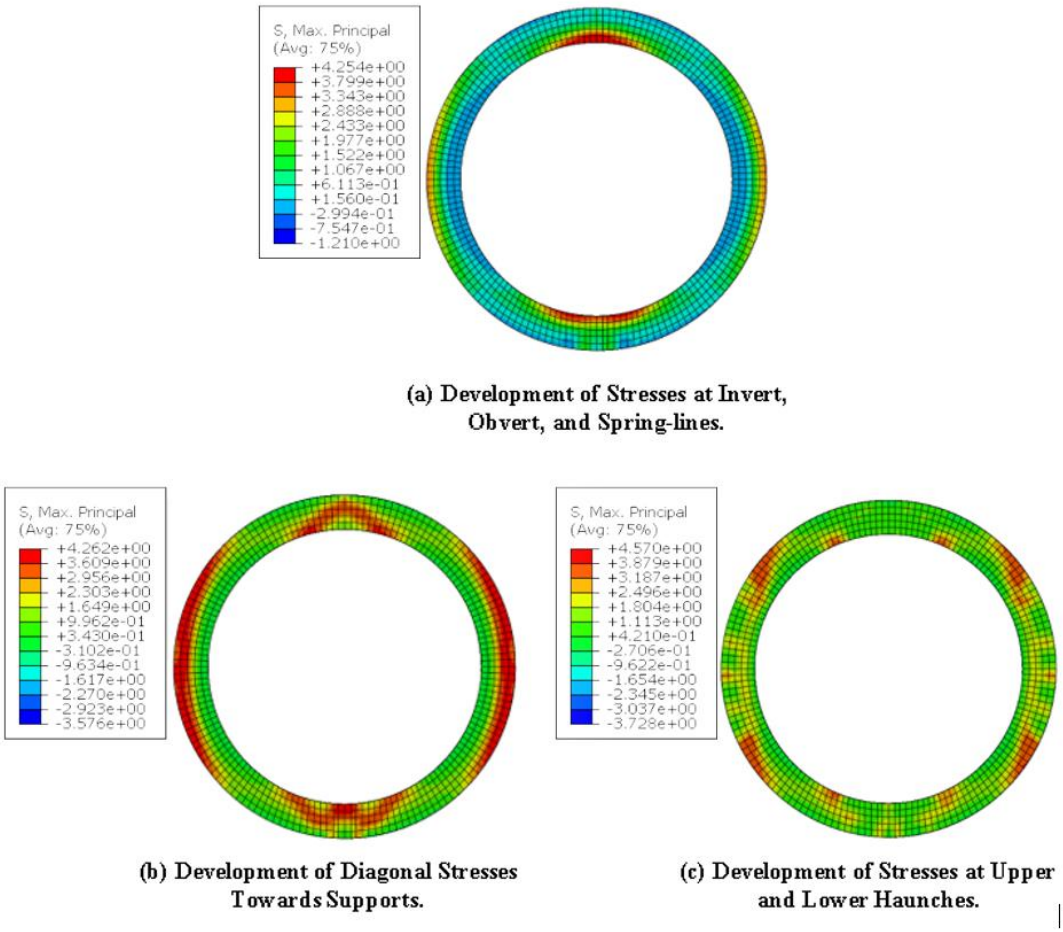

Figure 4.12- Progression of Principle Stress in Finite Element Model (a) In Elastic Phase Prior to $D_{\delta=0.36\%}$, (b) Beyond $D_{\delta=0.36\%}$, and (c) Plastic Phase Towards D_{10mm} (stress in MPa).

lower haunches of the pipe as the load resistance of the damaged concrete section decreased and stresses were transferred to the undamaged area of the concrete, indicating the formation of the plastic hinges at the upper and lower haunches (**Figure 4.12** (**c**)). However, stresses decreased at the outer face of the spring-lines of the pipe as the RCP deteriorated, indicating stress transfer towards the steel reinforcement in the plastic phase.

4.5 Discussion

4.5.1 Effect of Elliptical Reinforcing Cage Rotation

4.5.1.1 General Aspects

A parametric study was conducted using the constructed 1050 mm FEM to investigate the sensitivity of the pipe with SE cage reinforcement to the mis-orientation of the cage that can arise from the manufacturing or installation process. There are two main implications to the rotation of the single elliptical reinforcement that affect the structural capacity of the pipe: i) the rotation causes the cage to shift away from the tensile zones at the invert, obvert, and spring-lines of the pipe under the TEBT; and ii) the rotation results in an increase in the concrete cover at the invert and obvert of the pipe, which in turn affects structural capacity. The cage reinforcement was rotated at 5° increments up to 45° to consider various scenarios of cage rotations that can occur during manufacturing. Further scenarios at 60°, 75°, and 90° cage rotations were also analyzed. The 90° cage rotation is considered the most extreme case where the concrete cover at the invert is maximum. **Figure 4.13** shows an RCP with SE cage reinforcement in the original design position and how the concrete cover at the invert would get affected from a 45° rotation of the cage reinforcement. The increase in concrete cover leads to reduction of the effective depth of the compression zone under loading, thus influencing the serviceability crack and ultimate capacity of the pipe according to Heger (Heger, 1963).

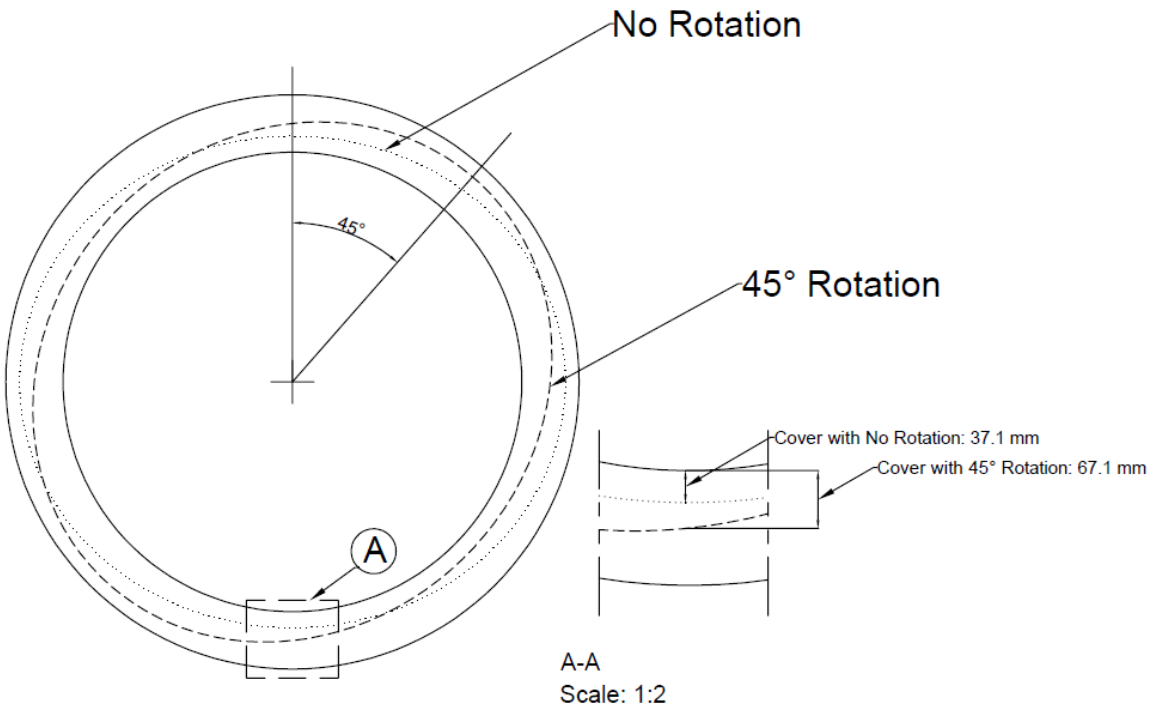

Figure 4.13-Effect of Cage Rotation on Concrete Cover at the Pipe Invert.

4.5.1.2 Serviceability and Stiffness of Pipe

Figure 4.14 shows the load-deflection curves obtained for the 1050 mm pipe at different rotation angles of the cage reinforcement. These load-deflection curves indicate that the overall load capacity of the pipes decreased as a result of rotation of the elliptical reinforcing steel cage. However, the general behaviour of the load deflection curves was comparable between pipes with rotated cages, with the pipe experiencing an increase in load capacity towards D_{10mm}. **Table 4.4** reports the load capacity results $D_{\delta=0.36\%}$ and D_{10mm} for pipe FEMs with different rotation angles. To assess the effect of the cage rotation on RCP structural performance, the load values at different deflection limits: (**i**) 0.2 mm deflection, (**ii**) 1 mm deflection, **(iii)** deflection at $D_{\delta=0.36\%}$ corresponding to 3.84 mm, **(iv)** 5 mm deflection, and **(v)** 10 mm deflection , D_{10mm}, with respect to the rotation angle were plotted in **Figure 4.15**.

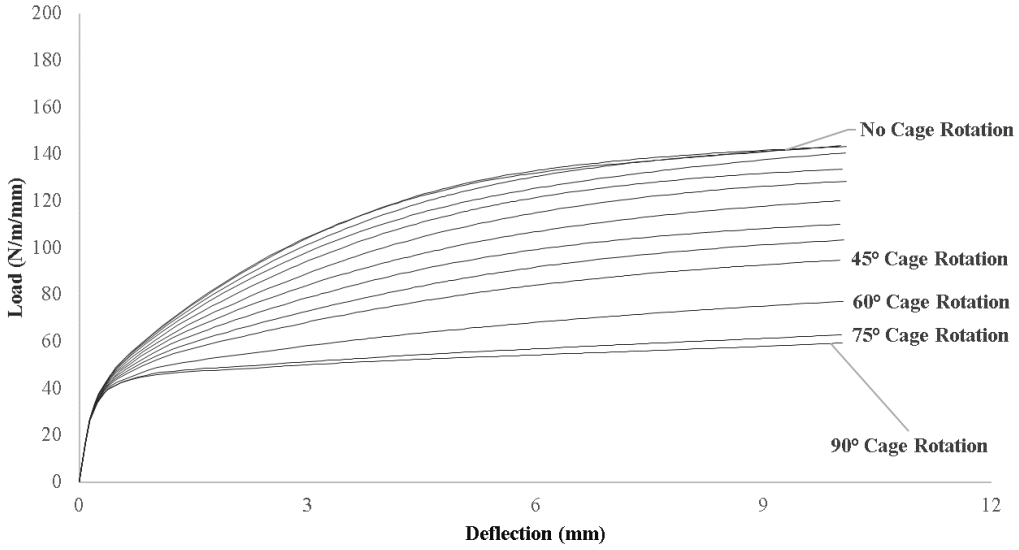

Figure 4.14-Load-Deflection Curves for 1050 mm Pipe with Cage Rotation at Different Angles.

Table 4.4- Numerical Results of $D_{\delta=0.36\%}$ and D_{10mm} (N/m/mm) for Different Angles of Cage Rotation

Rotation Angle	$D_{\delta=0.36\%}$ (N/m/mm)	D_{10mm} (N/m/mm)
0°	115.4	143.7
5°	115.4	143.3
10°	112.3	143.3
15°	108.6	140.6
20°	104.3	133.6
25°	98.4	128.4
30°	92.1	120.0
35°	85.9	110.0
40°	79.2	103.4
45°	73.4	94.8
60°	61.4	77.1
75°	53.1	62.8
90°	51.5	59.4

The cage rotation had no significant effect on the load when the pipe was deflected by 0.2 mm. A minor reduction in load occurred with respect to the cage rotation when the deflection reached 1 mm **(Figure 4.15).** In the initial stages of TEBT, the load was not substantial to affect the elastic performance of the pipe as micro-cracks started forming in the undamaged concrete. The stiffness of the pipe started decreasing when the magnitude of the load increased, and hairline cracks started to form. Massenzio *et. al* (Massenzio et

al., 2005) reported that steel reinforcement had no significant influence on natural frequency, which is a function of stiffness, in the pre-cracked concrete section. The minimal effect of the rotation on the pre-cracked stiffness of the pipe observed in the results is explained below.

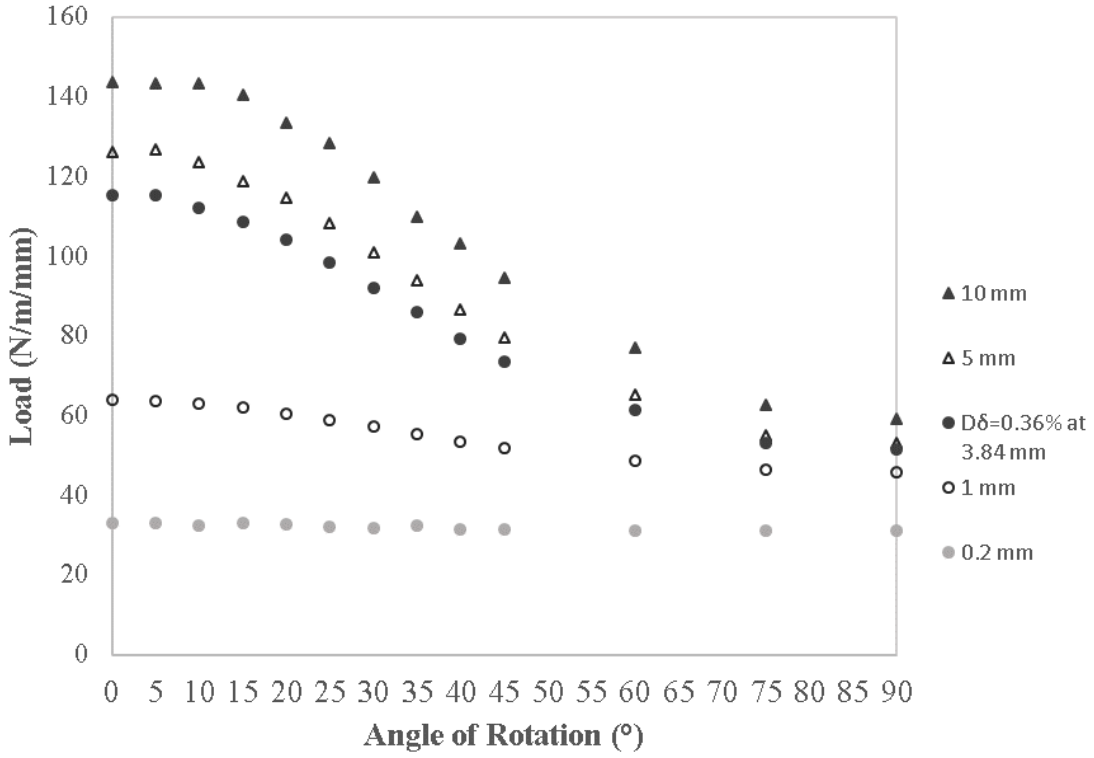

Figure 4.15- Load vs. Angle of Rotation at 0.2 mm Deflection, 1 mm Deflection, Deflection at $D_{\delta=0.36\%}$, 5 mm Deflection, 10 mm Deflection, D_{10mm}, Deflection Limits.

The increase TEBT load magnitude and formation of cracks resulted in transfer of stresses from the damaged concrete to the undamaged concrete sections. At this stage, the rotation of the cage reinforcement indicated greater influence on the serviceability of the pipe at **(iii)** $D_{\delta=0.36\%}$ (**Figure 4.15**). The $D_{\delta=0.36\%}$ load capacity value was greatly decreased from 0°, which is the intended design position, to 90° rotation, the most extreme rotation case. The service load capacity, $D_{\delta=0.36\%}$, decreased by 76.6% between these two scenarios. According to Massenzio *et. al* (Massenzio et al., 2005), the effect of the steel reinforcement had significant influence on the natural frequency, of concrete beyond concrete cracking. Thus, it was observed that the influence of the steel reinforcement grew from the lower

deflection limits towards the deflection limit at $D_{\delta=0.36\%}$, where multiple hairline cracks had formed.

Figure 4.16 illustrates the pipe stiffness, $S_{\delta=0.36\%}$, versus the rotation of the cage. As suggested in previous study (Massenzio et al., 2005), the RCP stiffness was more influenced by the steel reinforcement in the post-cracked concrete section. The stiffness values in **Figure 4.16** indicate that at the service load capacity $D_{\delta=0.36\%}$, the stiffness of the pipe was significantly decreased as a result of rotation of the cage reinforcement. The reduced effective depth of the reinforcement, as a result of the rotation, decreased the required load to reach the deflection limit of 3.84 mm.

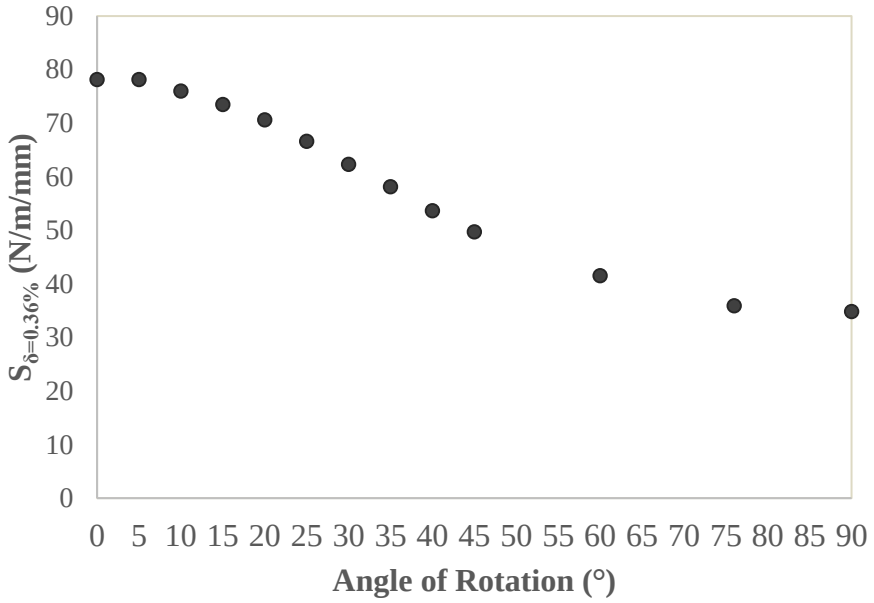

Figure 4.16- Stiffness $S_{\delta=0.36\%}$ vs. Angle of Rotation.

4.5.1.3 Plastic Behaviour and Load Capacity of Pipe

The loss of sectional capacity due to concrete cracking transfers the load bearing capacity of the pipe from the damaged concrete to the steel reinforcement. Thus, at the latter stages of loading, the steel reinforcement influence on the load resistance of the pipe becomes greater. The load capacity results at deflection limits of **(iv)** 5 mm and **(v)** 10 mm, D_{10mm}, in **Figure 4.15** suggest that the elliptical cage rotation had a significant effect on the load

capacity reduction in the plastic phase. The rate of load capacity reduction at 5 mm and 10 mm deflection was comparable, indicating that the rotation of the cage reinforcement influenced the capacity of the pipe early in the plastic behaviour where the steel reinforcement became fully effective. Overall, the reduction of load capacity, D_{10mm}, was 83% between 0° and 90° cage rotation. The rotation of the cage reinforcement had greater effect on the load capacity D_{10mm} than the service load $D_{\delta=0.36\%}$ since the steel reinforcement became fully effective in the plastic phase. It was found in the experimental study in Chapter 3 that using SE cage reinforcement affected the end behaviour of the pipe, which corroborates the suggestion that the rotation of the cage reinforcement had a bigger influence on D_{10mm}.

As per CSA A257 (CSA A257-14, 2014) and ASTM C76 (ASTM C76-16, 2016) requirements, variation in the nominal position of the reinforcement shall not be greater than 13 mm for the 1050 mm pipe. **Figure 4.15** indicates that at 5 mm and 10 mm deflection, the cage rotation up to 10° had minimal effect on the load capacity of the pipe. This can be attributed to the fact that the change of concrete cover at 10° was not significant and is within the variation limits specified by the standards. Moreover, the steel reinforcement was still within the tensile zones of the pipe under the TEBT and had not shifted greatly from the original position.

It was observed that the effect of the cage rotation on the load capacity of the pipe beyond 75° rotation was not significant. At 75° rotation, the reinforcement position shifted mostly from the tensile zone under TEBT into the compression zone. Thus, the steel reinforcement was not resisting the tensile forces in the pipe and was ineffective. Rather, the weaker concrete was resisting tensile forces, which explains why the pipes with 75° and 90° cage rotation did not regain much capacity in the plastic phase.

4.5.2 Effect of Non-Iso Symmetry of Single Elliptical Cage

The SE cage configuration used in the experimental study in Chapter 3 was a nonsymmetric circular-elliptical-circular profile in order to accommodate the joints at the bell and spigot. Ideally, the cage would be truly elliptical along the length of the pipe, as the circular-

elliptical-circular configuration influences the structural capacity. FEM was also used to investigate the effect of the non-iso-symmetrical profile of the cage by modelling the cage reinforcement as a truly symmetrical elliptical cage and comparing the load capacity results with the non-symmetrical elliptical cage. **Figure 4.17** compares the load-deflection behaviour for 1050 mm pipe between the iso-symmetrical and non-iso-symmetrical SE reinforcement. Minimal effect on the capacity was observed at the early loading stage where deflection was less than 2 mm. The capacity for the iso-symmetrical cage showed 5.9% increase compared to that of the non-iso-symmetrical cage at 10 mm deflection.

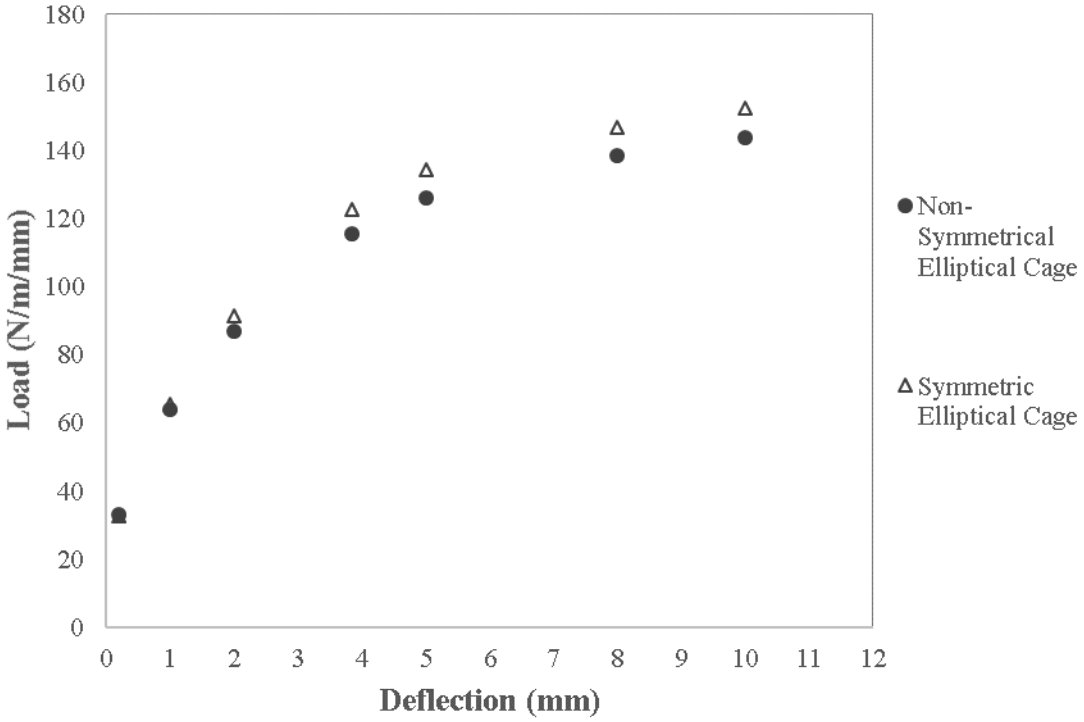

Figure 4.17- Effect of Non-Iso-Symmetrical Elliptical Cage vs. Iso-Symmetrical Elliptical Cage on Load vs. Deflection.

This is attributed to the fact that the reinforcement had greater significance on the structural performance post-cracking of the pipe. The true elliptical profile of the cage occupies 80% of the overall cage. The cage transitions into a circular profile for the remainder 20% of the pipe, which reduces the effective compressive depth to the steel at the pipe spring-lines, thus compromising the flexural capacity of the pipe. Furthermore, the circular portion of

the cage decreased the area of reinforcement in the tensile zones at the spring-lines of the pipe under TEBT loading. The cage transition is inevitable in the SE cage design; thus, the area of steel should be increased to compensate for the reduction in capacity.

4.5.3 Serviceability of Single Elliptical and Double Circular RCP

The FEM was used to assess differences in serviceability limit between the SE pipe and DC pipe. The serviceability limit was based on the correlation of the load values at δ=0.36% and $\delta=D_{0.3}$, representing the deflection values at 0.36% internal pipe diameter and at the crack load, $D_{0.3}$, respectively. **Figure 4.18** shows the correlation between $D_{\delta=0.36\%}$ and $D_{0.3}$ for pipes of different reinforcement area and cage configurations. Both experimental and FEM results were considered in the correlation. The correlation suggests that the $D_{\delta=0.36\%}$ serviceability limit suggested in previous research (Younis et al., 2020) is applicable for mid-size diameter pipes with SE cage reinforcement to predict the serviceability crack load, $D_{0.3}$. Little variation was observed between the SE and DC pipes for $D_{\delta=0.36\%}$ (**Table 4.5**). However, the variation was higher for $D_{0.3}$ for SE cage compared to DC cage, suggesting that the 0.3 mm crack limit is more difficult to observe in RCP with SE cage. The correlation in **Figure 4.18** suggests that serviceability performance of RCP with SE and DC cage configurations is comparable, as suggested in the experimental study in Chapter 3.

Table 4.5- Coefficient of Variance for $D_{0.3}$ and $D_{\delta=0.36\%}$ for SE and DC Pipe Measured in N/m/mm

Cage Configuration	Average $D_{0.3}$	Standard Deviation $D_{0.3}$	Coefficient of Variance $D_{0.3}$	Average $D_{\delta=0.36\%}$	Standard Deviation $D_{\delta=0.36\%}$	Coefficient of Variance $D_{\delta=0.36\%}$	Sample Number
SE Cage	111.7	35.4	31.7	120.8	16.5	13.7	6
DC Cage	125.6	23.0	18.3	125.9	20.3	16.1	5

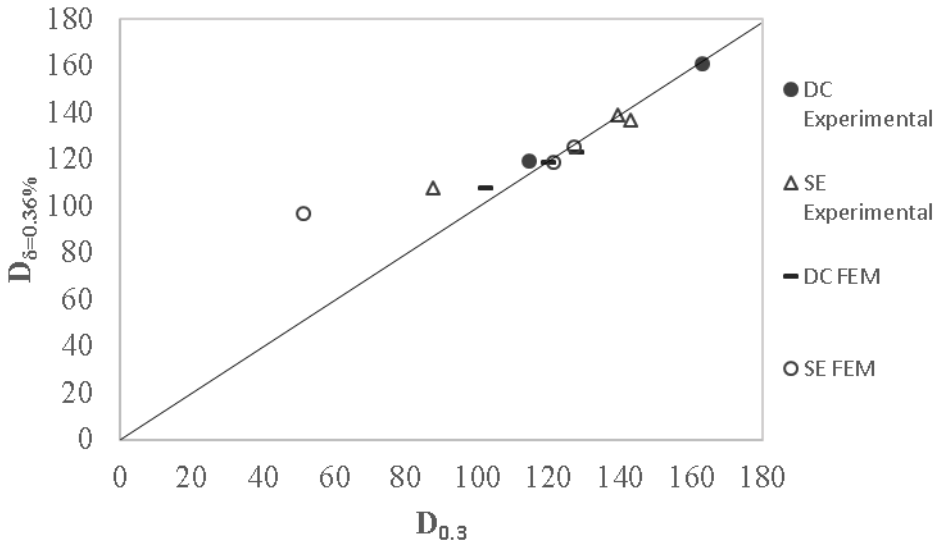

Figure 4.18-$D_{\delta=0.36\%}$ vs. $D_{0.3}$ for SE and DC Pipe Configurations.

4.6 Conclusions

Numerical modelling was used in this chapter to simulate the behaviour of precast concrete pipe reinforced with single elliptical steel cage and to capture the effect of steel cage reinforcement rotation on the load capacity of the pipe. Non-linear 3D FEM was developed and validated using experimental results on full-scale pipes. RCP under TEBT was modelled using the software ABAQUS. The FEM utilized the CDP model to simulate the compressive and tensile behaviour of concrete. From the numerical analysis, the following conclusions can be drawn:

1. The model had an average error of 9.8% and 9% for the serviceability load capacity, $D_{\delta=0.36\%}$, and load capacity at 10 mm deflection, D_{10mm}, respectively. The observed error was attributed to radial tension failure and concrete slabbing/delamination of the pipe with SE cage reinforcement.

2. The rotation of the elliptical cage reinforcement did not have a significant effect on the initial elastic behaviour of the pipe under the TEBT up to 1 mm deflection.

3. As the concrete pipe section became damaged and cracks begun to form, the stiffness and load capacity of RCP decreased with increased rotation of the cage as the load bearing resistance was transferred from the damaged concrete to the steel. FEM suggests that the rotation of the cage reinforcement up to 90° from the design position decreased the serviceability load by 76.6%.

4. The rotation of the elliptical cage reinforcement had a significant effect on the load capacity, D_{10mm}, with an 83% reduction in load capacity observed from 0° to 90° rotation. This signifies that rotation of the cage essentially affects the plastic behaviour of the pipe where the steel reinforcement becomes fully effective.

5. The rotation of the cage reinforcement up to 10° did not have a significant effect on the load D_{10mm} due to the small changes in effective compressive depth. Furthermore, it was found that at 75° and up to 90° rotation, the steel reinforcement became ineffective as most of the reinforcement had shifted away from the critical tensile zone.

6. It was concluded that the cage rotation reduced the depth of the concrete compressive section, which in turn led to reduction of the serviceability load and moment capacity of the pipe.

7. The non-symmetrical shape of the elliptical cage reinforcement did not significantly decrease the load capacity of the pipe, with only 5.9% difference observed between the symmetrical and non-symmetrical elliptical shape at 10 mm deflection.

8. The serviceability performance of RCP with DC and SE reinforcing cage configurations was comparable. Moreover, the deflection limit at 0.36% of pipe diameter was found to be a good indicator to predict the crack load in the SE cage pipes as is the case for DC pipes.

4.7 References

Alfarah, B., López-Almansa, F., & Oller, S. (2017). New methodology for calculating damage variables evolution in Plastic Damage Model for RC structures. *Engineering Structures*, *132*, 70–86. https://doi.org/10.1016/j.engstruct.2016.11.022

ASTM A1064/A1064M-18a. (2018). *Specification for Carbon-Steel Wire and Welded Wire Reinforcement, Plain and Deformed, for Concrete*. ASTM International. https://doi.org/10.1520/A1064_A1064M-18A

ASTM C76-16. (2016). *Specification for Reinforced Concrete Culvert, Storm Drain, and Sewer Pipe*. ASTM International. https://doi.org/10.1520/C0076-16

Blazejowski, M. (2012). *Flexural Behaviour of Steel Fibre Reinforced Concrete Tunnel Linings*. Western University.

CSA A257-14. (2014). *Standards for Concrete Pipe and Manhole Sections*. CSA Group.

de la Fuente, A., Escariz, R. C., de Figueiredo, A. D., Molins, C., & Aguado, A. (2012). A new design method for steel fibre reinforced concrete pipes. *Construction and Building Materials*, *30*, 547–555. https://doi.org/10.1016/j.conbuildmat.2011.12.015

Diehl, C. A. T. S., Rocha, A. da S., Epp, J., & Zoch, H.-W. (2017). Experimental analysis of residual stresses in pre-straightened SAE 1045 steel. *Materials Research*, *20*(6), 1554–1562. https://doi.org/10.1590/1980-5373-mr-2017-0344

Hamedani, R. N., & Esfahani, M. S. (2012). *Numerical Evaluation of Structural Behavior of the Simply Supported FRP-RC Beams*.

Heger, F. (1963). Structural Behavior of Circular Reinforced Concrete Pipe-Development of Theory. *ACI Journal Proceedings*, *60*(11). https://doi.org/10.14359/7905

Hillerborg, A., Modéer, M., & Petersson, P.-E. (1976). Analysis of crack formation and crack growth in concrete by means of fracture mechanics and finite elements. *Cement and Concrete Research*, *6*(6), 773–781. https://doi.org/10.1016/0008-8846(76)90007-7

Kataoka, M. N., da Silva, J. L., de Oliveira, L. M. F., & El Debs, M. K. (2017). FE analysis of RC pipes under three-edge-bearing test: Pocket and diameter influence. *Computers and Concrete*, *20*(4), 483–490. https://doi.org/10.12989/CAC.2017.20.4.483

Lee Jeeho, & Fenves Gregory L. (1998). Plastic-Damage Model for Cyclic Loading of Concrete Structures. *Journal of Engineering Mechanics*, *124*(8), 892–900. https://doi.org/10.1061/(ASCE)0733-9399(1998)124:8(892)

Lubliner, J., Oliver, J., Oller, S., & Oñate, E. (1989). A plastic-damage model for concrete. *International Journal of Solids and Structures*, *25*(3), 299–326. https://doi.org/10.1016/0020-7683(89)90050-4

Massenzio, M., Jacquelin, E., & Ovigne, P. A. (2005). Natural frequency evaluation of a cracked RC beam with or without composite strengthening for a damage

assessment. *Materials and Structures*, *38*(10), 865–873. https://doi.org/10.1007/BF02482253

Mohamed, N., & Nehdi, M. L. (2016). Rational finite element assisted design of precast steel fibre reinforced concrete pipes. *Engineering Structures*, *124*, 196–206. https://doi.org/10.1016/j.engstruct.2016.06.014

Smith, Michael. (2009). *ABAQUS/Standard User's Manual, Version 6.9*. Dassault Systèmes Simulia Corp.

Tehrani, A. D. (2016). *Finite Element Analysis for ASTM C-76 Reinforced Concrete Pipes with Reduced Steel Cage*. University of Texas Arlington.

Younis, A.-A., Ramadan, A., Wong, L. S., & Nehdi, M. L. "New rational test for reinforced-concrete pipe eliminating subjective crack-width criteria" submitted to *Structures*, 2020.

Chapter 5

5 Conclusions, Recommendations, and Future Research

5.1 Conclusions

The research conducted in this study aimed at exploring the structural behaviour of RCP with single elliptical (SE) cage reinforcement as an alternative to the conventional double cage (DC) configuration. While Canadian and American standards permit using SE cage reinforcement in lieu of the DC configuration, SE reinforced pipes are rarely produced due to technological limitations for manufacturing true elliptical shape reinforcing cage. There is also lack of understanding of the structural behaviour of SE reinforced RCP. An extensive experimental and numerical study was conducted herein to fill this knowledge gap and provide the precast concrete industry with information on the manufacturing, structural performance and challenges of utilizing SE reinforced pipe. Successful employment of SE reinforced pipe can lead to material cost savings of up to 30%.

Chapter 3 assessed the structural behaviour of SE reinforced pipe under TEBT loading and focused on the manufacturing of the SE cage. The performance was compared with that of control RCP with conventional DC cage reinforcement and design standard requirements and was analyzed through experimental deflection data. Experimental results showed that, given similar amount of reinforcing steel at the tension zone of the inner face of the invert and obvert of the pipe, RCP with SE reinforcing cage meets lower equivalent class than that of RCP with conventional double reinforcing cage. The absence of a second layer of reinforcement in the SE pipes produced more brittle failure characterized by radial tension, followed by concrete slabbing. Increasing the steel reinforcement ratio improved the 0.3-mm crack load and ultimate load capacity up to a certain threshold, beyond which adding more steel did not enhance the results. Results indicate that RCP with SE reinforcement designed per current standards did not meet the specified 0.3-mm crack and ultimate load

capacity. Hence, pertinent provisions in CSA A257.2 and ASTM C76 for RCP need to be updated with specific and more suitable guidance for single elliptical cage RCP.

In Chapter 4, a non-linear 3D finite element model was developed to evaluate the load capacity of SE reinforced RCP. The concrete damage plasticity model was used to develop constitutive relationships for the concrete compressive and tensile behaviour based on studies in the literature. Model predictions were validated using experimental results on corresponding full-scale pipes from Chapter 3. The model simulated load-deflection curves of RCP under the TEBT and predicted its load capacity with an average error of 9%. A parametric study was conducted to investigate the effects of SE cage rotation on the load capacity of RCP. It was found that SE cage rotation had minimal effect on the elastic behaviour and stiffness of the pipe up to 1 mm vertical deflection. However, SE cage rotation had greater significance on the plastic response of the pipe when the steel reinforcement became fully engaged. Furthermore, the model assessed the effect of the non-symmetrical shape of the elliptical cage reinforcement. Results indicate that the non-symmetrical shape does not have a significant effect on the capacity of the pipe, showing a 5.9% reduction at 10 mm deflection compared to symmetrical elliptical reinforcement. The proposed model could provide a basis for developing design charts for RCP with SE reinforcement and quantify possible effects of SE reinforcing cage rotation on pipe load capacity.

5.2 Major Contributions

This research investigates the applicability of RCP with SE cage reinforcement as an alternative to the conventional DC cage reinforcement used in mid-sized diameter pipes. Accordingly, a knowledge gap is filled concerning the structural performance of RCP with SE cage reinforcement. Specific research contributions include:

1. Investigating the manufacturing process of elliptical steel cage reinforcement. Findings outlined the challenges and modifications undergone in order to manufacture elliptical reinforcing steel cages.

2. Studying the structural performance of RCP with SE cage reinforcement under the three-edge bearing test. The study compared the performance of SE RCP with that of RCP reinforced with conventional steel double cage in order to assess applicability of SE pipe to the RCP industry.
3. Developing a finite element model for RCP with SE cage reinforcement to assess the load capacity of the pipe. The model evaluated the effect of SE cage rotation manufacturing or installation process and assessed the effect of the cage rotation on the structural capacity of the pipe.

5.3 Recommendations and Future Research

While current Canadian and American standards allow for using SE reinforcement in RCP as an alternative to conventional DC reinforcement, no research on the structural behaviour of RCP with SE reinforcement was available in the open literature. Thus, the work reported in this thesis blazes the trail for future research and further studies as follows:

1. In practice, the load distribution around RCP confined in soil is far more distributed around the pipe in comparison to the TEBT loading where the load is severely concentrated. The observed slabbing failure mode of RCP specimens with SE reinforcement may be less problematic in real soil conditions. However, further research is needed to evaluate the failure mode of RCP with SE reinforcement in buried soil conditions compared to the more severe TEBT.

2. One promising research direction would be combining steel fibre reinforcement and single elliptical reinforcing cage to enhance load capacity, ductility and stability of RCP. Steel fibre reinforcement can improve the shear performance of the RCP. Incorporating steel fibres with SE reinforced pipes could reduce radial tension cracking. However, experimental work is needed to validate this.

3. The effect of the cage orientation on the structural capacity might differ in practical applications. It is recommended to carry out modelling of RCP with SE cage reinforcement under realistic soil conditions rather than the TEBT to assess true

structural performance. Furthermore, full-scale tests should be performed in-situ under real soil conditions to assess the effects of rotation of the SE reinforcing cage.

4. Producing full-scale experimental tests on RCP with SE cage reinforcement is a costly and time-consuming process. However, the benefits gained from the material cost savings to the industry make the return on investment worthwhile if design of the SE pipe is optimized. This research provides the building blocks for future research in this area; further studies are indeed needed to validate this research. Further research to assess pipes of different diameters and lengths should be conducted; thus, increasing the sample size.

Appendix A

Three-Edge Bearing Test Reports

THREE-EDGE BEARING TEST REPORT

Test Date	03/12/2018	Mfg. Date	27/11/2018	Test ID	E01
Pipe Size	1200	Class	140D	Length	2.44 m
				Wall	127 mm

Cage Design:

Inner:		@		mm2
Outer:		@		0 mm2
Elliptical:	D12	@	50	1548 mm2

RFT Area

As Inner: 1548 mm2

As Outer:

Age: 7 days

Hairline:	244 kN	82.1 N/m/mm	(Obsv.)	Cover:	mm
M. Hairline:	381 kN	128.2 N/m/mm	(Obsv.)	f'c:	57.8 MPa
0.3-mm:	414 kN	139.3 N/m/mm	(Obsv.)	Equivalent Class:	100 D
Ultimate:	445.2 kN	149.8 N/m/mm	UL/DL:	108%	

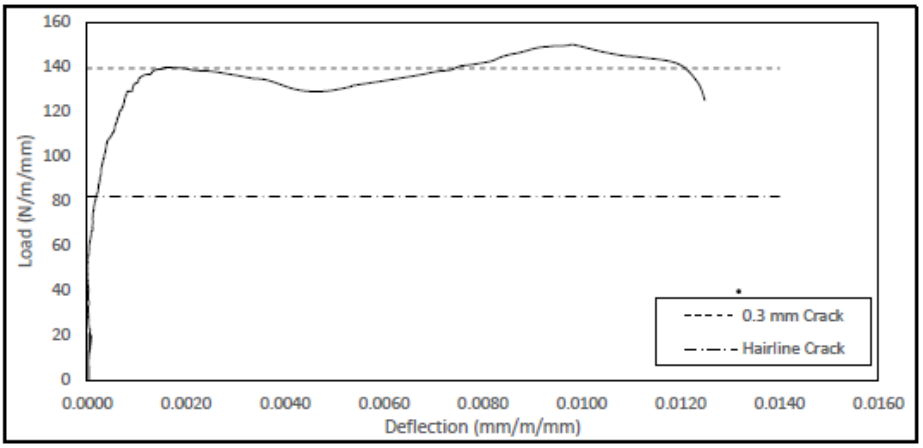

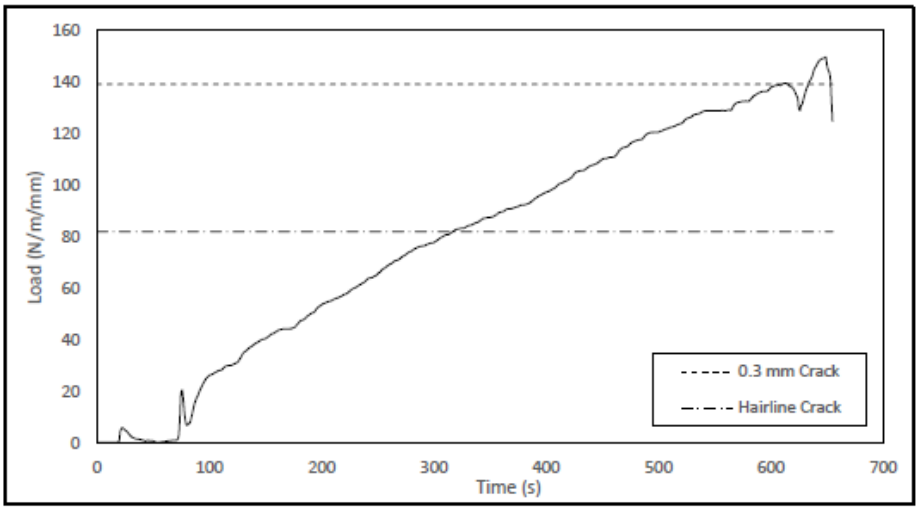

THREE-EDGE BEARING TEST REPORT

Test Date	04/12/2018	Mfg. Date	27/11/2018	Test ID	E02
Pipe Size	1200	Class	100D	Length	2.44 m
				Wall	127 mm

Cage Design:

Inner:		@		mm2	As Inner: 821 mm2
Outer:		@		0 mm2	As Outer:
Elliptical:	D7	@	55	821 mm2	

RFT Area

Age: 8 days

Hairline:	206 kN	69.3 N/m/mm	(Obsv.)	Cover:	mm
M. Hairline:	kN	N/m/mm	(Obsv.)	f'c:	58.5 MPa
0.3-mm:	261 kN	87.8 N/m/mm	(Obsv.)	Equivalent Class:	77.0 D
Ultimate:	341.9 kN	115.0 N/m/mm		UL/DL:	131%

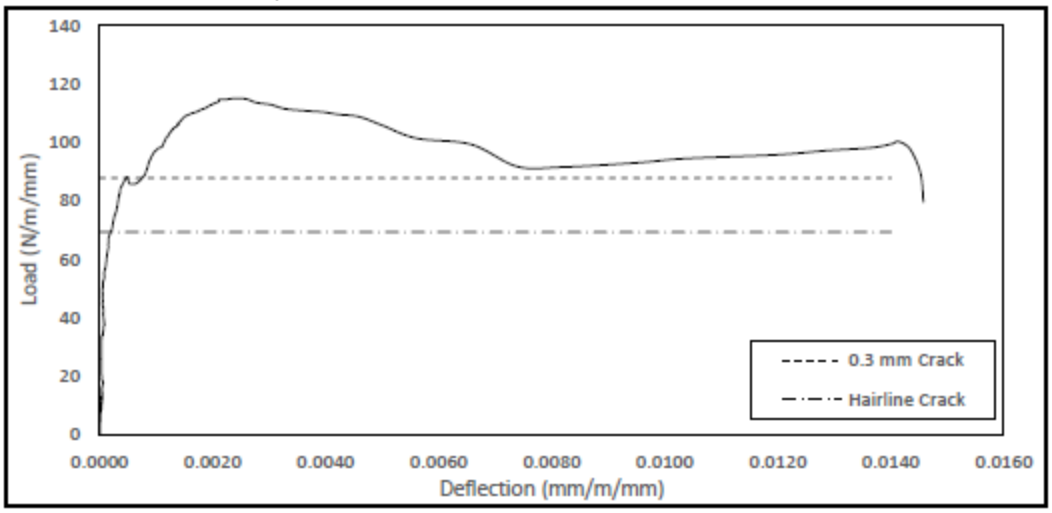

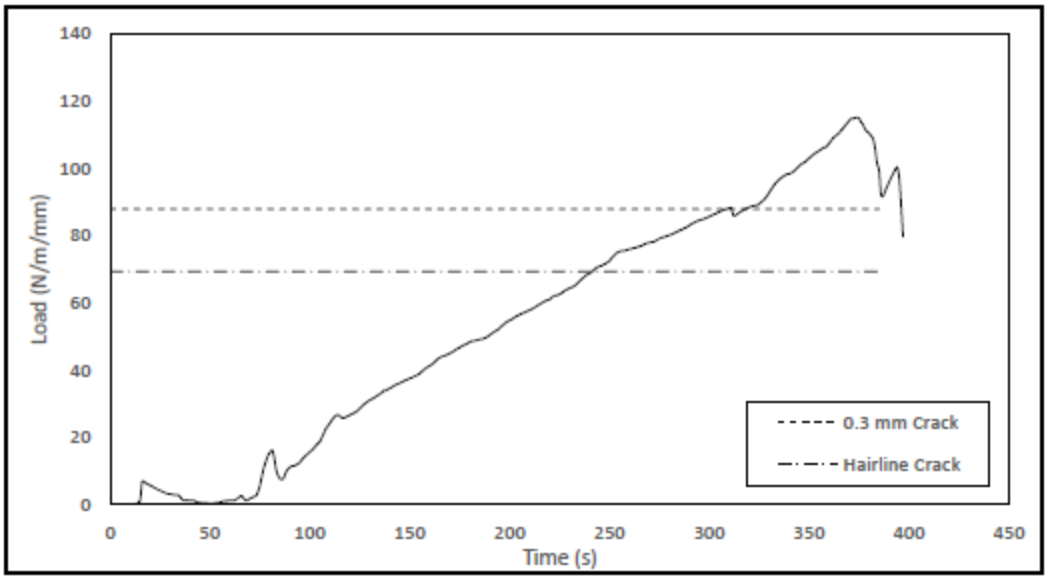

THREE-EDGE BEARING TEST REPORT

Test Date	18/03/2019	Mfg. Date	20/02/2019	Test ID	E08
Pipe Size	1050	Class	100D	Length	2.44 m
				Wall	133 mm

Cage Design: RFT Area

Inner:		@		mm2	As Inner: 581 mm2
Outer:		@		0 mm2	As Outer:
Elliptical:	W4.5	@	50	581 mm2	

Age: 27 days

Hairline:	264 kN	101.5 N/m/mm	(Obsv.)	Cover:	mm
M. Hairline:	kN	N/m/mm	(Obsv.)	f'c:	64.8 MPa
0.3-mm:	410 kN	157.6 N/m/mm	(Obsv.)	Equivalent Class:	151.0 D
Ultimate:	491.3 kN	188.9 N/m/mm		UL/DL:	120%

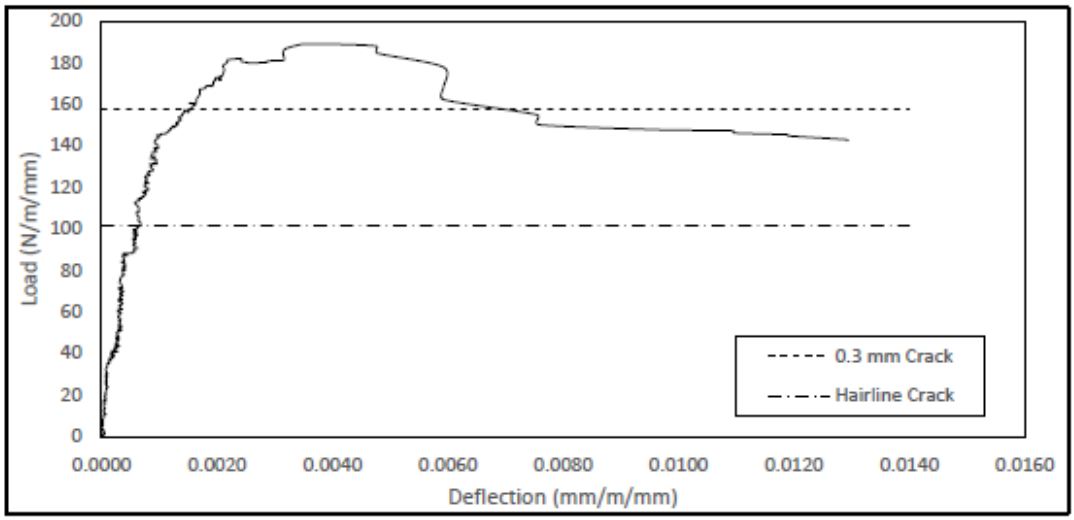

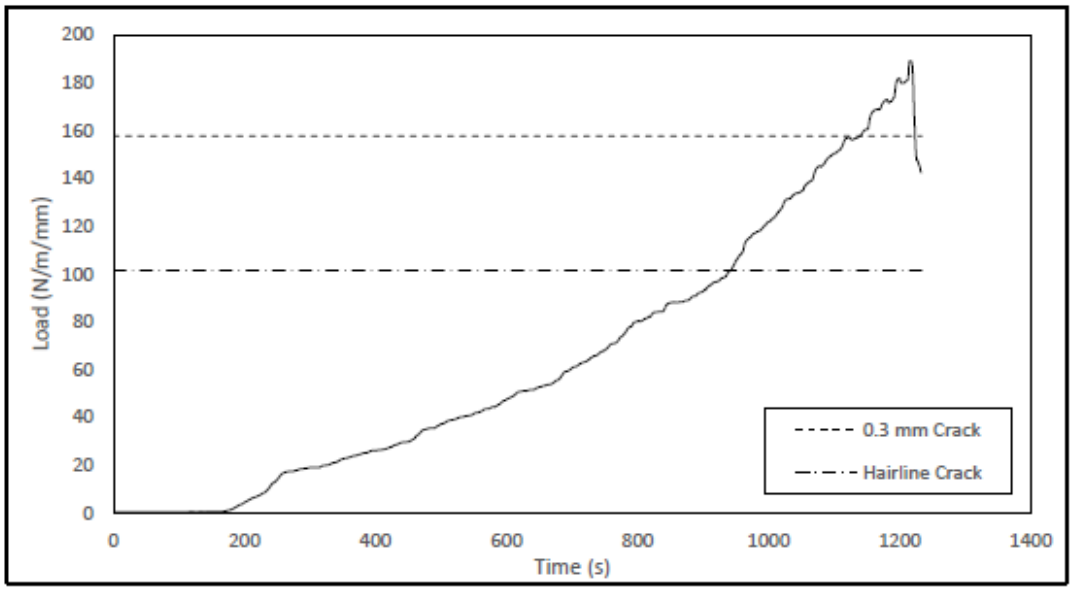

THREE-EDGE BEARING TEST REPORT

Test Date	18/03/2019	Mfg. Date	22/02/2019	Test ID	E09
Pipe Size	1200	Class	100D	Length	2.44 m
				Wall	127 mm

Cage Design: RFT Area

Inner:	@		mm2	As Inner: 903	mm2
Outer:	@		0 mm2	As Outer:	
Elliptical:	D7 @	50	903 mm2		

Age: 25 days

Hairline:	236 kN	79.4 N/m/mm	(Obsv.)	Cover:	mm
M. Hairline:	kN	N/m/mm	(Obsv.)	f'c:	64.4 MPa
0.3-mm:	351 kN	118.1 N/m/mm	(Obsv.)	Equivalent Class:	97 D
Ultimate:	434.4 kN	146.2 N/m/mm		UL/DL:	124%

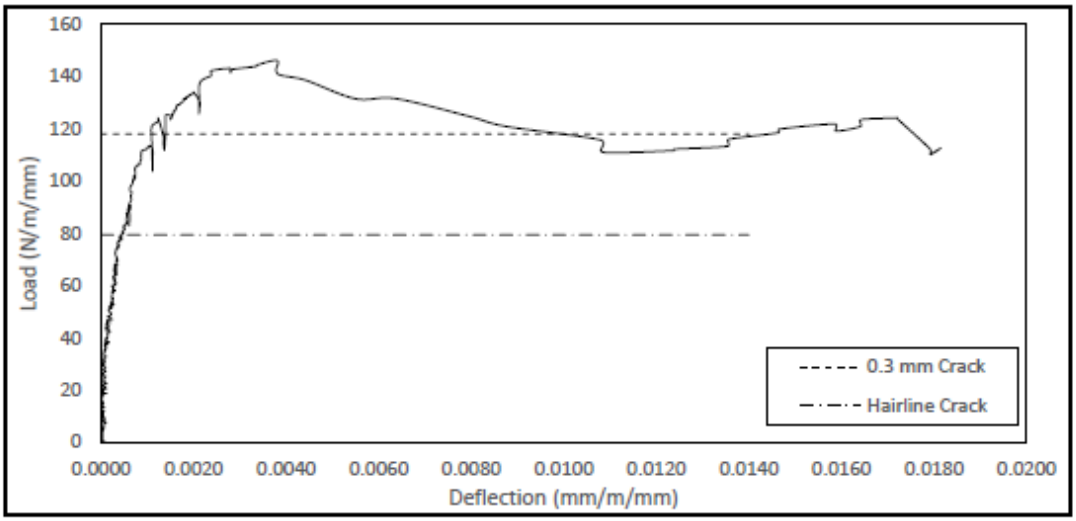

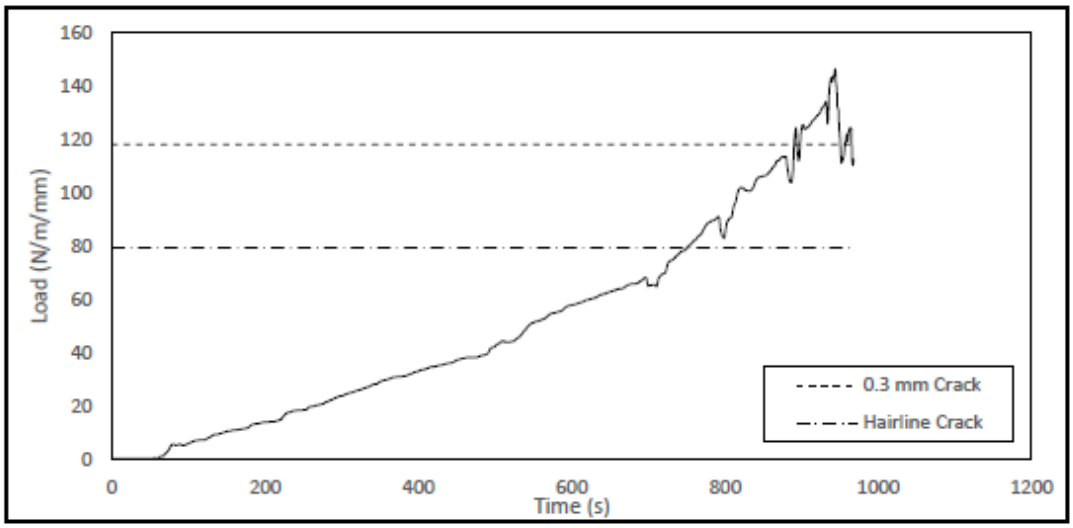

THREE-EDGE BEARING TEST REPORT

Test Date	18/03/2019	Mfg. Date	22/02/2019	Test ID	E10
Pipe Size	1200	Class	100D	Length	2.44 m
				Wall	127 mm

Cage Design:

Inner:		@		mm2	As Inner: 903 mm2
Outer:		@		0 mm2	As Outer:
Elliptical:	D7	@	50	903 mm2	

Age: 25 days

Hairline:	233 kN	78.4 N/m/mm	(Obsv.)	Cover:	mm
M. Hairline:	0 kN	N/m/mm	(Obsv.)	f'c:	64.4 MPa
0.3-mm:	359 kN	120.8 N/m/mm	(Obsv.)	Equivalent Class:	91 D
Ultimate:	404.8 kN	136.2 N/m/mm		UL/DL:	113%

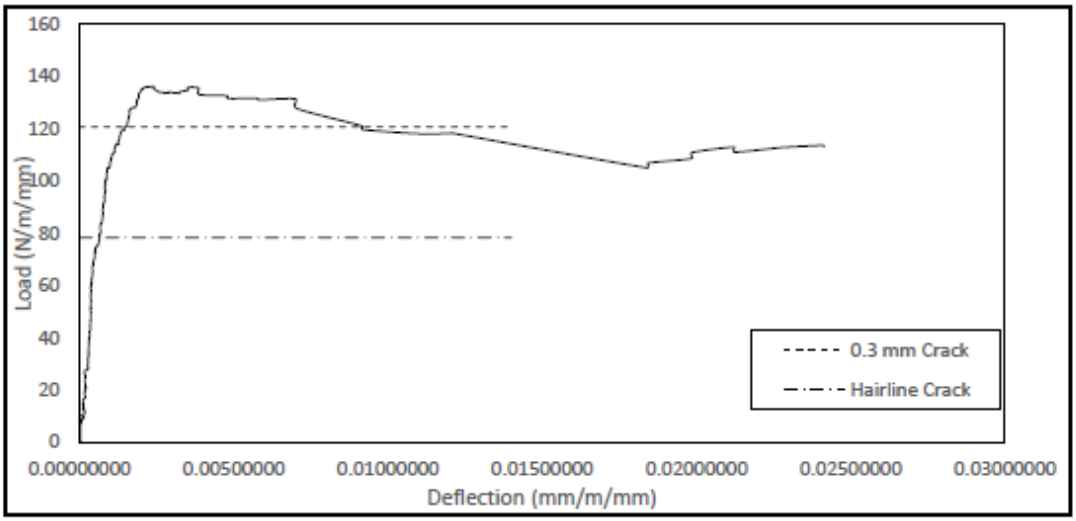

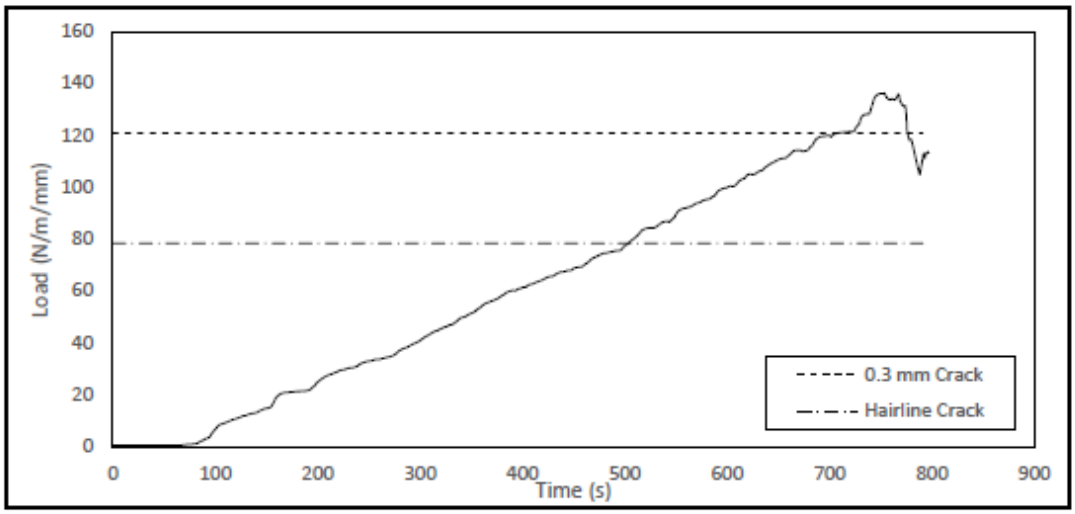

THREE-EDGE BEARING TEST REPORT

Test Date	18/03/2019	Mfg. Date	22/02/2019	Test ID	E11
Pipe Size	1200	Class	100D	Length	2.44 m
				Wall	127 mm

Cage Design: RFT Area

Inner:	@		mm2	As Inner: 903	mm2
Outer:	@		0 mm2	As Outer:	
Elliptical:	D7 @	50	903 mm2		

Age: 25 days

Hairline:	202 kN	68.0 N/m/mm	(Obsv.)	Cover:	mm
M. Hairline:	kN	N/m/mm	(Obsv.)	f'c:	64.4 MPa
0.3-mm:	351 kN	118.1 N/m/mm	(Obsv.)	Equivalent Class:	99 D
Ultimate:	439.2 kN	147.8 N/m/mm	UL/DL:	125%	

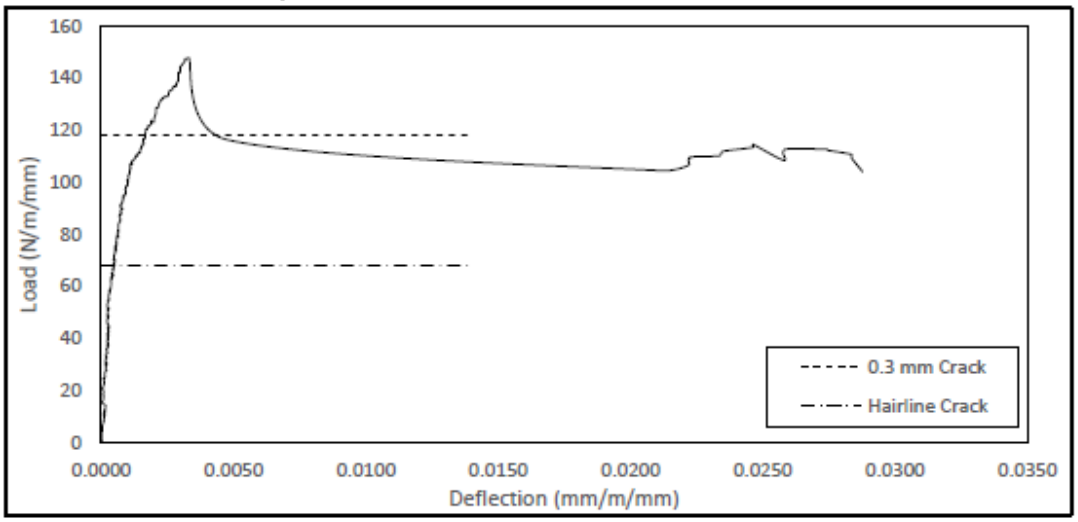

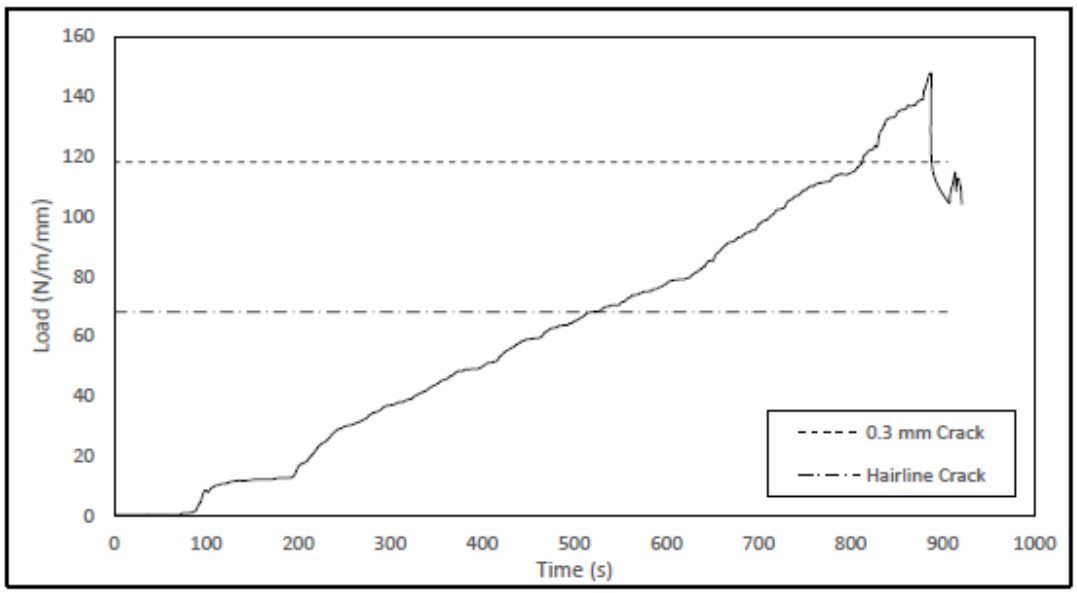

THREE-EDGE BEARING TEST REPORT

Test Date	25/03/2019	Mfg. Date	22/02/2019	Test ID	E12
Pipe Size	1200	Class	100D	Length	2.44 m
				Wall	127 mm

Cage Design: RFT Area

Inner:	@	mm2	As Inner:	993	mm2
Outer:	@	0 mm2	As Outer:		
Elliptical:	D10 @ 65	993 mm2			

Age: 32 days

Hairline:	227 kN	76.4 N/m/mm	(Obsv.)	Cover:	mm
M. Hairline:	kN	N/m/mm	(Obsv.)	f'c:	65.7 MPa
0.3-mm:	368 kN	123.8 N/m/mm	(Obsv.)	Equivalent Class:	93 D
Ultimate:	415.6 kN	139.8 N/m/mm	UL/DL:	113%	

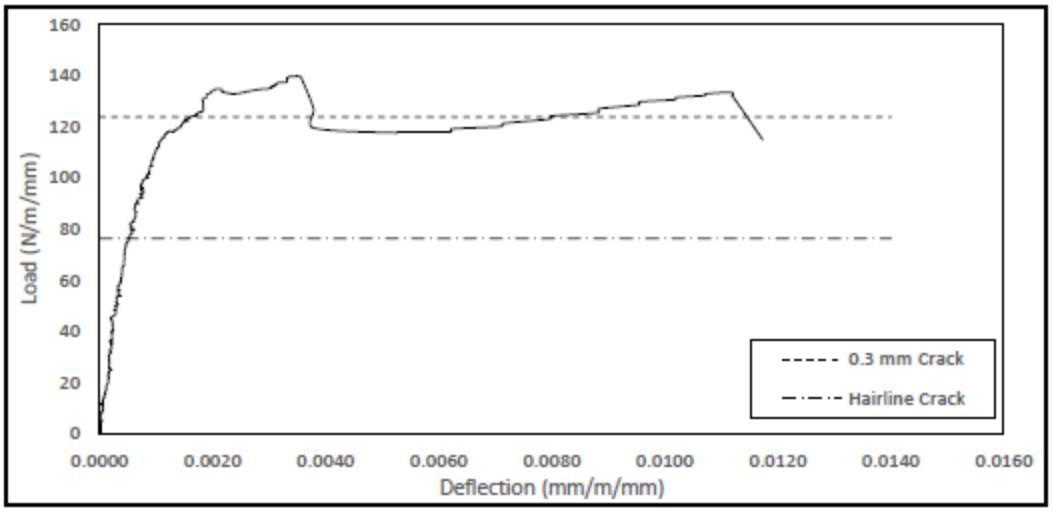

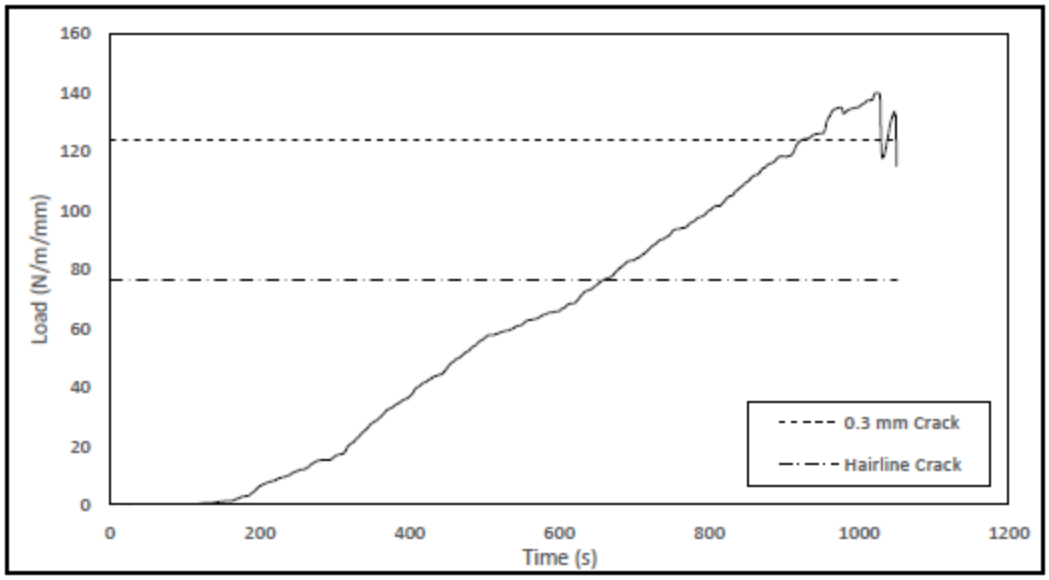

THREE-EDGE BEARING TEST REPORT

Test Date	25/03/2019	Mfg. Date	22/02/2019	Test ID	E13
Pipe Size	1200	Class	100D	Length	2.44 m
				Wall	127 mm

Cage Design: RFT Area

Inner:		@		mm2	As Inner: 993 mm2
Outer:		@		0 mm2	As Outer:
Elliptical:	D10	@	65	993 mm2	

Age: 32 days

Hairline:	176 kN	59.2 N/m/mm	(Obsv.)	Cover:	mm
M. Hairline:	kN	N/m/mm	(Obsv.)	f'c:	65.7 MPa
0.3-mm:	342 kN	115.1 N/m/mm	(Obsv.)	Equivalent Class:	91 D
Ultimate:	404.8 kN	136.2 N/m/mm		UL/DL:	118%

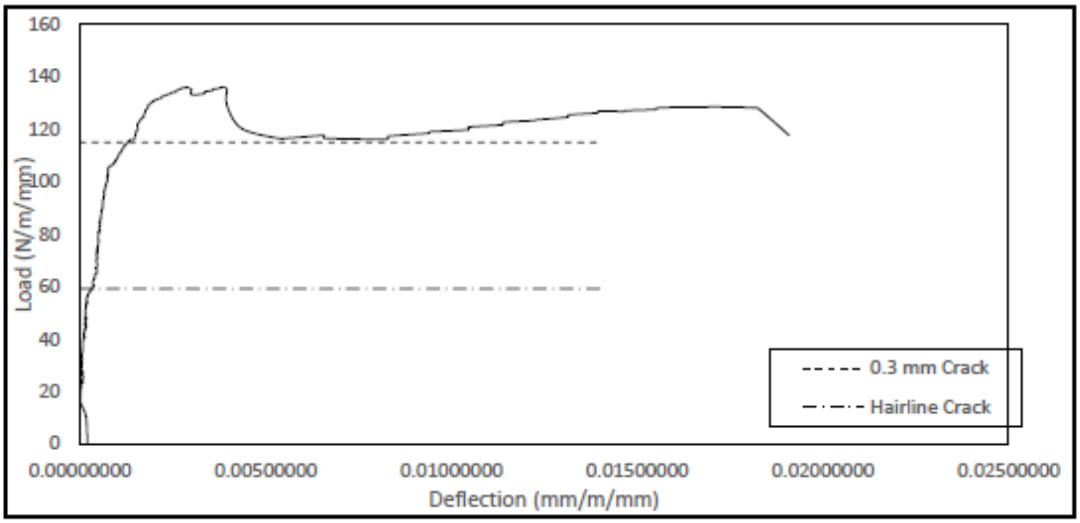

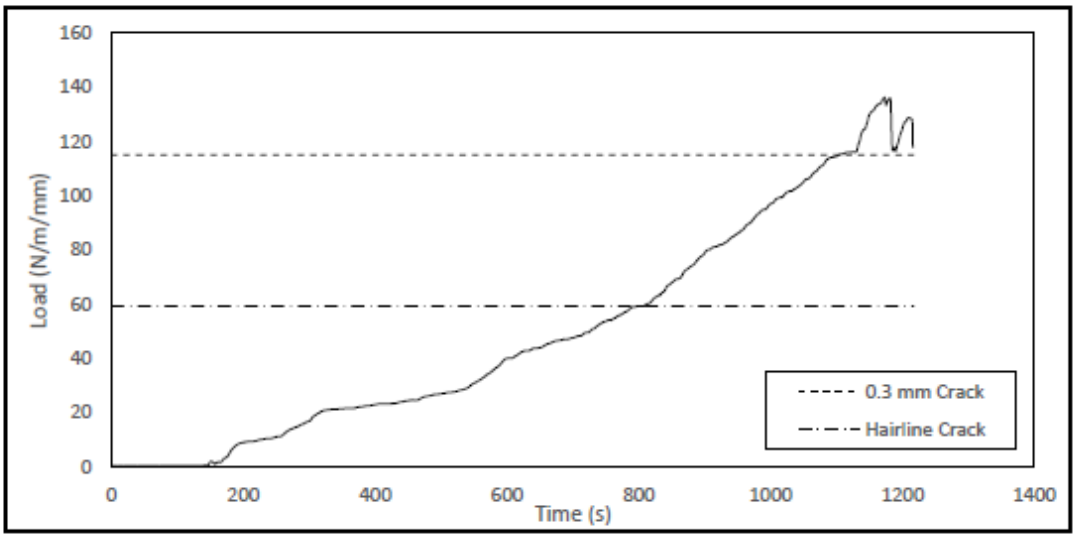

THREE-EDGE BEARING TEST REPORT

Test Date	25/03/2019	Mfg. Date	22/02/2019	Test ID	E14
Pipe Size	1200	Class	100D	Length	2.44 m
				Wall	127 mm

Cage Design: RFT Area

Inner:		@		mm2	As Inner: 993 mm2
Outer:		@		0 mm2	As Outer:
Elliptical:	D10	@	65	993 mm2	

Age: 32 days

Hairline:	168 kN	56.5 N/m/mm	(Obsv.)	Cover:	mm
M. Hairline:	kN	N/m/mm	(Obsv.)	f'c:	65.7 MPa
0.3-mm:	344 kN	115.7 N/m/mm	(Obsv.)	Equivalent Class:	99 D
Ultimate:	442.8 kN	149.0 N/m/mm		UL/DL:	129%

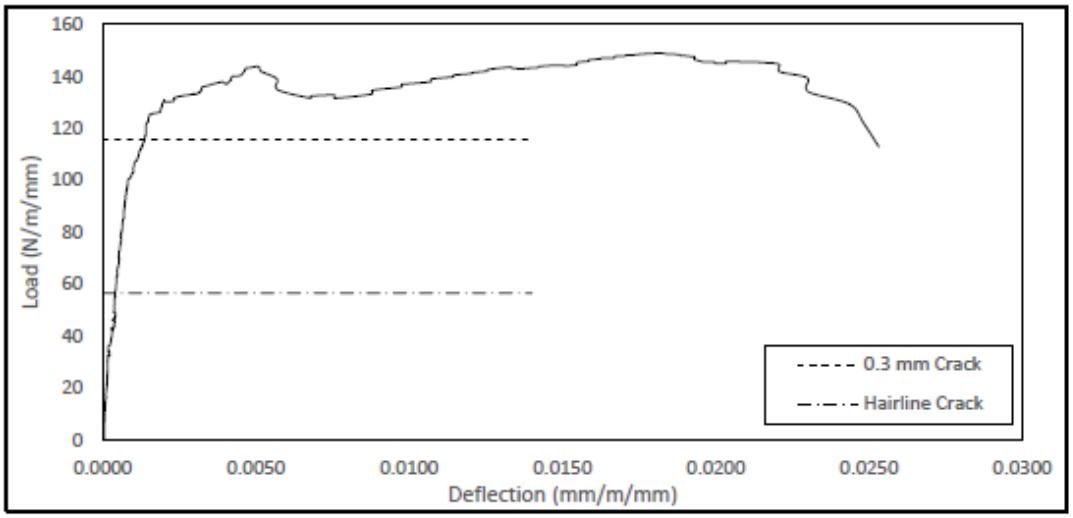

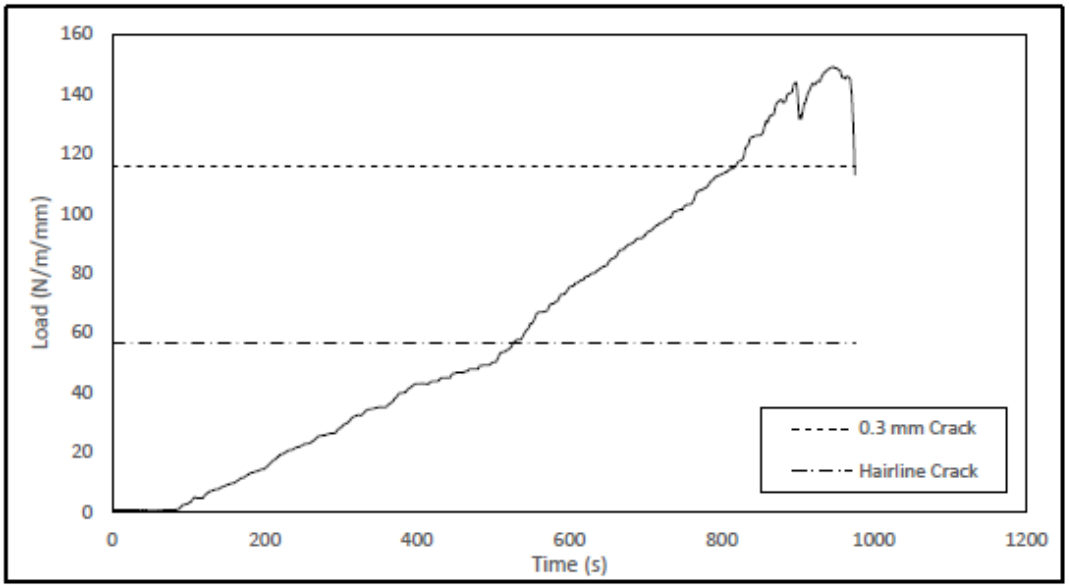

THREE-EDGE BEARING TEST REPORT

Test Date	31/05/2019	Mfg. Date	22/05/2019	Test ID	E15
Pipe Size	1200	Class	140D	Length	2.44 m
				Wall	127 mm

Cage Design: **RFT Area**

Inner:	@		mm2	As Inner:	1936 mm2
Outer:	@		0 mm2	As Outer:	
Elliptical:	D12 @	40	1936 mm2		

Age: 9 days

Hairline:	235 kN	79.1 N/m/mm	(Obsv.)	Cover:	mm
M. Hairline:	kN	N/m/mm	(Obsv.)	f'c:	59.1 MPa
0.3-mm:	425 kN	143.0 N/m/mm	(Obsv.)	Equivalent Class:	143 D
Ultimate:	571 kN	192.1 N/m/mm	UL/DL:	134%	

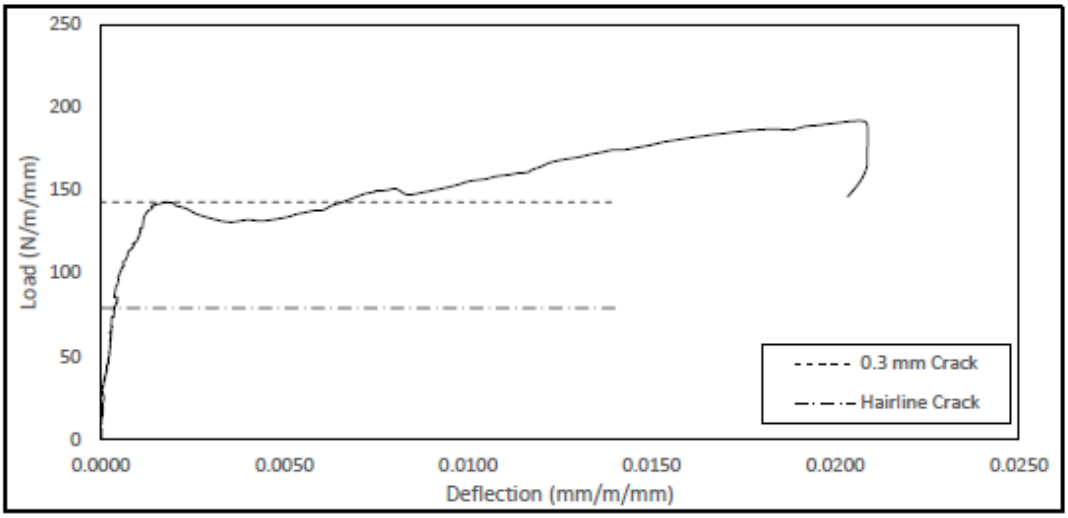

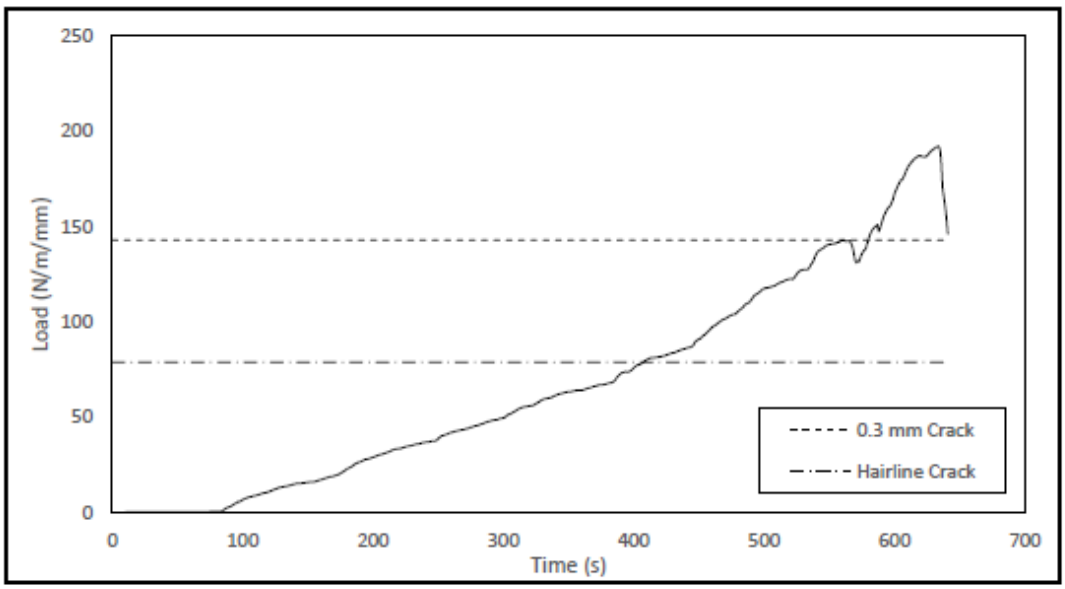

THREE-EDGE BEARING TEST REPORT

Test Date	31/05/2019	Mfg. Date	22/05/2019	Test ID	E16
Pipe Size	1200	Class	140D	Length	2.44 m
				Wall	127 mm

Cage Design: RFT Area

Inner:		@		mm2	As Inner: 1936 mm2
Outer:		@		0 mm2	As Outer:
Elliptical:	D12	@	40	1936 mm2	

Age: 9 days

Hairline:	201 kN	67.6 N/m/mm	(Obsv.)	Cover:	mm
M. Hairline:	kN	N/m/mm	(Obsv.)	f'c:	59.1 MPa
0.3-mm:	418 kN	140.6 N/m/mm	(Obsv.)	Equivalent Class:	141 D
Ultimate:	546.4 kN	183.8 N/m/mm		UL/DL:	131%

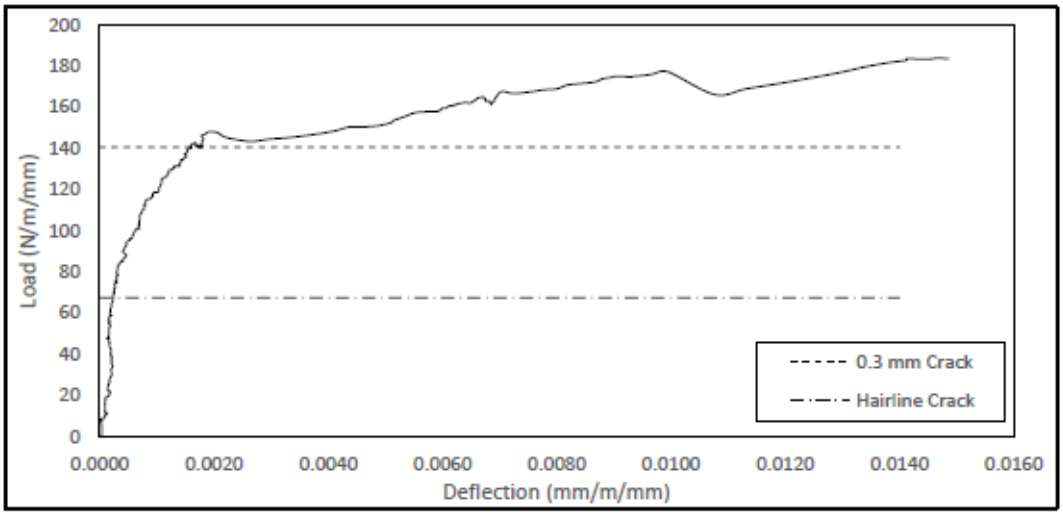

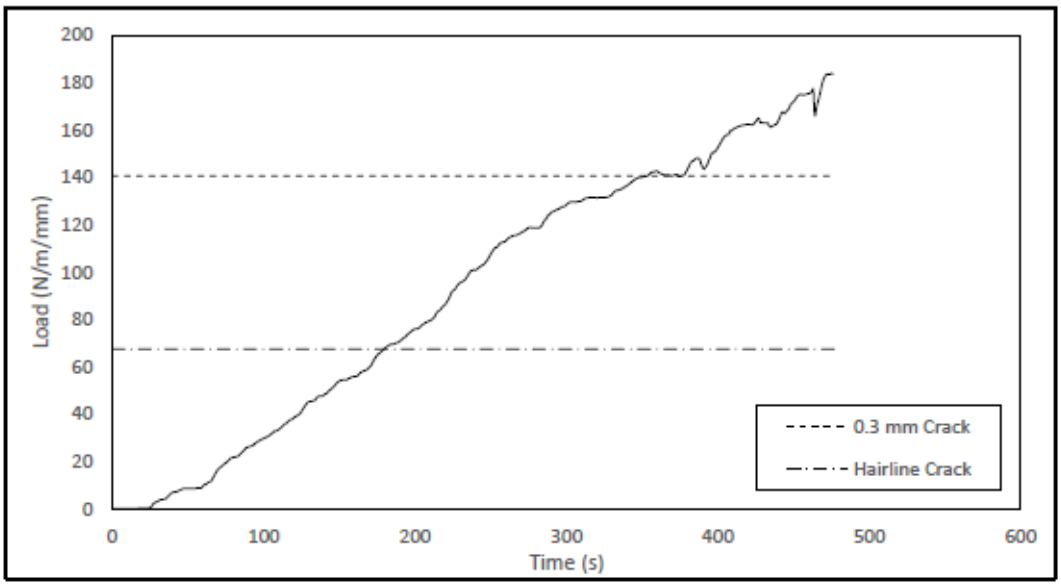

THREE-EDGE BEARING TEST REPORT

Test Date	31/05/2019	Mfg. Date	22/05/2019	Test ID	E17
Pipe Size	1200	Class	140D	Length	2.44 m
				Wall	127 mm

Cage Design:

Inner:		@		mm2	As Inner: 1936 mm2
Outer:		@		0 mm2	As Outer:
Elliptical:	D12	@	40	1936 mm2	

RFT Area

Age: 9 days

Hairline:	165 kN	55.5 N/m/mm	(Obsv.)	Cover:	mm
M. Hairline:	kN	N/m/mm	(Obsv.)	f'c:	59.1 MPa
0.3-mm:	425 kN	143.0 N/m/mm	(Obsv.)	Equivalent Class:	143 D
Ultimate:	554.2 kN	186.5 N/m/mm		UL/DL:	130%

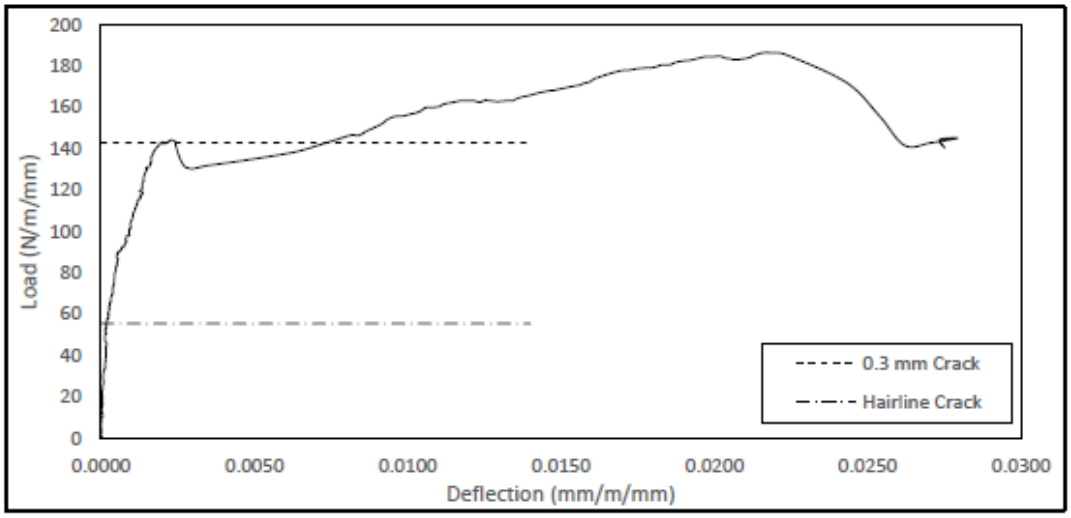

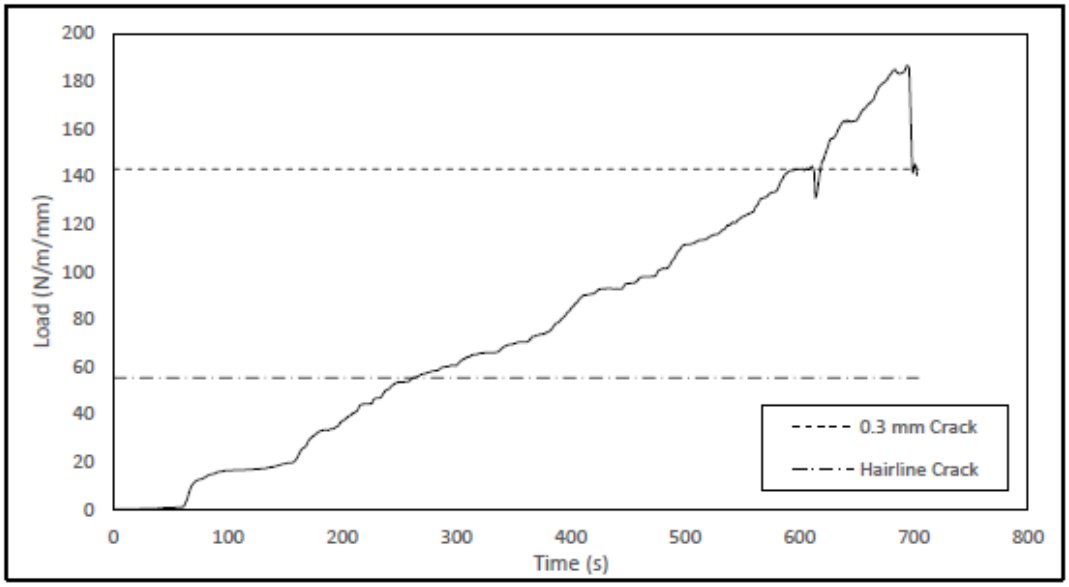

THREE-EDGE BEARING TEST REPORT

Test Date	03/06/2019	Mfg. Date	22/5/2019	Test ID	E18
Pipe Size	1200	Class	100D	Length	2.44 m
				Wall	127 mm

Cage Design: RFT Area

Inner:	@		mm2	As Inner:	1290 mm2
Outer:	@		0 mm2	As Outer:	
Elliptical:	D10	@ 50	1290 mm2		

Age: 12 days

Hairline:	167 kN	56.2 N/m/mm	(Obsv.)	Cover:	mm
M. Hairline:	kN	N/m/mm	(Obsv.)	f'c:	60.6 MPa
0.3-mm:	369 kN	124.1 N/m/mm	(Obsv.)	Equivalent Class:	96 D
Ultimate:	426.9 kN	143.6 N/m/mm		UL/DL:	116%

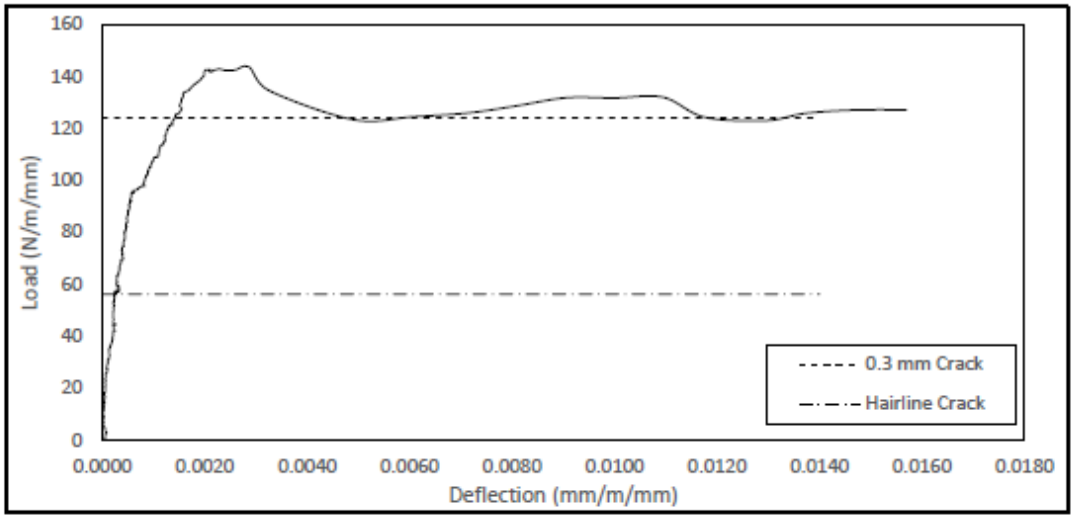

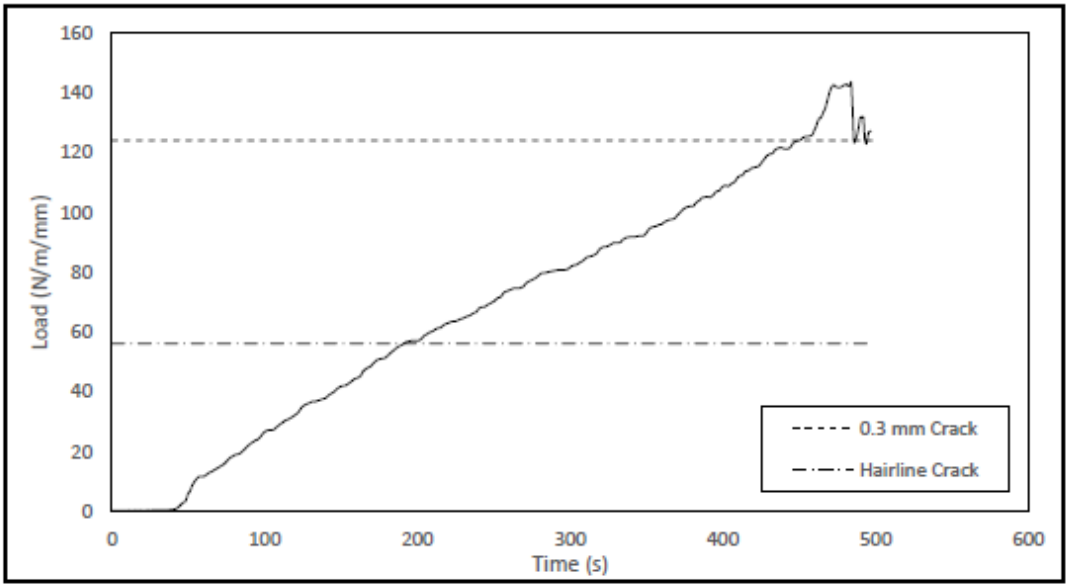

THREE-EDGE BEARING TEST REPORT

Test Date	03/06/2019	Mfg. Date	22/05/2019	Test ID	E19
Pipe Size	1200	Class	100D	Length	2.44 m
				Wall	127 mm

Cage Design: **RFT Area**

Inner:	@	mm2	As Inner:	1290	mm2
Outer:	@	0 mm2	As Outer:		
Elliptical:	D10 @ 50	1290 mm2			

Age: 12 days

Hairline:	147 kN	49.5 N/m/mm	(Obsv.)	Cover:	
M. Hairline:	kN	N/m/mm	(Obsv.)	f'c:	60.6 MPa
0.3-mm:	302 kN	101.6 N/m/mm	(Obsv.)	Equivalent Class:	84 D
Ultimate:	373.6 kN	125.7 N/m/mm	UL/DL:	124%	

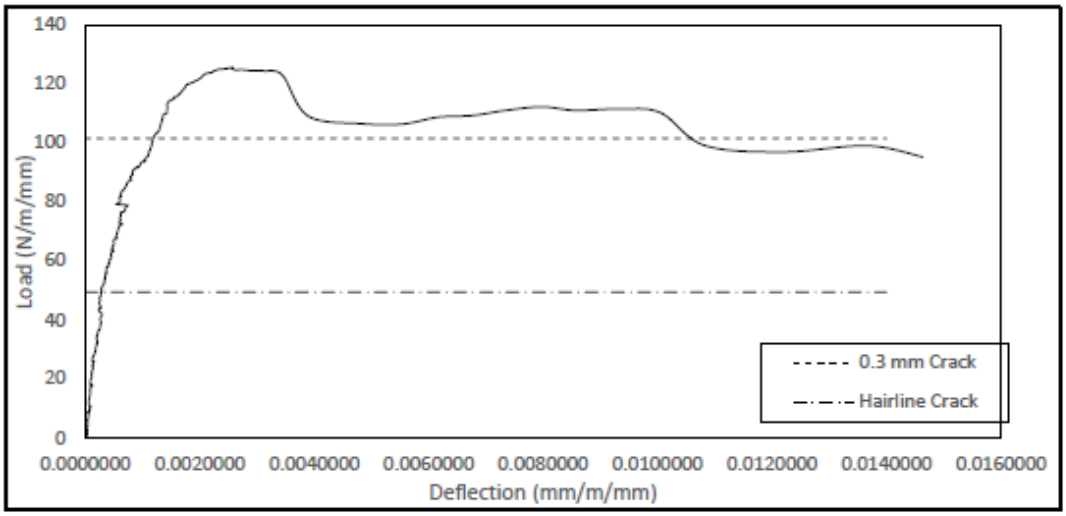

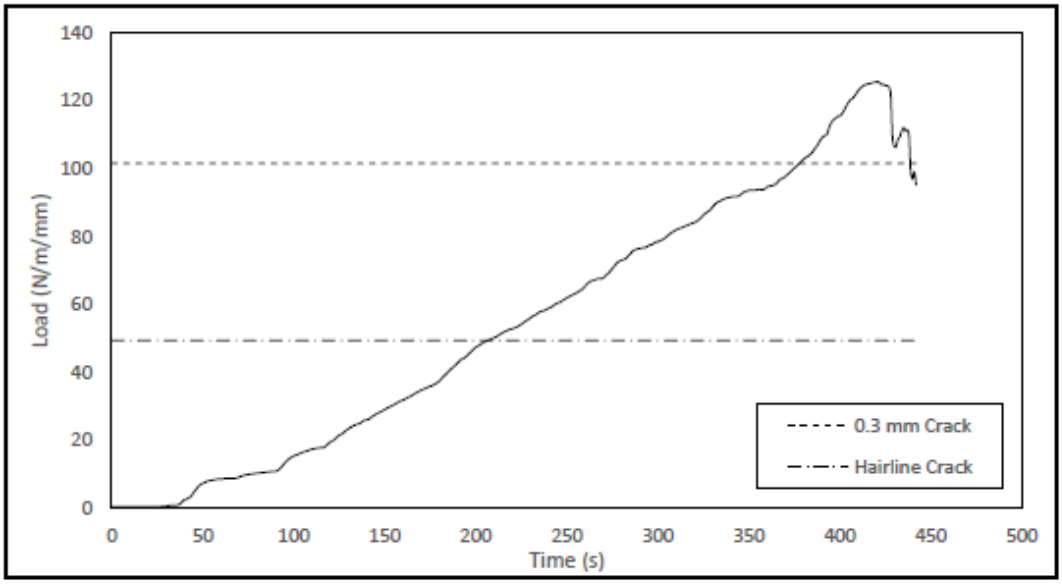

THREE-EDGE BEARING TEST REPORT

Test Date	03/06/2019	Mfg. Date	22/05/2019	Test ID	E20
Pipe Size	1200	Class	100D	Length	2.44 m
				Wall	127 mm

Cage Design: RFT Area

Inner:		@		mm2	As Inner: 1290 mm2
Outer:		@		0 mm2	As Outer:
Elliptical:	D10	@	50	1290 mm2	

Age: 12 days

Hairline:	161 kN	54.2 N/m/mm	(Obsv.)	Cover:	mm
M. Hairline:	kN	N/m/mm	(Obsv.)	f'c:	60.6 MPa
0.3-mm:	329 kN	110.7 N/m/mm	(Obsv.)	Equivalent Class:	93 D
Ultimate:	415.6 kN	139.8 N/m/mm		UL/DL:	126%

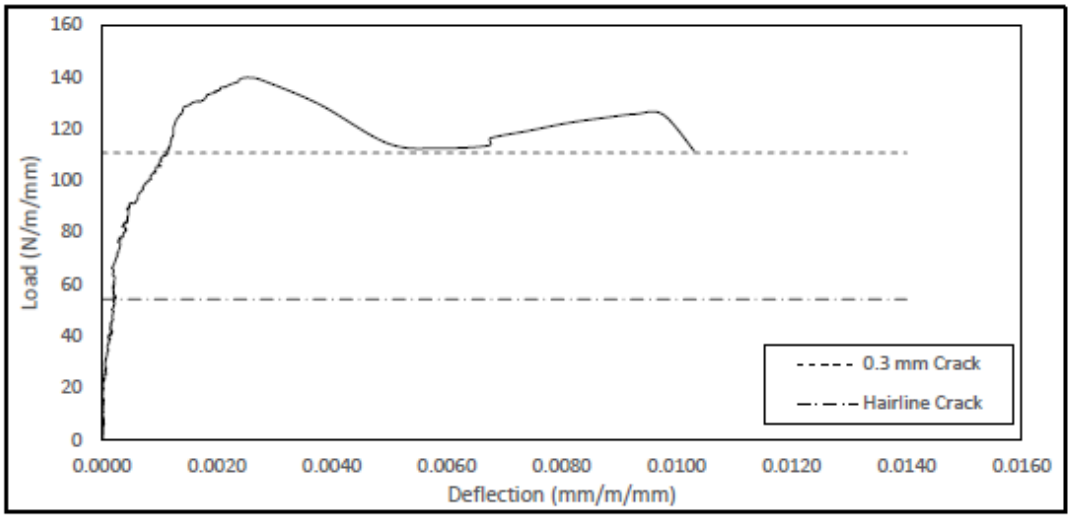

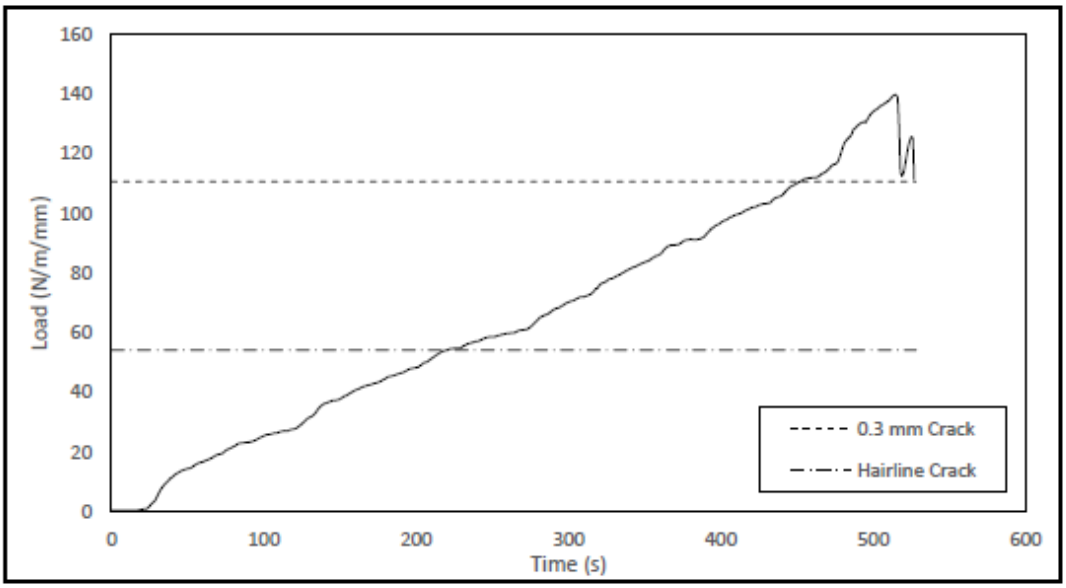

THREE-EDGE BEARING TEST REPORT

Test Date	25/06/2019	Mfg. Date	14/06/2019	Test ID	E21
Pipe Size	1050	Class	100D	Length	2.44 m
				Wall	133 mm

Cage Design: **RFT Area**

Inner:		@		mm2	As Inner: 581 mm2
Outer:		@		0 mm2	As Outer:
Elliptical:	W4.5	@	50	581 mm2	

Age: 11 days

Hairline:	206 kN	79.2 N/m/mm	(Obsv.)	Cover:	mm
M. Hairline:	kN	N/m/mm	(Obsv.)	f'c:	60.2 MPa
0.3-mm:	297 kN	114.2 N/m/mm	(Obsv.)	Equivalent Class:	97 D
Ultimate:	377.8 kN	145.3 N/m/mm		UL/DL:	127%

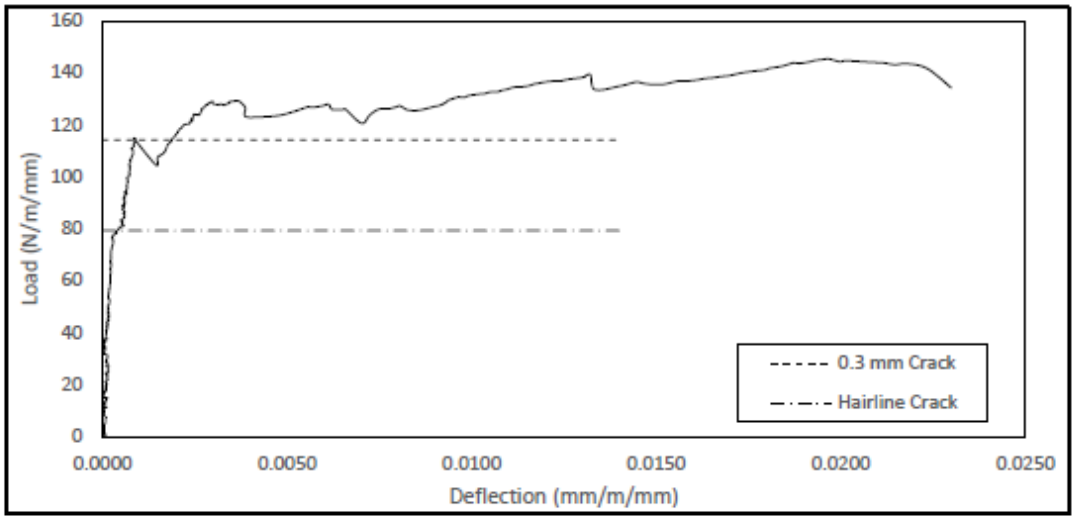

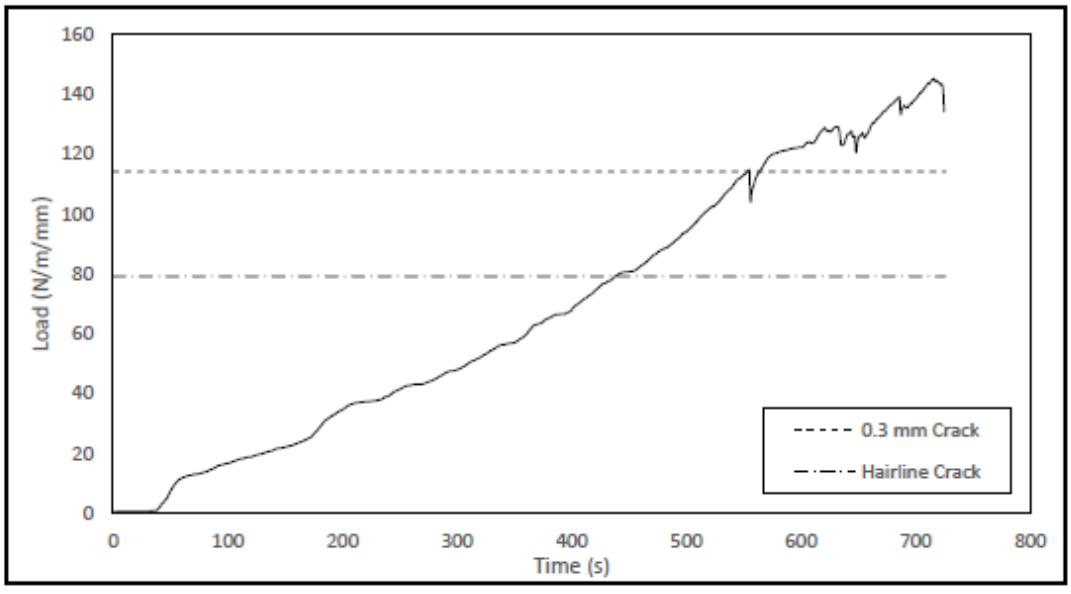

THREE-EDGE BEARING TEST REPORT

Test Date	25/06/2019	Mfg. Date	14/06/2019	Test ID	E23
Pipe Size	1050	Class	100D	Length	2.44 m
				Wall	133 mm

Cage Design: **RFT Area**

Inner:	@		mm2	As Inner: 581	mm2
Outer:	@		0 mm2	As Outer:	
Elliptical:	W4.5 @	50	581 mm2		

Age: 11 days

Hairline:	161 kN	61.9 N/m/mm	(Obsv.)	Cover:	mm
M. Hairline:	kN	N/m/mm	(Obsv.)	f'c:	60.2 MPa
0.3-mm:	234 kN	90.0 N/m/mm	(Obsv.)	Equivalent Class:	86 D
Ultimate:	335.3 kN	128.9 N/m/mm		UL/DL:	143%

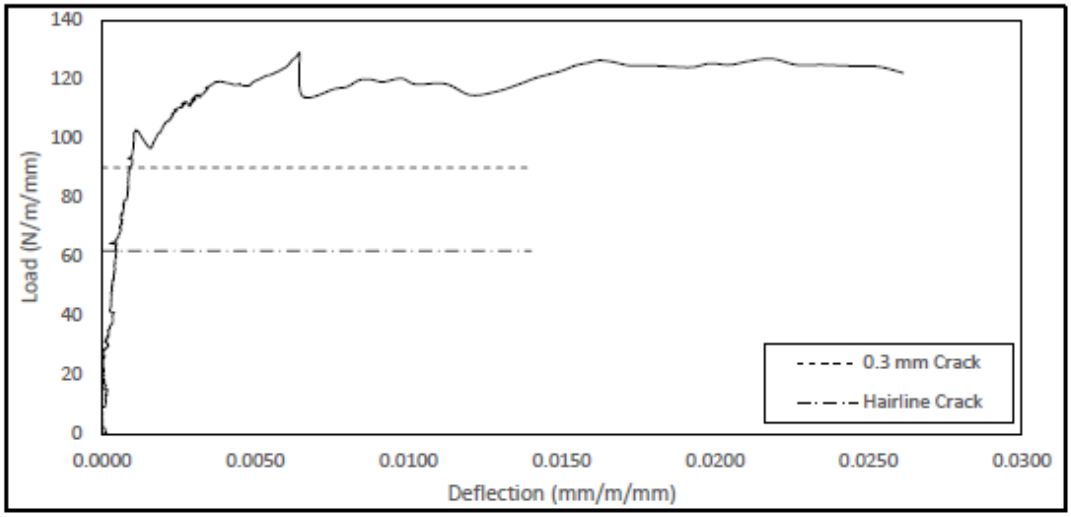

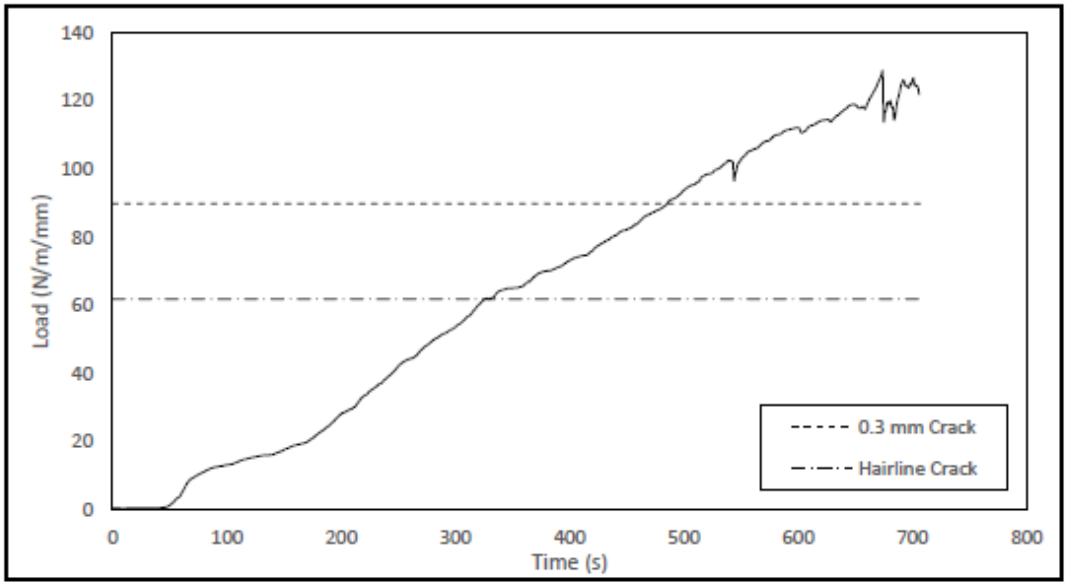

THREE-EDGE BEARING TEST REPORT

Test Date	25/06/2019	Mfg. Date	14/06/2019	Test ID	E24
Pipe Size	1050	Class	140D	Length	2.44 m
				Wall	133 mm

Cage Design:

Inner:		@		RFT Area	mm2
Outer:		@		0	mm2
Elliptical:	D7	@	50	903	mm2

As Inner: 903 mm2

As Outer:

Age: 11 days

Hairline:	182 kN	70.0 N/m/mm	(Obsv.)	Cover:	mm
M. Hairline:	kN	0.0 N/m/mm	(Obsv.)	f'c:	60.2 MPa
0.3-mm:	296 kN	113.8 N/m/mm	(Obsv.)	Equivalent Class:	76 D
Ultimate:	296.4 kN	113.9 N/m/mm		UL/DL:	100%

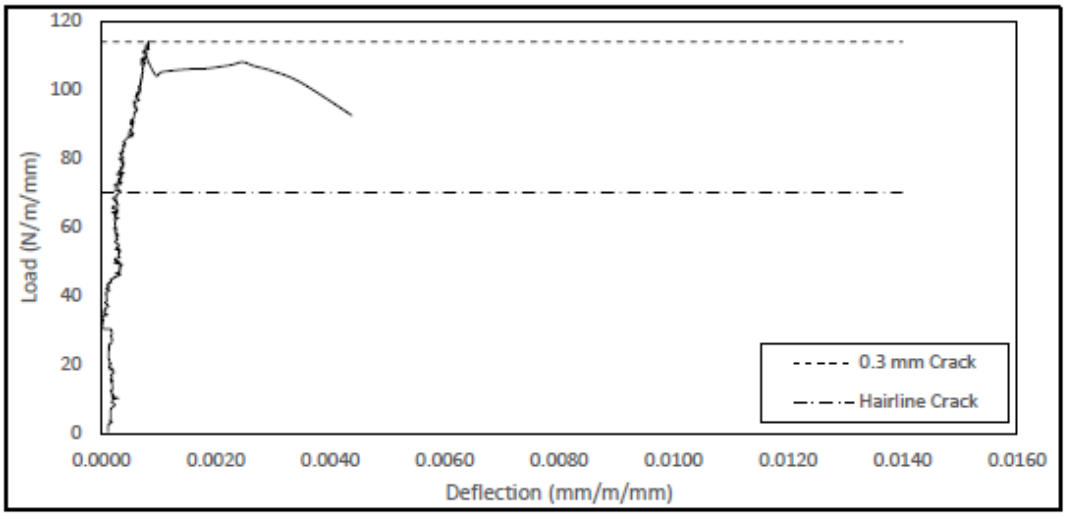

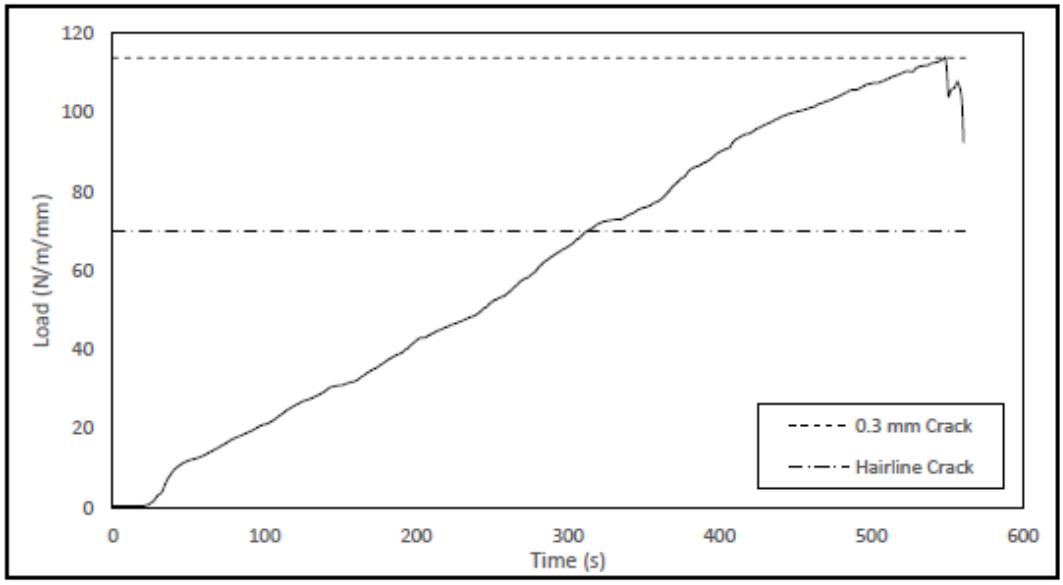

THREE-EDGE BEARING TEST REPORT

Test Date	25/06/2019	Mfg. Date	14/06/2019	Test ID	E25
Pipe Size	1050	Class	140D	Length	2.44 m
				Wall	133 mm

Cage Design: RFT Area

Inner:	@		mm2	As Inner: 903	mm2
Outer:	@		0 mm2	As Outer:	
Elliptical:	D7 @	50	903 mm2		

Age: 11 days

Hairline:	207 kN	79.6 N/m/mm	(Obsv.)	Cover:	mm
M. Hairline:	351 kN	135.0 N/m/mm	(Obsv.)	f'c:	60.2 MPa
0.3-mm:	351 kN	135.0 N/m/mm	(Obsv.)	Equivalent Class:	106 D
Ultimate:	400.9 kN	154.1 N/m/mm		UL/DL:	114%

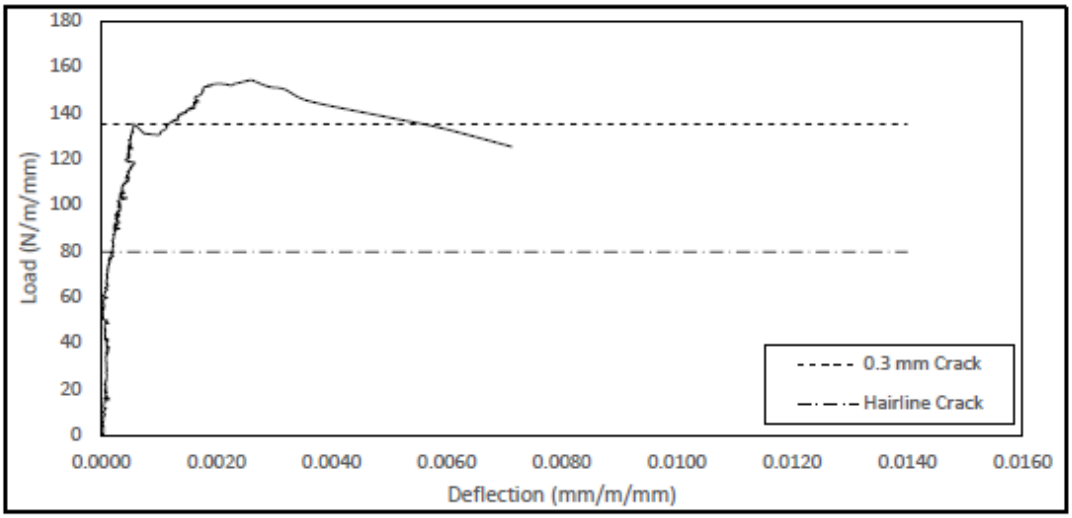

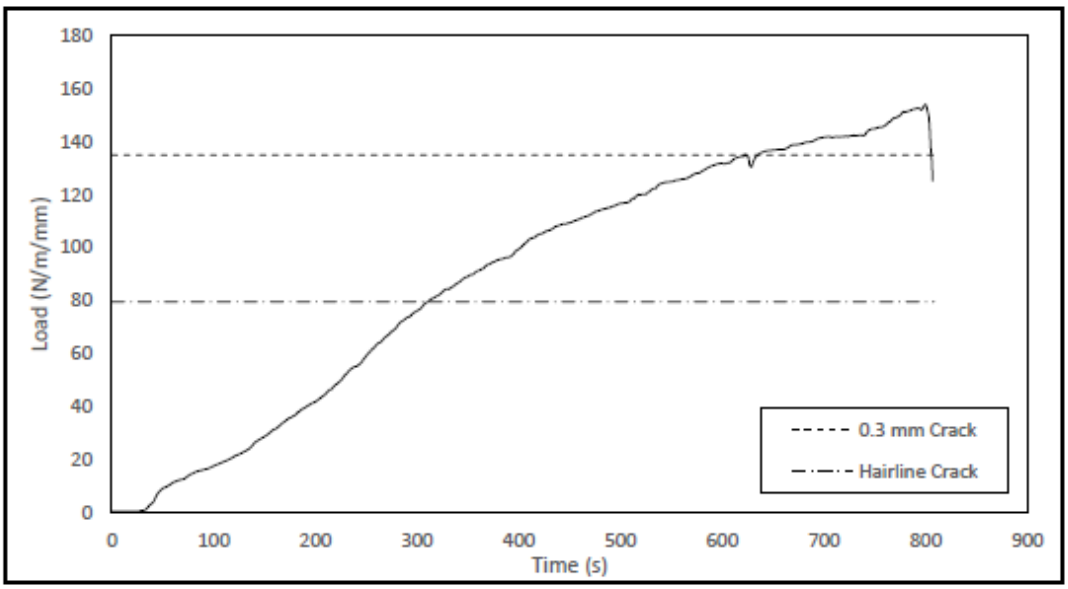

THREE-EDGE BEARING TEST REPORT

Test Date	25/06/2019	Mfg. Date	14/06/2019	Test ID	E26
Pipe Size	1050	Class	140D	Length	2.44 m
				Wall	133 mm

Cage Design: RFT Area

Inner:	@		mm2	As Inner:	903 mm2
Outer:	@		0 mm2	As Outer:	
Elliptical:	D7	@ 50	903 mm2		

Age: 11 days

Hairline:	189 kN	72.7 N/m/mm	(Obsv.)	Cover:	mm
M. Hairline:	kN	N/m/mm	(Obsv.)	f'c:	60.2 MPa
0.3-mm:	321 kN	123.4 N/m/mm	(Obsv.)	Equivalent Class:	101 D
Ultimate:	390.7 kN	150.2 N/m/mm		UL/DL:	122%

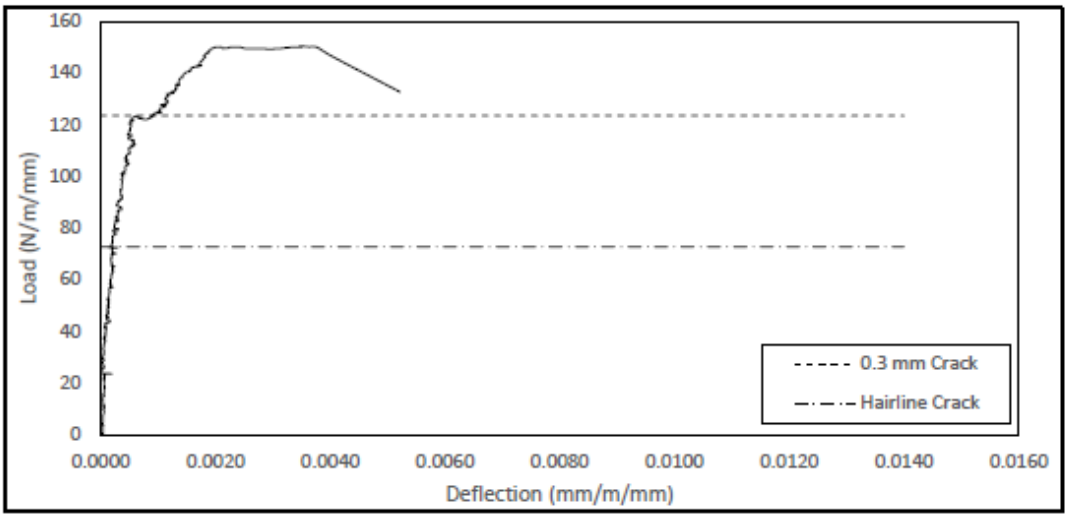

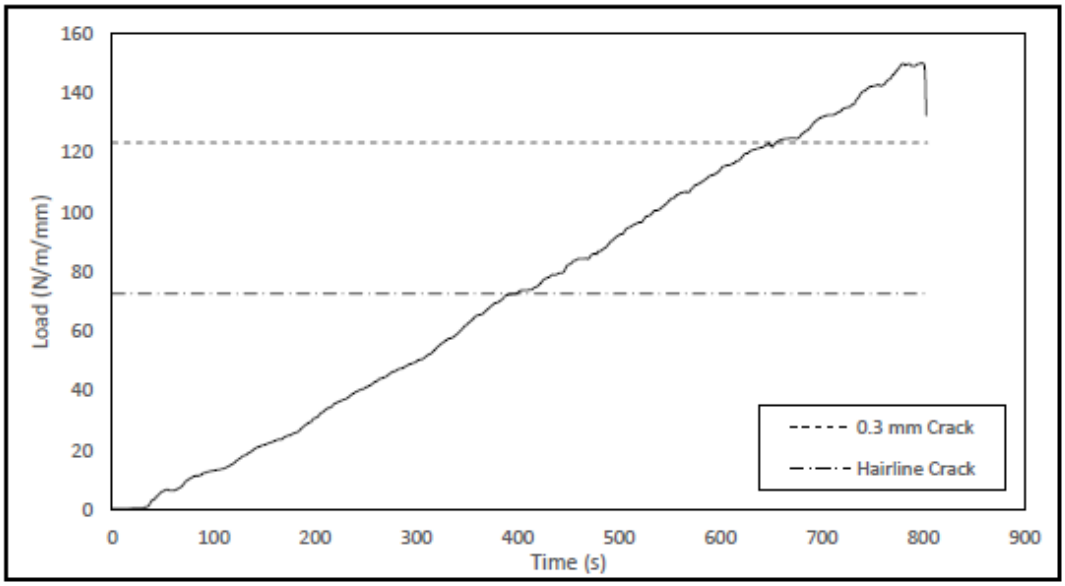

Appendix B

Heger Crack Load, Moment Capacity, and Ultimate Load Capacity Calculation

RCP Geometry Inputs:

- **Internal Pipe Diameter:** $\boldsymbol{Di} = 1066.8\ mm$

  Convert *Di* to imperial: $Di = \frac{1066.8}{25.4} = 42\ inches = 3.5ft$

- **Pipe Wall Thickness:** $\boldsymbol{h} = 133\ mm$

  Convert *h* to imperial: $h = \frac{133}{25.4} = 5.24\ inches$

Reinforcing Steel Inputs

- **Area of Steel:** $\boldsymbol{As_1} = 903\ mm^2/m$

  Convert As_1 to in^2/ft: $As_1 = \frac{\frac{903}{645.15}}{3.2808} = 0.427\ in^2/ft$

- **Bar Diameter:** $\boldsymbol{\varphi} = 0.3\ inches$

- **Longitudinal Wire Spacing:** $\boldsymbol{l_o}$

  Number of Longitudinal Steel Bars *n*: $n = 24\ Bars$

  Concrete Cover *c*: $c = 0.90\ inches$

  Effective depth *d*: $d = h - c - \frac{\boldsymbol{\varphi}}{\mathbf{2}} = 5.24 - 0.9 - \frac{0.3}{2} = 4.19\ inches$

  Circumference cf_1: $cf_1 = \pi(Di + 2d) = \pi\big(42 + 2(4.19)\big) = 158.27\ inches$

  $lo = \frac{cf_1}{n} = \frac{158.27}{24} = 6.59\ inches$

Materials Input:

- **Concrete Compressive Strength *fc'***: $fc' = 60.2\ MPa$

  Convert *fc'* to psi: $fc' = 60.2 * 145.038 = 8752.2\ psi$

- **Steel Yield Strength *fs'***: $fs' = 630\ MPa$

  Convert *fs'* to psi: $fs' = 630 * 145.038 = 91374\ psi$

- **Density ρ**: $\rho = 2400\frac{kg}{m^3} = 149.827\ lb/ft^3$

- **Pipe Weight *W***: $\frac{(\frac{\pi\left((Di+h^2)^2-Di^2\right)}{4}*\rho*9.81)}{1000^3} = 11.8\frac{kN}{m} = 808.8\ lbf/ft$

Heger Crack Load Capacity:

$$(DL)_{0.01} = \frac{(1.15 \times 10^5)A_{s1}d}{l_o D_i^2} + \frac{0.3 l_o h d\sqrt{f_c'}}{\varphi D_i^2} - \frac{0.72W}{D_i}$$

$$(DL)_{0.01} = \frac{(1.15 \times 10^5) * 0.427 * 4.19}{6.59 * 3.5^2} + \frac{0.3 * 6.59 * 5.24 * 4.19\sqrt{8752.2}}{0.3 * 42^2} - \frac{0.72 * 808.8}{3.5}$$

$$= 24.22\frac{lbf}{in^2} = \mathbf{167.0\ N/m/mm}$$

Heger Moment Capacity:

$$M_{p1} = f_s' A_{s1}(d - 0.5a)\left(\frac{1}{12}\right)$$

$$a = 0.1\frac{f_s' A_{s1}}{f_c'}$$

$$a = 0.1\frac{91374 * 0.427}{808.8} = 0.4468$$

$$M_{p1} = 91374 * 0.427(4.1.9 - 0.5 * 0.4468)\left(\frac{1}{12}\right) = 12896\ ft - lb = \mathbf{17485\ N - m}$$

Heger Ultimate Load Capacity:

$$(DL)_u = \frac{7.3M_{p1}}{D_i^2} - \frac{0.5W}{D_i}$$

$$(DL)_u = \frac{7.3 * 12896}{3.5^2} - \frac{0.5 * 808.8}{3.5} = 7569\frac{lbf}{ft^2} = \mathbf{361.6\ N/m/mm}$$

Curriculum Vitae

Name:	Abdullah Samir Ramadan
Post-secondary Education and Degrees:	Western University London, Ontario, Canada 2012-2017 B.E.Sc.
Honours and Awards:	Western University Continuing Admissions Scholarship 2012 Western University International Learning Award 2016
Related Work Experience	Research & Teaching Assistant Western University 2018-2020

Publications:

Ramadan, A., Younis, A.-A., Wong, L. S., and Nehdi, M. L. "Investigation of structural behavior of precast concrete pipe with single elliptical steel cage reinforcement," *Engineering Structures, Elsevier,* Vol. 219, pp. 1-17, 2020.

Ramadan, A., Shehata, A., Younis, A.-A., Wong, L. S., and Nehdi, M. L. "Modeling structural behavior of precast concrete pipe with single elliptical cage reinforcement," *Structures*, Elsevier, Vol. 27, October 2020 Issue, pp. 1-14, 2020.

Ramadan, A., Younis, A.-A., Wong, L. S., and Nehdi, M. L. (2019) "Reinforced Concrete Pipe Design with Single Elliptical Steel Cage Reinforcement" 7th International Specialty Conference on Engineering Mechanics and Materials, Proceeding of the Annual Conference of the Canadian Society for Civil Engineering, Laval, Canada

Younis, A.-A., **Ramadan, A.**, Wong, L. S., and Nehdi, M. L. "New rational test for reinforced-concrete pipe eliminating subjective crack-width criteria," submitted to *Structures*, 2020.

Younis, A.-A., Shehata, A., **Ramadan, A.**, Wong, L. S., and Nehdi, M. L. "Modeling structural behavior of reinforced-concrete pipe with single, double, and triple cage reinforcement," submitted to *Engineering Structures*, 2020.